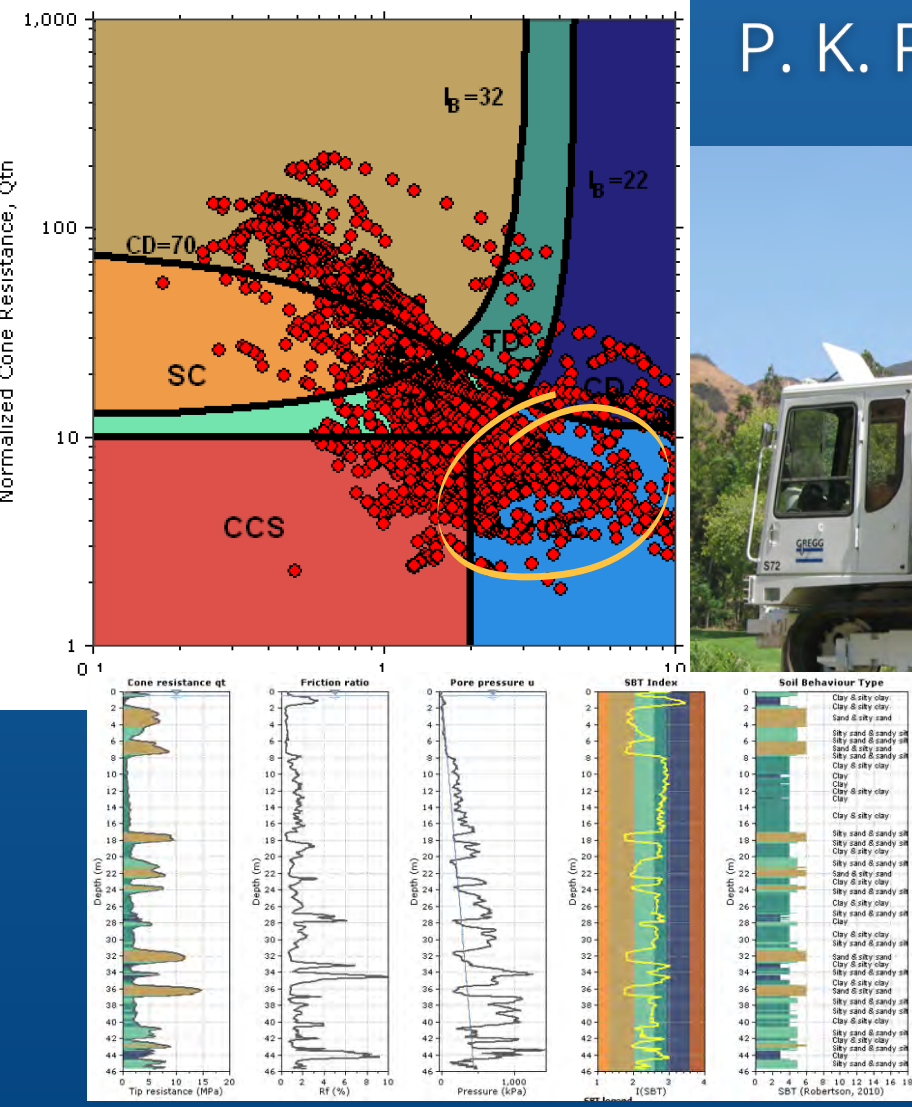


CONE PENETRATION TESTING

Modified Robertson (2016) SBTn



P. K. Robertson & K. Cabal



7th Edition

Gregg Drilling LLC
Corporate Headquarters
2726 Walnut Ave.
Signal Hill, CA 90755

Tel: 562-427-6899
Email: info@greggdrilling.com
www.greggdrilling.com

The publisher and the author make no warranties or representations of any kind concerning the accuracy or suitability of the information contained in this guide for any purpose and cannot accept any legal responsibility for any errors or omissions that may have been made.

Copyright © 2022 Gregg Drilling LLC. All rights reserved.

**GUIDE TO
CONE PENETRATION
TESTING**

**BY
P.K. ROBERTSON
& K. CABAL**

GREGG DRILLING LLC

**SEVENTH EDITION
DECEMBER 2022**



TABLE OF CONTENTS

Glossary	i
Introduction.....	1
Risk Based Site Characterization	2
Role of the CPT	3
Cone Penetration Test (CPT).....	6
<i>Introduction</i>	6
<i>History</i>	7
<i>Test Equipment and Procedures</i>	10
<i>Additional Sensors/Modules</i>	11
<i>Delivery systems</i>	12
<i>Depth of Penetration</i>	18
<i>Test Procedures</i>	18
<i>Cone Design</i>	22
<i>CPT Interpretation</i>	25
Groundwater Conditions and Piezometric Profile	26
Soil Profiling and Soil Classification	27
Non-Normalized SBT Charts	27
Equivalent SPT N ₆₀ Profiles	36
Soil Unit Weight (γ)	39
Undrained Shear Strength (s _u)	41
Soil Sensitivity (S _t)	42
Undrained Shear Strength Ratio (s _u / σ' _{vo})	43
Overconsolidation Ratio (OCR) and Yield Stress (σ' _y)	44
Consistency between values of k (for OCR) and N _{kt} (for s _u)	46
In-Situ Stress Ratio (K _o)	47
Relative Density (Dr)	48
State Parameter (ψ)	51
Peak Friction Angle (ϕ')	53
Stiffness and Modulus	55
Modulus from Shear Wave Velocity	56
Estimating Shear Wave Velocity (V _s) from CPT	57
Identification of soils with microstructure	58
Hydraulic Conductivity (k)	60
Consolidation Characteristics	63
Constrained Modulus	67
<i>Applications of CPT Results</i>	68
Shallow Foundation Design	69
Shallow Foundation - Bearing Capacity	70

Indirect Methods Based on Soil Parameters	72
Direct Approach to estimate Bearing Capacity (In-Situ Tests)	73
Shallow Foundation Design – Settlement	75
Seismic Shear Wave Velocity	79
Deep Foundation Design	89
Ground Improvement Compaction Control	101
Design of Wick or Sand Drains	104
<i>Liquefaction</i>	106
Liquefaction Definitions	106
Cyclic Liquefaction (Level or Gently Sloping Ground Sites)	110
Flow (static) Liquefaction (Steeply Sloping Sites)	135
Software	148
Main References	151

Glossary

This glossary contains the most used terms related to CPT and are presented in alphabetical order.

CPT

Cone penetration test.

CPTu

Cone penetration test with pore pressure measurement – *piezocene* test.

Cone

The part of the cone penetrometer on which the cone resistance is measured.

Cone penetrometer

The assembly containing the cone, friction sleeve, and any other sensors, as well as the connections to the push rods.

Cone resistance, q_c

The force acting on the cone, Q_c , divided by the projected area of the cone, A_c .

$$q_c = Q_c / A_c$$

Corrected cone resistance, q_t

The cone resistance q_c corrected for pore water effects.

$$q_t = q_c + u_2(1 - a)$$

Data acquisition system

The system used to record the measurements made by the cone.

Dissipation test

A test when the decay of the pore pressure is monitored during a pause in penetration.

Filter element

The porous element inserted into the cone penetrometer to allow transmission of pore water pressure to the pore pressure sensor, while maintaining the correct dimensions of the cone penetrometer.

Friction ratio, R_f

The ratio, expressed as a percentage, of the sleeve friction resistance, f_s , to the cone resistance, q_t , both measured at the same depth.

$$R_f = (f_s/q_t) \times 100\%$$

Friction reducer

A local enlargement on the push rods placed a short distance above the cone penetrometer, to reduce the friction on the push rods.

Friction sleeve

The section of the cone penetrometer upon which the friction resistance is measured.

Normalized cone resistance, Q_t

The cone resistance expressed in a non-dimensional form and taking account of the in-situ vertical stresses.

$$Q_t = (q_t - \sigma_{vo}) / \sigma'_{vo}$$

Normalized cone resistance, Q_{tn}

The cone resistance expressed in a non-dimensional form taking account of the in-situ vertical stresses and where the stress exponent (n) varies with soil type and stress level. When $n = 1$, $Q_{tn} = Q_t$.

$$Q_{tn} = \left(\frac{q_t - \sigma_{vo}}{P_{a2}} \right) \left(\frac{P_a}{\sigma'_{vo}} \right)^n$$

Net cone resistance, q_n

The corrected cone resistance minus the vertical total stress.

$$q_n = q_t - \sigma_{vo}$$

Excess pore pressure (or net pore pressure), Δu

The measured pore pressure less the in-situ equilibrium pore pressure.

$$\Delta u = u_2 - u_0$$

Pore pressure

The pore pressure generated during cone penetration and measured by a pore pressure sensor:

u_1 when measured on the cone face

u_2 when measured just behind the cone.

Pore pressure ratio, B_q

The net pore pressure normalized with respect to the net cone resistance.

$$B_q = \Delta u / q_n$$

Push rods

Thick-walled tubes used to advance the cone penetrometer

Sleeve friction resistance, f_s

The frictional force acting on the friction sleeve, F_s , divided by its surface area, A_s .

$$f_s = F_s / A_s$$

Introduction

The purpose of this guide is to provide a concise resource for the application of the CPT to geotechnical engineering practice. This guide is a supplement and update to the book ‘CPT in Geotechnical Practice’ by Lunne, Robertson and Powell (1997). This guide is applicable primarily to data obtained using a standard electronic cone with a 60-degree apex angle and either a diameter of 35.7 mm or 43.7 mm (10 or 15 cm² cross-sectional area).

Recommendations are provided on applications of CPT data for soil profiling, material identification and evaluation of geotechnical parameters and design. The companion book (Lunne et al., 1997) provides more details on the history of the CPT, equipment, specification, and performance. The companion book also provides extensive background on interpretation techniques. This guide provides only the basic recommendations for the application of the CPT for geotechnical design.

A list of the main references is included at the end of this guide. A more comprehensive reference list can be found in the companion CPT book and the recently listed technical papers. Other technical papers on the CPT can be downloaded from www.cpt-robertson.com and <https://usucger.org/books/>.

Additional details on CPT interpretation are provided in a series of free webinars that can be viewed at:
<https://www.youtube.com/user/GreggCPTWebinars>.
<https://www.greggdrilling.com/resources/webinars/>

The interpretations described in this Guide have been incorporated into easy-to-use CPT-based software (CPeT-IT and CLiq) that can be downloaded from <https://geologismiki.gr/products/>.

Risk Based Site Characterization

Risk and uncertainty are characteristics of the ground and are never fully eliminated. The appropriate level of sophistication for site characterization and analyses should be based on the following criteria:

- Precedent and local experience
- Design objectives
- Level of geotechnical risk
- Potential cost savings

The evaluation of geotechnical risk is dependent on hazards, probability of occurrence and the consequences. Risk is defined as the product of likelihood and consequences and, in basic terms, projects can be classified as either: low, moderate or high risk, depending on the above criteria. Table 1 shows a generalized flow chart to illustrate the likely geotechnical ground investigation approach associated with risk. The level of sophistication in a site investigation is also a function of the project design objectives and the potential for cost savings.

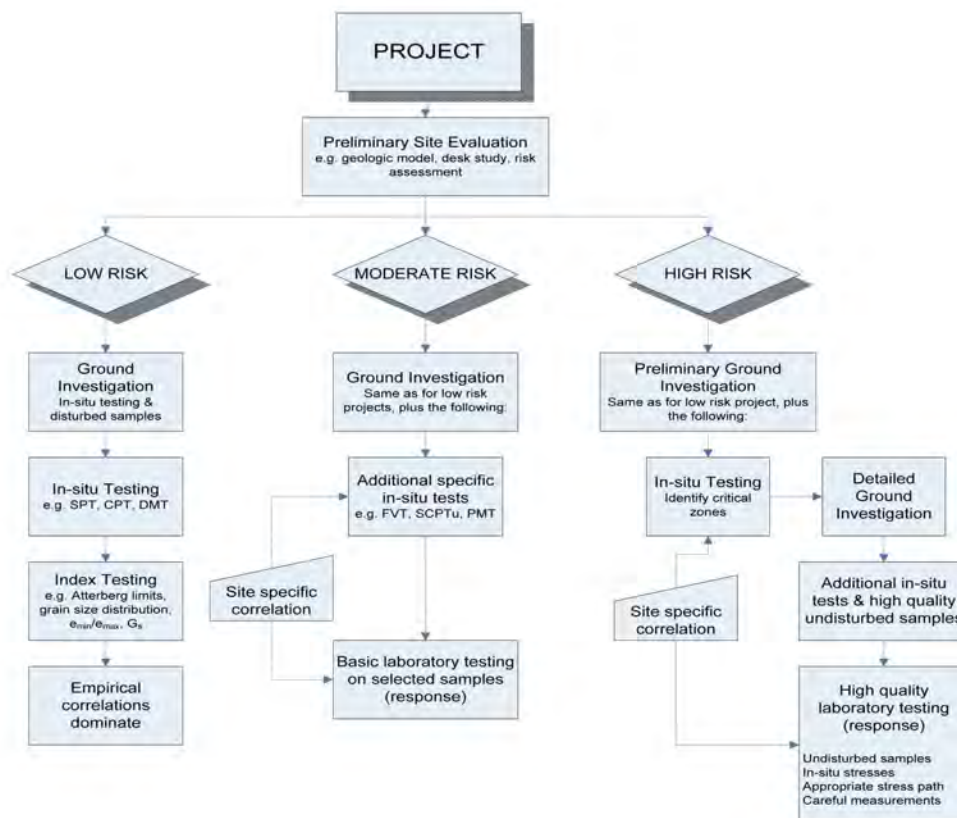


Table 1 Risk-based flowchart for site characterization

Role of the CPT

The objectives of any subsurface investigation are to determine the following:

- Nature and sequence of the subsurface strata (geologic regime)
- Groundwater conditions (hydrologic regime)
- Physical and mechanical properties of the subsurface strata.

For geo-environmental site investigations where contaminants are possible, the above objectives have the additional requirement to determine:

- Distribution and composition of contaminants.

The above requirements are a function of the proposed project and the associated risks. An ideal investigation program should include a mix of field and laboratory tests depending on the risk of the project. Geophysical testing is often an ideal complement to CPT (e.g., surface seismic using MASW).

Table 2 presents a partial list of the major in-situ tests and their perceived applicability for use in different ground conditions.

Group	In-situ Test	Geotechnical Parameter											Ground Type						
		Soil type	Profile	u_0	OCR	$D_{R-\psi}$	ϕ^*	s_u	$G_o - E$	$\sigma-\varepsilon$	$M - C_c$	k	c_v	hard rock	soft rock	gravel	sand	silt/clay	peat-organic
Penetrometer/ Direct Push	Dy. Probing (DP)	C	B	-	C	C	C	C	C	-	-	-	-	-	C	B	A	B	B
	SPT	B	B	-	C	B	C	C	C	-	-	-	-	-	C	B	A	B	B
	CPT	B	A	-	B	B	B	B	B	C	C	C	-	-	B	B	A	A	A
	CPTu	A	A	A	B	A	B	A	B	C	B	A	A	-	B	B	A	A	A
	SCPTu	A	A	A	A	A	B	A	B	B	B	A	A	-	B	B	A	A	A
	DMT	B	B	B	B	C	B	B	B	C	B	C	B	-	C	C	A	A	A
	SDMT	B	B	B	A	B	B	B	A	B	B	C	B	-	C	C	A	A	A
	Full-flow (T-ball)	C	B	B	B	C	C	A	C	C	C	C	C	-	-	C	B	A	A
	Field vane (FVT)	B	C	-	B	-	A	-	-	-	-	-	-	-	-	-	A	B	
Pressuremeter	Pre-bored	B	B	-	C	C	C	B	B	C	C	-	C	A	A	B	B	B	B
	Self-bored	B	B	A ¹	B	B	B	A	A	B	B	A ¹	-	C	-	B	A	B	
	Full-displacement	B	B	B	C	C	C	B	A	A	B	B	A	-	C	-	B	A	A
Other	Screw/plate load	C	-	-	B	C	C	B	B	B	B	C	C	C	A	B	B	B	B
	Borehole shear	C	-	-	-	-	B	C	-	-	-	-	-	C	B	C	C	C	-
	Permeameter	C	-	A	-	-	-	-	-	-	-	A	B	A	A	A	A	B	
	Borehole seismic	C	C	-	B	C	-	-	A	C	-	-	A	A	A	A	A	A	B
	Surface seismic	-	C	-	B	C	-	-	A	C	-	-	A	A	A	A	A	A	A
	Hydraulic fracture	-	-	B	-	-	-	-	-	-	-	C	C	B	B	-	-	B	C

Applicability: A = high, B = moderate, C = low, - = none

Geotechnical parameters: u_0 = in-situ static pore pressure, OCR = over-consolidation ratio, $D_{R-\psi}$ = relative density and/or state parameter, ϕ^* = peak friction angle, s_u = undrained shear strength (peak and/or remolded), $G_o - E$ = small strain shear and/or Young's modulus, $\sigma-\varepsilon$ = stress-strain relationship, $M - C_c$ = constrained modulus and/or compression index, k = permeability, c_v = coefficient of consolidation

ϕ^* will depend on soil type; ¹ only when pore pressure sensor fitted.

Table 2. The applicability and usefulness of in-situ tests
(Lunne, Robertson & Powell, 1997, updated by Robertson, 2012)

The Cone Penetration Test (CPT) and its enhanced versions such as the piezocone (CPTu) and seismic (SCPT), have extensive applications in a wide range of soils. Although the CPT was initially limited mainly to softer soils, with modern pushing equipment and more robust cones, the CPT can be performed in stiff to very stiff soils, and in some cases soft rock.

Advantages of CPT:

- Fast and continuous profiling
- Repeatable and reliable data (independent of operator)
- Economical and productive
- Strong theoretical basis for interpretation
- Significant number of case histories

Disadvantage of CPT:

- Relatively high capital investment
- Requires somewhat skilled/trained operators
- No soil sample, during a CPT
- Penetration can be restricted in some gravel and /or cemented layers

Although it is not possible to obtain a soil sample during a CPT, it is possible to obtain soil samples using CPT direct push equipment. The continuous nature of CPT results provides a detailed stratigraphic profile to guide in selective sampling appropriate for the project. The recommended approach is to first perform several CPT soundings to define the stratigraphic profile and to provide initial estimates of geotechnical parameters, then follow with selective sampling. The type and amount of sampling will depend on the project requirements and geotechnical risks as well as the stratigraphic profile. Typically, sampling will be focused in critical zones for the project, as defined by the CPT, and carried out adjacent to and immediately after a CPT. Testing and interpretation should always be done within a geologic framework.

A variety of push-in discrete depth samplers are available. Most are based on designs like the original Gouda or MOSTAP samplers from the Netherlands. The samplers are pushed to the required depth in a closed position. The Gouda type samplers have an inner cone tip that is retracted to the locked position leaving a hollow sampler with small diameter (typically 25mm/1 inch) stainless steel or brass sample tubes. The hollow sampler is then pushed to collect a sample. The filled sampler and push rods are then retrieved to the ground surface. The

MOSTAP type samplers contain a wire to fix the position of the inner cone tip before pushing to obtain a sample. Modifications have also been made to include a wireline system so that soil samples can be retrieved at multiple depths rather than retrieving and re-deploying the sampler and rods at each interval. The wireline systems tend to work better in soft soils. Figure 1 shows a schematic of typical (Gouda-type) CPT-based soil sampler. The speed of sampling depends on the maximum speed of the pushing equipment but is not limited to the standard 2cm/s used for the CPT. Some specialized CPT trucks can take samples at a rate of up to 40cm/s. Hence, push-in soil sampling can be fast and efficient. In very soft soils, special 800mm (32 in) long push-in piston samplers have been developed to obtain 63mm (2.5 in) diameter essentially undisturbed soil samples.

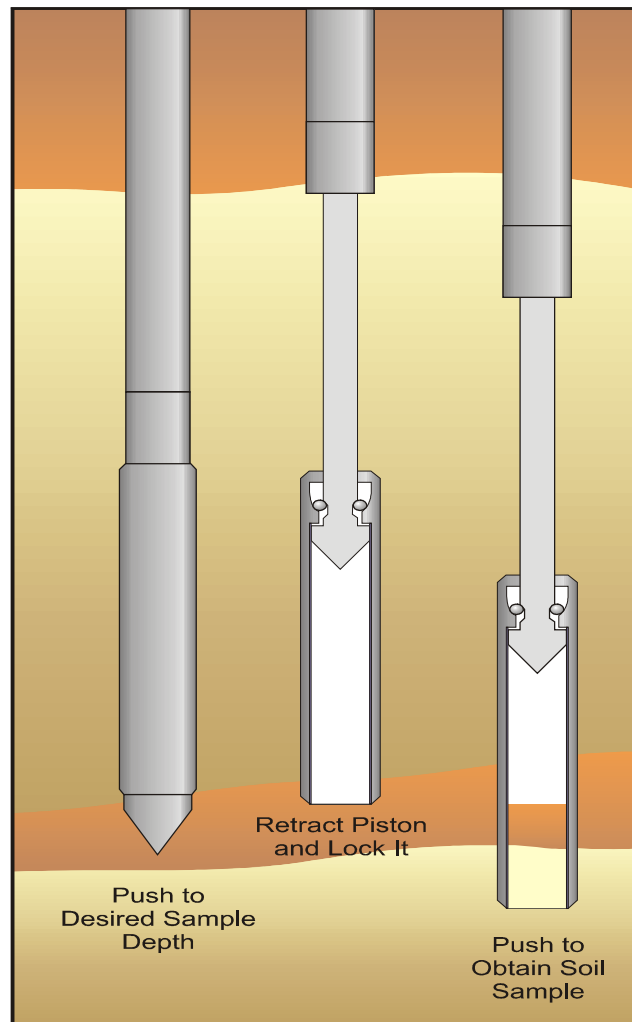


Figure 1. Schematic of simple direct-push (CPT-based) soil sampler
(www.greggdrilling.com)

Cone Penetration Test (CPT)

Introduction

In the Cone Penetration Test (CPT), a cone on the end of a series of rods is pushed into the ground at a constant rate and near-continuous measurements are made of the resistance to penetration of the cone and of a surface sleeve. Figure 2 illustrates the main terminology regarding cone penetrometers.

The total force acting on the cone, Q_c , divided by the projected area of the cone, A_c , produces the cone resistance, q_c . The total force acting on the friction sleeve, F_s , divided by the surface area of the friction sleeve, A_s , produces the sleeve resistance, f_s . In a *piezocene*, pore pressure is also measured, typically behind the cone in the u_2 location, as shown in Figure 2. If pore pressures are measured on the face of the cone, it is the u_1 location. Some cones can measure both u_1 and u_2 pore pressures simultaneously.

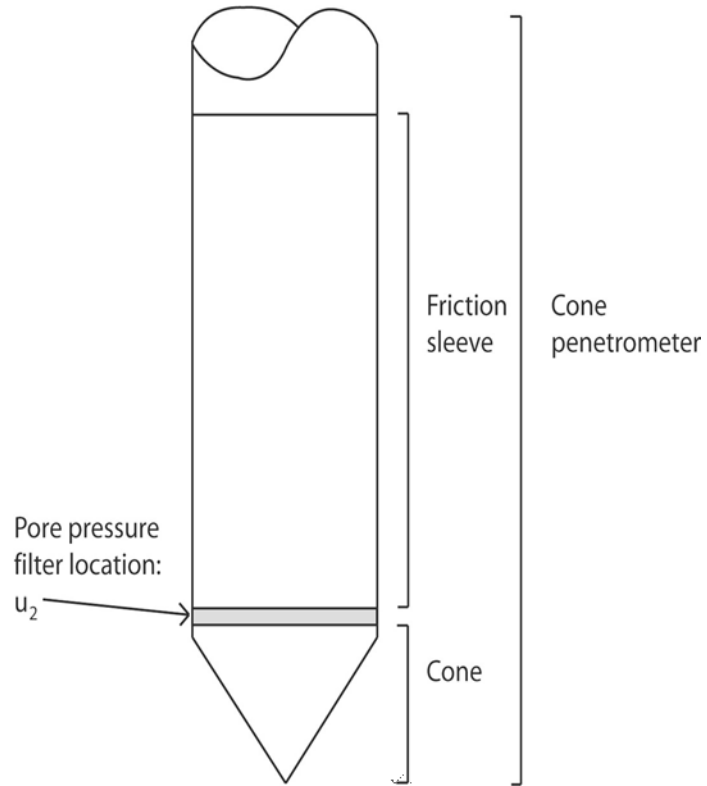


Figure 2. Terminology for cone penetrometers

History

1932

The first cone penetrometer tests were made using a 35 mm outside diameter gas pipe with a 15 mm steel inner push rod. A cone tip with a 10 cm^2 projected area and a 60° apex angle was attached to the steel inner push rods, as shown in Figure 3.

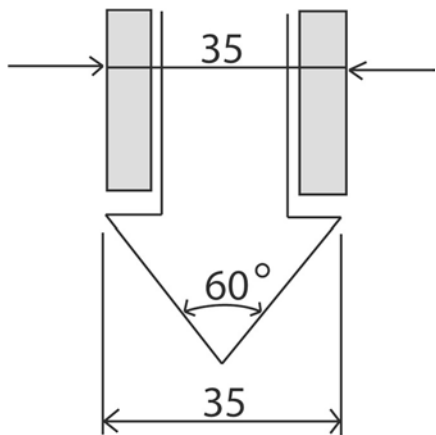


Figure 3. Early Dutch mechanical cone (after Sanglerat, 1972)

1935

Delft Soil Mechanics Laboratory designed the first manually operated 10ton (100kN) cone penetration push machine, see Figure 4.

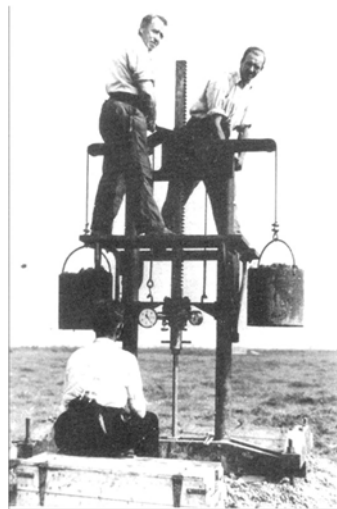


Figure 4. Early Dutch mechanical cone (after Delft Geotechnics)

1948

The original Dutch mechanical cone was improved by adding a conical part just above the cone. The purpose of the geometry was to prevent soil from entering the gap between the casing and inner rods. The basic Dutch mechanical cones, shown in Figure 5, are still in use in some parts of the world.

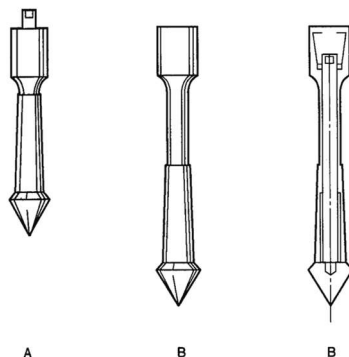


Figure 5. Dutch mechanical cone penetrometer with conical mantle

1953

A friction sleeve ('adhesion jacket') was added behind the cone to include measurement of the local sleeve resistance (Begemann, 1953), see Figure 6. Measurements were made every 20 cm, (8 inches) and for the first time, friction ratio was used to classify soil type (see Figure 7).

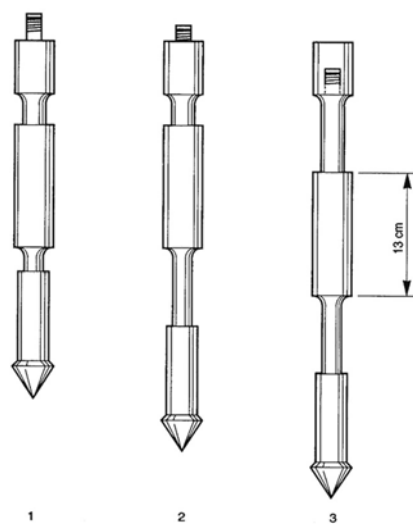


Figure 6. Begemann type cone with friction sleeve

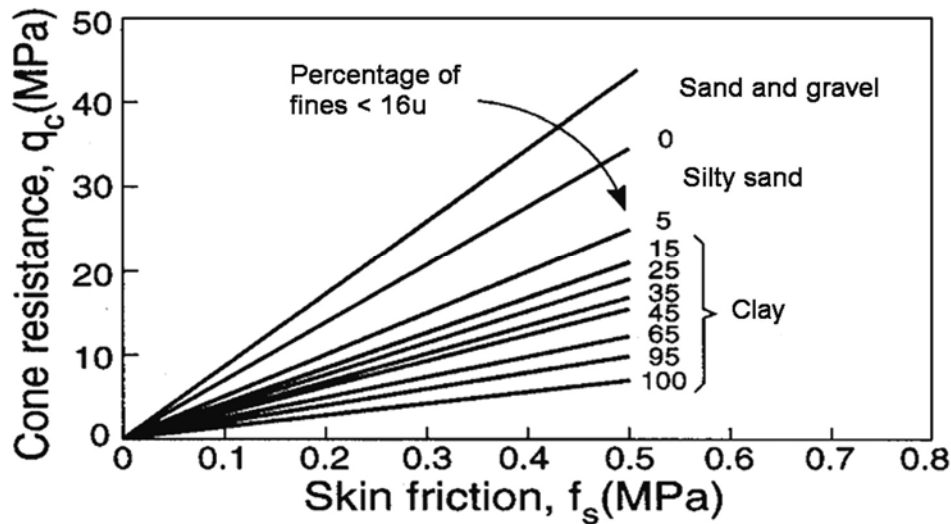


Figure 7. First CPT-based soil classification for Begemann mechanical cone

1965

Fugro developed an electric cone, of which the shape and dimensions formed the basis for the modern cones and the International Standard and ASTM procedure. The main improvements relative to the mechanical cone penetrometers were:

- Elimination of incorrect readings due to friction between inner rods and outer rods and weight of inner rods.
- Continuous testing with continuous rate of penetration without the need for alternate movements of different parts of the penetrometer and no undesirable soil movements influencing the cone resistance.
- Simpler and more reliable electrical measurement of cone resistance and sleeve friction resistance.

1974

Cone penetrometers that could also measure pore pressure (*piezocones*) were introduced. Early designs had various shapes and pore pressure filter locations. Gradually the practice has become more standardized so that the recommended position of the filter element is close behind the cone at the u_2 location. With the measurement of pore water pressure, it became apparent that it was necessary to correct the cone resistance for pore water pressure effects (q_t), especially in soft clay.

Test Equipment and Procedures

There are several elements in a CPT ranging from the probe and sensing elements to the delivery and deployment systems.

Cone Penetrometers

Cone penetrometers come in a range of sizes with the 10 cm^2 and 15 cm^2 probes the most common and specified in most standards. Figure 8 shows a range of cones from a mini cone at 2 cm^2 to a large cone at 40 cm^2 . The mini cones are used for shallow investigations, whereas the large cones can be used in gravelly soils.



Figure 8. Range of CPT probes (from left: 2 cm^2 , 10 cm^2 , 15 cm^2 , 40 cm^2)

Additional Sensors/Modules

Since the introduction of the electric cone in the early 1960's, many additional sensors have been added to the cone, such as:

- Temperature
- Geophones/accelerometers (seismic wave velocities, V_s and V_p)
- Pressuremeter (cone pressuremeter)
- Camera (visible light)
- Radioisotope (gamma/neutron)
- Electrical resistivity/conductivity
- Dielectric
- pH
- Oxygen exchange (redox)
- Laser/ultraviolet induced fluorescence (LIF/UVOST)
- Membrane interface probe (MIP)

The latter items are primarily for geo-environmental applications.

One of the more common additional sensors is a geophone or accelerometer to allow the measurement of seismic wave velocities. A schematic of the seismic CPT (SCPT) procedure is shown in Figure 9.

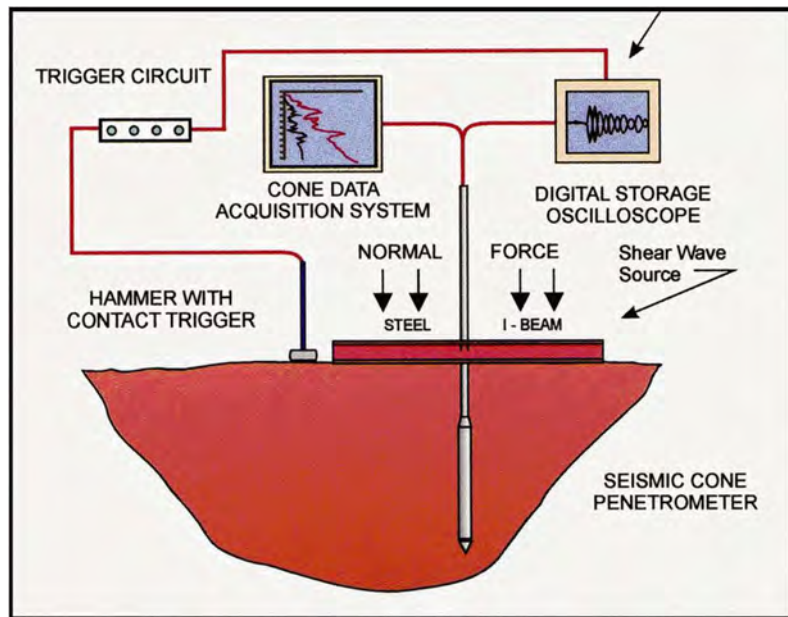


Figure 9. Schematic of Seismic CPT (SCPT) test procedure

Delivery systems

The CPT equipment can reach a location using a wide range of delivery systems.

On Land

Delivery systems for land (onshore) applications generally consist of specially built units that are either wheeled or track mounted as well as a wide range of anchored systems. Figures 10 to 13 show a range of on shore delivery systems.



Figure 10. Truck mounted 250kN (25 ton) CPT unit



Figure 11. Track mounted 200kN (20 ton) CPT unit



Figure 12. Small, anchored drill-rig unit



Figure 13. Portable ramset for CPT inside buildings or limited access



Figure 14. Mini CPT system with coiled rod delivery attached to small track mounted auger rig

Over Water

There are a variety of delivery systems for over water investigations depending on the depth of water. Floating or jack-up barges are common in shallow water (depth less than 30m/100 ft), see Figures 15 and 16.



Figure 15. Mid-size jack-up boat



Figure 16. Quinn Delta (Gregg) ship with spuds

In deeper water offshore (>100m, 350ft) it is common to place the CPT delivery systems on the seafloor using specially designed underwater systems, such as shown in Figure 17. Seabed systems can push full size cones ($10\text{ and }15\text{cm}^2$ cones) and smaller systems for mini cones ($2\text{ and }5\text{cm}^2$ cones) using continuous pushing systems. Rods can be connected before lowering to the seafloor and supported via a tension system or support tower, or a coiled tubing system can be straightened and pushed into the soil as the cone is advanced into the subsurface.



Figure 17. Seafloor CPT systems for pushing full size cones in deep water (ranging from 1500-4,000 msw) Clockwise from left: 1st Generation Gregg Marine Seabed CPT, a. p. van den berg ROSON system, 2nd Generation Gregg Marine coiled tubing CPT.

It is also possible to push the CPT from the bottom of a borehole using down-hole equipment. The advantage of down-hole CPT in a drilled borehole is that much

deeper penetration can be achieved and hard layers can be drilled through. Down-hole methods can be applied both on-shore and off-shore. Recently, remotely controlled seabed drill rigs have been developed that can drill and sample and push CPT in up to 4,000m (13,000 ft) of water (e.g., Lunne, 2010).

Deployment Systems

Deployment of the cone penetrometer into the ground is usually done using a hydraulic pushing system. For onshore systems it is common that the push rods are 1m in length and are connected after each push by an operator. This has traditionally meant that there is a short pause after each 1m push to add another rod. Recently there are several systems designed to provide continuous pushing. One system is a trademarked ‘SingleTwist’ rod connection system that allows a coiled string of short rods to be stored and quickly assembled by robotics. The rods require only a 1/6th turn to become rigidly connected for deployment. An alternate system is a coiled tubing system where the rods are coiled and straightened when passing through the continuous pushing system.

Robotic delivery and deployment systems also allow for unmanned remotely operated systems.



Figure 18. Gregg's Bumblebee remotely controlled, un-manned CPT system with 5cm² cone and coiled tubing

Depth of Penetration

CPT's can be performed to depths exceeding 100m (300ft) in soft soils and with large capacity pushing equipment. To improve the depth of penetration, the friction along the push rods should be reduced. This can be done using an expanded coupling (i.e., friction reducer) a short distance, typically 0.5m (1.5ft), behind the cone. Penetration will be limited if very hard soils, gravel layers or rock are encountered. It is common in North America to use 15cm² cones to increase penetration depth, since 15cm² cones are more robust and have a slightly larger diameter than the standard 10cm² push rods, hence there is no need for an additional friction reducer. The push rods can also be lubricated with drilling mud to remove rod friction for deep soundings. Depth of penetration can also be increased using down-hole techniques with a drill rig including wire-line CPT systems.

CPT systems have also been added to sonic drill rigs so that standard CPT can be performed using the drill rig. If hard layers are encountered, vibrations from the sonic drill head can be activated to aid penetration through the hard layer. After penetration through the hard layer, standard (no vibrations) CPT can be resumed. For CPT using sonic rigs, the basic cones are more robust to withstand the high acceleration from the high frequency vibrations.

Test Procedures

Pre-drilling

For penetration through coarse-grained fill or hard soil, it may be necessary to pre-drill to avoid damaging the cone. Pre-drilling, in certain cases, may be replaced by first pre-punching a hole through the upper problem material with a solid steel 'dummy' probe with a diameter slightly larger than the cone. It is also common to hand auger the first 1.5m (5ft) in urban areas to avoid underground utilities.

Verticality

The thrust machine should be set up to obtain a thrust direction as near as possible to vertical. The deviation of the initial thrust direction from vertical should not exceed 2 degrees and push rods should be checked for straightness. Modern cones have simple slope sensors incorporated to enable a measure of the non-verticality of the sounding. This is useful to avoid damage to equipment and breaking of push rods. For depths less than 15m (50ft), significant non-verticality

is unusual, provided the initial thrust direction is vertical. Non-vertical CPTs have also been carried out for special projects (e.g., inside tunnels).

Reference Measurements

Modern cones have the potential for a high degree of accuracy and repeatability (~0.1% of full-scale output, FSO). Tests have shown that the output of the sensors at zero load can be sensitive to changes in temperature, although most cones now include some temperature compensation. It is common practice to record zero load readings of all sensors to track these changes. Zero load readings should be monitored and recorded (in engineering units) at the start and end of each CPT and is required practice in most standards.

Rate of Penetration

The standard rate of penetration is 2cm/s (approximately 0.8in/s). Hence, a 20m (60ft) sounding can be completed (start to finish) in about 30 minutes. In coarse-grained soils, such as sand, the standard cone penetration is essentially fully drained and in fine-grained soils, such as clay, the penetration is essentially fully undrained. Hence, the measurements are generally not sensitive to slight variations in rate of penetration. However, in some soils, such as silt, the standard penetration may occur under partially drained conditions.

Interval of readings

Electric cones produce continuous analogue data. However, most systems convert the data to digital form at selected intervals. Most standards require the interval to be no more than 200mm (8in). In general, most systems collect data at intervals of between 10 to 50mm, with 20 mm (~1in) becoming the most common.

Dissipation Tests

During a pause in penetration, any excess pore pressure generated around the cone will start to dissipate. The rate of dissipation depends upon the coefficient of consolidation, which in turn, depends on the compressibility and permeability of the soil. The rate of dissipation also depends on the diameter of the probe. A dissipation test can be performed at any required depth by stopping the penetration and measuring the change of pore pressure with time. It is common to record the time to reach 50% dissipation (t_{50}), as illustrated in Figure 19.

If the equilibrium pore pressure (u_e) is required, the dissipation test should continue until no further dissipation is observed, as shown in Figure 19. This can

occur rapidly in sands, but may take many hours in plastic clays. Dissipation rate also increases as probe size decreases.

In soft, contractive clay, it is common to record large positive penetration pore pressures that decay with time toward the equilibrium pressure (u_o). In very stiff clay and dense silty sand, the penetration pore pressures can be negative of u_o due to the dilative nature of the soil and pore pressures will increase toward equilibrium during a dissipation test. At shallow depth, it is possible to measure penetration pore pressures that are below zero, where the shear induced pore pressures due to dilation exceed u_o and negative pore pressures are recorded up to a maximum of -1 atmosphere (~-100kPa or -15psi). Penetration pore pressures approaching -1 atmosphere can result in cavitation of the sensor fluid (i.e., small air bubbles) for onshore CPT causing the sensor to become unsaturated. During the dissipation test any small air bubbles caused by cavitation can go back into solution to regain full saturation of the sensor.

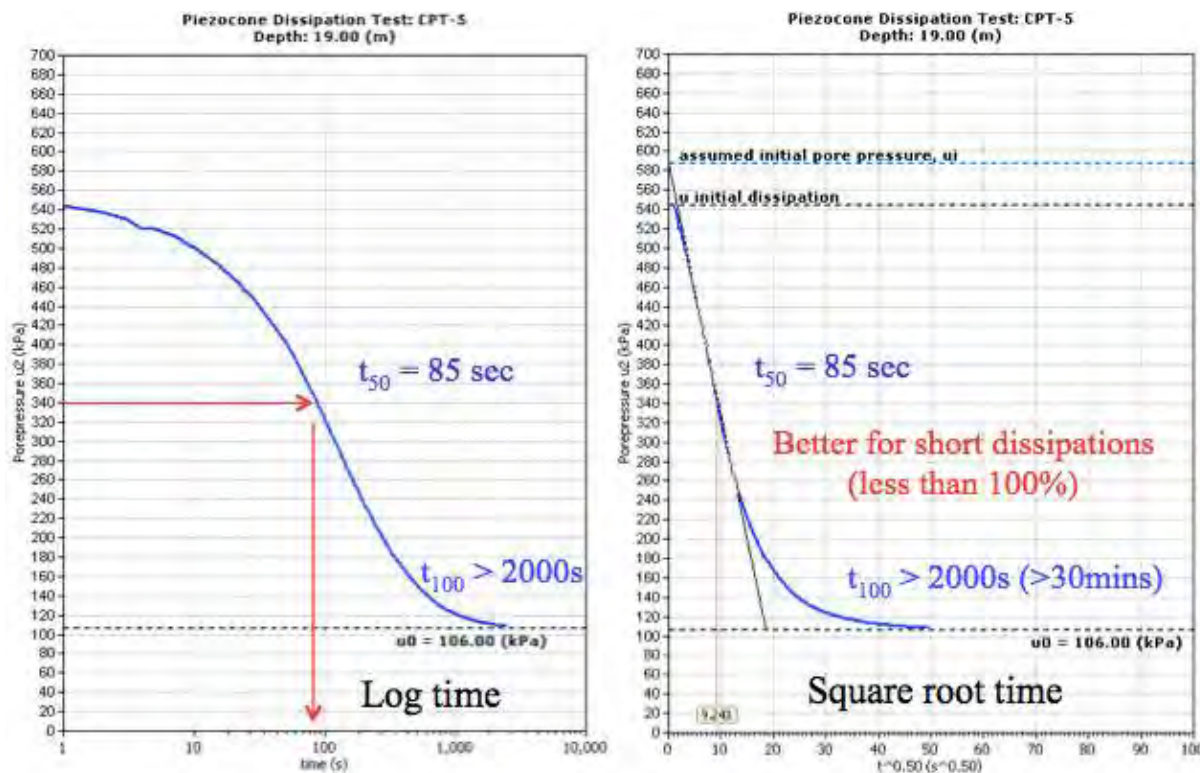


Figure 19. Example dissipation test to determine t_{50} and u_o .

Calibration and Maintenance

Calibrations should be carried out at intervals based on the stability of the zero load readings. Typically, if the zero load readings remain stable, the load cells do not require a check calibration. For major projects, check calibrations may be carried out before and after the field work, with functional checks during the work. Functional checks should include recording and evaluating the zero load measurements (baseline readings).

With careful design, calibration, and maintenance, strain gauge load cells and pressure transducers can have an accuracy and repeatability of better than +/- 0.1% of full-scale output (FSO).

Table 3 shows a summary of checks and recalibrations for the CPT.

<i>Maintenance</i>	<i>Start of Project</i>	<i>Start of Test</i>	<i>End of Test</i>	<i>End of Day</i>	<i>Once a Month</i>	<i>Every 3 months*</i>
<i>Wear</i>	x	x			x	
<i>O-ring seals</i>	x			x		
<i>Push-rods</i>		x			x	
<i>Pore pressure-filter</i>	x	x				
<i>Calibration</i>						x*
<i>Computer</i>					x	
<i>Cone</i>					x	
<i>Zero-load</i>		x	x			
<i>Cables</i>	x				x	

Table 3 Summary of checks and recalibrations for the CPT

*Note: recalibrations are normally carried out only when the zero-load readings drift outside manufacturers recommended range

Cone Design

Penetrometers use strain gauge load cells to measure the resistance to penetration. Basic cone designs use either separate load cells or subtraction load cells to measure the tip resistance (q_c) and sleeve resistance (f_s). In subtraction cones the sleeve friction is derived by ‘subtracting’ the tip load from the tip + friction load. Figure 20 illustrates the general principle behind load cell designs using either separated load cells or subtraction load cells.

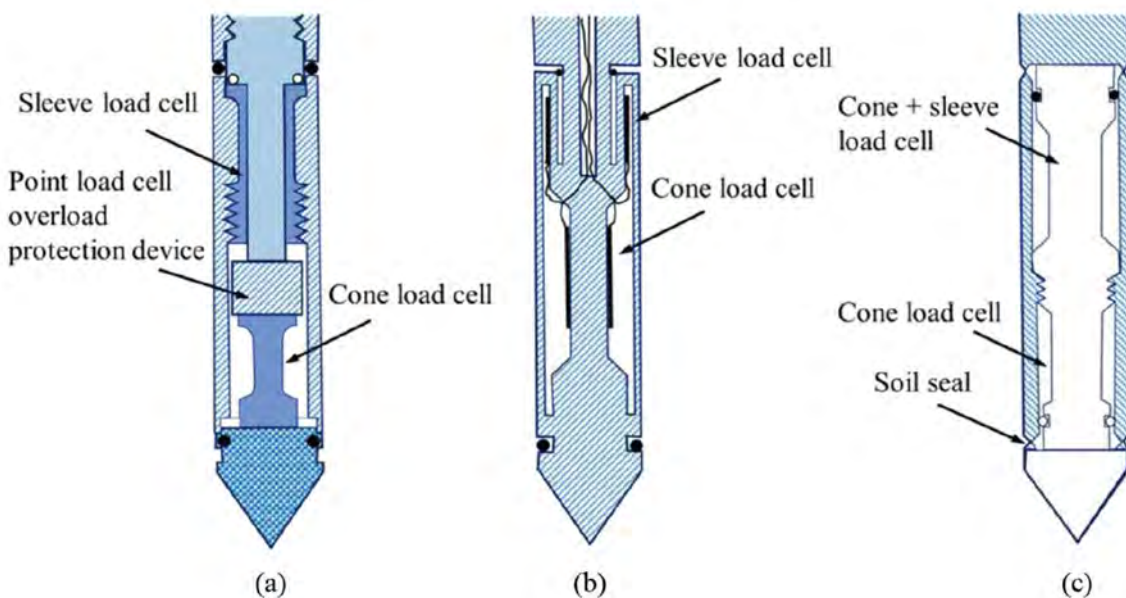


Figure 20. Designs for cone penetrometers (a) tip and sleeve load cells in compression, (b) tip load cell in compression and sleeve load cell in tension, (c) subtraction type load cell design (modified from Lunne et al., 1997)

In the 1980's subtraction cones became popular because of improved overall robustness of the penetrometer. However, in soft soils, subtraction cone designs suffer from a lack of accuracy in the determination of sleeve resistance due primarily to variable zero load stability of the two load cells. In subtraction cone designs, different zero load errors for each load cell can produce cumulative errors in the derived sleeve resistance values. For accurate sleeve resistance measurements in soft sediments, it is recommended that cones have separate (compression) load cells.

With good design (separate load cells, equal end area friction sleeve) and quality control (zero load measurements, tolerances, and surface roughness) it is possible to obtain very repeatable tip and sleeve resistance measurements. However, f_s measurements, in general, will be less accurate than tip resistance, q_c , especially in soft sensitive fine-grained soils, where the sleeve resistance values can be smaller than the accuracy of some cones (e.g., $f_s < 5\text{kPa}$). In soft soils, cones with smaller capacity (i.e., smaller FSO) can be used for improved accuracy.

Pore pressure (water) effects

Due to the inner geometry of the cone the ambient water pressure acts on the shoulder behind the cone and on the ends of the friction sleeve. This effect is often referred to as the unequal end area effect (Campanella et al., 1982). Figure 21 illustrates the key features for water pressure acting behind the cone and on the end areas of the friction sleeve. In soft clays and silts and in over water work, the measured q_c must be corrected for pore water pressures acting on the cone geometry, thus obtaining the corrected cone resistance, q_t :

$$q_t = q_c + u_2 (1 - a)$$

Where 'a' is the net area ratio determined from laboratory calibration with a typical value between 0.70 and 0.85. In sandy soils $q_c = q_t$ due to higher values of q_c and smaller values of u_2 .

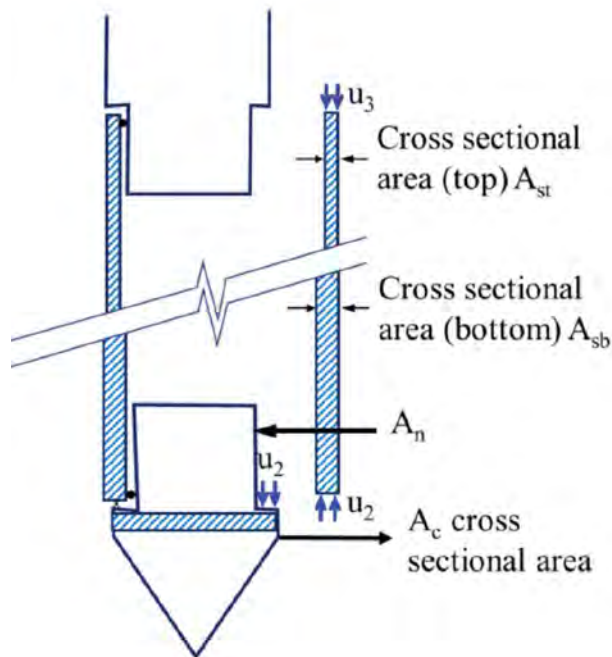


Figure 21. Unequal end area effects on cone tip and friction sleeve

A similar correction should be applied to the sleeve resistance.

$$f_t = f_s - (u_2 A_{sb} - u_3 A_{st}) / A_s$$

where:

- f_s = measured sleeve resistance
- u_2 = water pressure at base of sleeve
- u_3 = water pressure at top of sleeve
- A_s = surface area of sleeve
- A_{sb} = cross-section area of sleeve at base
- A_{st} = cross-sectional area of sleeve at top

However, most standards require that cones have an equal end area friction sleeve (i.e., $A_{st} = A_{sb}$) that reduces the need for such a correction. For 15cm² cones, where A_s is large compared to A_{sb} and A_{st} , (and $A_{st} = A_{sb}$) the correction is generally very small. All cones should have equal end area friction sleeves to minimize the effect of water pressure on the sleeve resistance measurements. Careful monitoring of the zero load readings is also required.

For deeper overwater CPTs, it is common to record the zero load readings at the mudline line (soil surface) since the effective stress at the mudline is always zero. For some shallow over water work the zero load readings are sometimes taken at the water surface. In this case, the cone will record readings through the water which can be helpful to identify when soil is encountered. In some cases, there can be a transition from heavy mud to a soil boundary. When interpreting overwater CPT data, it is important to know where the zero load readings were made to ensure that the calculated effective stress is zero at the mudline.

In the offshore industry, where CPT can be carried out in very deep water (> 1,000m), cones are sometimes compensated (filled with oil) so that the pressure inside the cone is equal to the hydrostatic water pressure outside the cone. For compensated cones the correction for cone geometry to obtain q_t is slightly different than shown above, since the cone can automatically record zero q_c at the mudline.

CPT Interpretation

Numerous semi-empirical correlations have been developed to estimate geotechnical parameters from the CPT for a wide range of soils. Most correlations have some theoretical framework but remain semi-empirical due to the complex behavior of most natural soils. These correlations vary in their reliability and applicability. Because the CPT has additional sensors (e.g., pore pressure, CPTu and seismic, SCPT), the applicability to estimate soil parameters varies. Since CPT with pore pressure measurements (CPTu) is commonly available, Table 4 shows an estimate of the perceived applicability of the CPTu to estimate soil parameters. If seismic (V_s) is added, the ability to estimate soil stiffness (E, G & G_0) is further improved.

Soil Type	D_r	Ψ	K_o	OCR	S_t	s_u	ϕ'	E, G*	M	G_0^*	k	c_h
Coarse-gained (sand-like)	2-3	2-3	5	5			2-3	2-3	2-3	2-3	3-4	3-4
Fine-grained (clay-like)			2	1	2	1-2	4	2-4	2-3	2-4	2-3	2-3

Table 4 Perceived applicability of CPTu for deriving soil parameters
 1=high, 2=high to moderate, 3=moderate, 4=moderate to low, 5=low reliability, Blank=no applicability, * improved with SCPT

Where:

D_r	Relative density	ϕ'	Peak friction angle
Ψ	State Parameter	K_o	In-situ stress ratio
E, G	Young's and Shear moduli	G_0	Small strain shear moduli
OCR	Over consolidation ratio	M	1-D Compressibility
s_u	Undrained shear strength	S_t	Sensitivity
c_h	Coefficient of consolidation	k	Permeability

Most semi-empirical correlations apply primarily to young, uncemented, predominately silica-based soils that have little to no microstructure.

A major advantage of using the SCPTu is that it can make 6 to 7 measurements in one sounding (q_t , f_s , u_2 , V_s (V_p), t_{50} , u_o). These multiple measurements provide an improved understanding of the soil behavior and groundwater conditions. There is no other in-situ test that can provide this level of information in a near-continuous and cost-effective manner.

Groundwater Conditions and Piezometric Profile

Soil behavior is controlled by the in-situ effective stresses and knowledge of the groundwater conditions is important to determine the correct in-situ effective stresses. The CPTu provides detailed information on soil behavior including the pore pressure (piezometric) profile. If dissipation tests are performed, the resulting equilibrium pore pressure (u_o) measurements provide an opportunity to define the piezometric profile at the time of the CPT.

It is often assumed that groundwater conditions are hydrostatic. However, this is not always the case, especially in sloping ground or close to an embankment, where downward (lateral) flow is common, as well as near lakes and rivers, where upward flow is common. In conditions of downward flow, the piezometric profile will be less than hydrostatic and in conditions of upward flow, the piezometric profile will be greater than hydrostatic and can result in artesian conditions. When piezometric conditions are non-hydrostatic it is important to perform multiple dissipation tests to better define the piezometric profile. Since dissipation to equilibrium (u_o) can be time consuming in some fine-grained clay layers, it is preferred, if possible, to perform dissipation tests in coarse-grained sand and silt layers, where possible, since u_o can be obtained quickly. However, frequent dissipation tests can also influence the penetration (dynamic) pore pressures that can then influence interpretation. In low permeability clay layers the CPT penetration pore pressures (u_2) can respond rapidly and penetration will be undrained early in the penetration. However, in more permeable silt layers, it can take some penetration depth (e.g., up to 1m) to achieve full undrained conditions and frequent dissipation tests may reduce the ability to achieve these undrained conditions during cone penetration. Ideally, under these conditions, it is preferred to perform a standard CPTu with no dissipations (and with rapid rod additions if using incremental 1m push rods) followed by an adjacent CPTu where frequent dissipation tests are performed to determine the correct piezometric profile. If the 2nd sounding includes seismic measurements (SCPT) then frequent stops/pauses are required to make the seismic measurements and it can be helpful to also record the dissipation data during these stops/pauses. It is more common to perform a single CPTu sounding with a small number (e.g., 3 or 4) dissipation tests, as a

compromise between achieving undrained conditions where appropriate and determining the approximate piezometric profile.

There can be conditions, such as in mine tailings, where there is ongoing deposition of tailings and water at the surface, combined with strong downward flow. It is possible that any fine tailings, with high air entry values, are saturated, but dissipation tests indicate little or no equilibrium pressures (i.e., $u_o \sim 0$) due to the strong downward flow. In this case, it is incorrect to assume that the tailings are unsaturated with no groundwater. It is more correct to assume that the phreatic surface is at the ground surface (consistent with observed surface water from ongoing tailings deposition) but with strong downward flow such that $u_o \sim 0$. Likewise, it is possible that interlayered tailings (alternate sand and silt layers) can indicate that the sand tailings maybe essentially unsaturated (due to a small air entry value), with slightly negative CPT penetration pore pressures ($u_2 < 0$) but the finer silt tailings are either saturated or close to saturated with large positive penetration positive CPT pore pressures ($u_2 > 0$). Near saturated fine-grained soils can be expected to behave similar to saturated soils in undrained shear. Fine grained soils have high air entry values and can remain essentially saturated (saturation > 85%) even under conditions when u_o is close to zero.

Soil Profiling and Soil Classification

One of the major applications of the CPT is for *soil profiling and soil classification*. Typically, the cone resistance, (q_t) is high in sands and low in clays, and the friction ratio ($R_f = f_s/q_t$) is low in sands and high in clays (see Figure 7). Traditional soil classification systems (e.g., USCS) are based on laboratory determined *physical characteristics*, such as, grain size distribution and plasticity that are measured on remolded samples. CPT measurements respond to in-situ *mechanical behavior* of the soil, such as, strength, stiffness, and compressibility. The CPT measurements provide a repeatable index of the aggregate behavior of the in-situ soil in the immediate area of the probe. Hence, the prediction of soil type based on CPT measurements is referred to as the ***Soil Behavior Type (SBT)***.

Non-Normalized SBT Charts

The most used CPT soil behavior type (SBT) chart was suggested by Robertson et al. (1986), and the updated, dimensionless version (Robertson, 2010) is shown in Figure 22. This chart uses the basic CPT parameters of cone resistance, q_t and friction ratio, $R_f = (f_s/q_t)100\%$. The chart is global in nature and can provide reasonable predictions of SBT for CPT soundings up to about 20m (60ft) in depth. Overlap in some zones should be expected and the zones can be modified

somewhat based on local experience. The non-normalized SBT chart (Fig. 22) is often used real-time during the CPT to identify the basic soil types, since it uses measured q_c and f_s .

Normalized SBT_n Charts

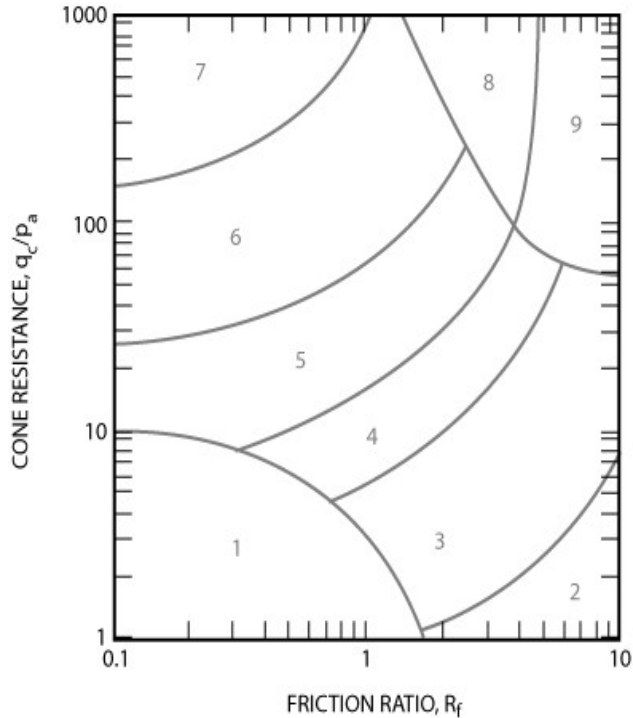
Since both the penetration resistance (q_c) and sleeve resistance (f_s) increase with depth due to the increase in effective overburden stress, the CPT data requires normalization for overburden stress to remove the influence of depth.

A popular CPT soil behavior chart based on normalized CPT data is that first proposed by Robertson (1990) and shown in Figure 23. The linear normalization suggested by Wroth (1984) was used:

$$Q_t \text{ or } Q_{t1} = (q_t - \sigma'_{vo}) / \sigma'_{vo}$$

$$F_r = 100 (f_s / (q_t - \sigma'_{vo})) \%$$

As a reference, included on the SBT chart are lines of normalized friction resistance (f_s/σ'_{vo}). The line for $f_s/\sigma'_{vo} = 0.01$ represents the approximate lower limit of accuracy for most cones and the line for $f_s/\sigma'_{vo} = 10$ represents the approximate upper limit of capacity for most cones. Most CPT data in normally to lightly overconsolidated soils with little or no microstructure plot in the central region between $0.1 < f_s/\sigma'_{vo} < 1.0$. The chart is also global in nature and provides only a guide to soil behavior type (SBT). Overlap in some zones should be expected and the zones can be modified somewhat based on local experience.

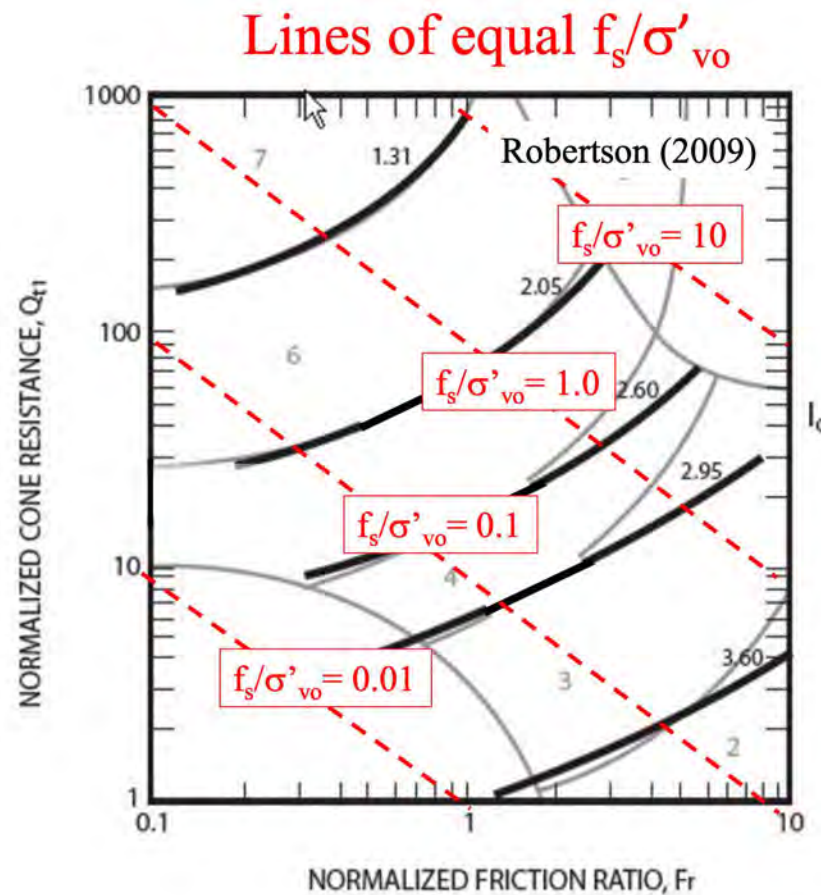


<i>Zone</i>	<i>Soil Behavior Type</i>
1	Sensitive, fine grained
2	Organic soils - clay
3	Clay – silty clay to clay
4	Silt mixtures – clayey silt to silty clay
5	Sand mixtures – silty sand to sandy silt
6	Sands – clean sand to silty sand
7	Gravelly sand to dense sand
8	Very stiff sand to clayey sand*
9	Very stiff fine grained*

* Heavily overconsolidated or cemented

P_a = atmospheric pressure = 100 kPa = 1 tsf

Figure 22. Non-normalized CPT Soil Behavior Type (SBT) chart (Robertson et al., 1986, updated by Robertson, 2010).



<i>Zone</i>	<i>Soil Behavior Type</i>	I_c
1	<i>Sensitive, fine grained</i>	N/A
2	<i>Organic soils – clay</i>	> 3.6
3	<i>Clays – silty clay to clay</i>	2.95 – 3.6
4	<i>Silt mixtures – clayey silt to silty clay</i>	2.60 – 2.95
5	<i>Sand mixtures – silty sand to sandy silt</i>	2.05 – 2.6
6	<i>Sands – clean sand to silty sand</i>	1.31 – 2.05
7	<i>Gravelly sand to dense sand</i>	< 1.31
8	<i>Very stiff sand to clayey sand*</i>	N/A
9	<i>Very stiff, fine grained*</i>	N/A

* Heavily overconsolidated or cemented

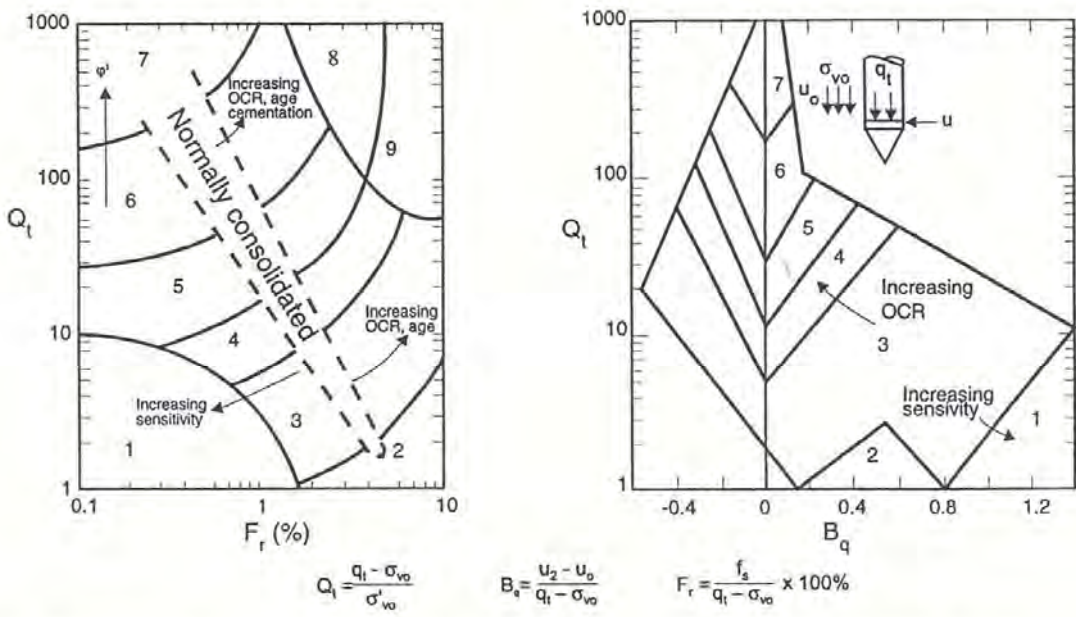
Figure 23. Normalized CPT Soil Behavior Type (SBT_n) chart, Q_t - F_r that include contours of SBT_n Index, I_c (Modified from Robertson, 1990 and Robertson, 2009).

The full normalized SBT_n charts suggested by Robertson (1990) also included an additional chart based on normalized pore pressure parameter, B_q, as shown on Figure 24, where:

$$B_q = \Delta u / q_n$$

and excess pore pressure, $\Delta u = u_2 - u_0$
 net cone resistance, $q_n = q_t - \sigma_{vo}$

The Q_t – B_q chart can aid in the identification of soft, saturated fine-grained soils where excess CPT penetration pore pressures can be large. In general, the Q_t - B_q chart is not always used for onshore CPT due to the sometimes lack of repeatability of the pore pressure results (e.g., poor saturation or loss of saturation of the filter element, etc.).



Zone	Soil behaviour type
1.	Sensitive, fine grained;
2.	Organic soils-peats;
3.	Clays-clay to silty clay;

Zone	Soil behaviour type
4.	Silt mixtures clayey silt to silty clay
5.	Sand mixtures; silty sand to sand silty
6.	Sands: clean sands to silty sands

Zone	Soil behaviour type
7.	Gravelly sand to sand;
8.	Very stiff sand to clayey sand
9.	Very stiff fine grained

Figure 24. Normalized CPT Soil Behavior Type (SBT_n) charts
 Q_t – F_r and Q_t - B_q (after Robertson, 1990).

If no prior CPT experience exists in a geologic environment, it is advisable to obtain samples from appropriate locations to verify the soil type. However, keep in mind that traditional classification systems based on samples are not the same as the CPT-based SBT and difference can occur. If significant CPT experience, within a geology environment, is available and the charts have been evaluated based on this experience, frequent sampling may not be required.

Soil behavior type can be improved if pore pressure measurements are also collected, as shown on Figure 24. In soft clays and silts the penetration pore pressures can be very large, whereas, in stiff heavily over-consolidated clays or dense silts and silty sands the penetration pore pressures (u_2) can be small and sometimes negative relative to the equilibrium pore pressures (u_0). The rate of pore pressure dissipation during a pause in penetration can also guide in the soil type. In sand and silt soils any excess CPT pore pressures will dissipate very quickly ($t_{50} < 60\text{s}$), whereas, in clay the rate of dissipation can be very slow ($t_{50} > 600\text{s}$).

To simplify the application of the CPT-based SBT_n chart shown in Figure 23, the normalized cone parameters Q_t and F_r can be combined into a Soil Behavior Type index, I_c , where I_c is the radius of the essentially concentric circles that represent the boundaries between each SBT_n zone. I_c can be defined as follows:

$$I_c = ((3.47 - \log Q_t)^2 + (\log F_r + 1.22)^2)^{0.5}$$

where:

$$\begin{aligned} Q_t &= \text{normalized cone penetration resistance (dimensionless)} \\ &= (q_t - \sigma'_{vo})/\sigma'_{vo} \\ F_r &= \text{normalized friction ratio, in \%} \\ &= (f_s/(q_t - \sigma_{vo})) \times 100\% \end{aligned}$$

The term Q_t represents the simple normalization with a stress exponent (n) of 1.0, which applies well to clay-like soils. Robertson (2009) suggested that the normalized SBT_n charts shown in Figures 23 and 24 should be used with the normalized cone resistance (Q_{tn}) calculated using a stress exponent (n) that varies with soil type via I_c (i.e., Q_{tn} , see Figure 48 for full details).

The approximate boundaries of soil behavior types are then given in terms of the SBT_n index, I_c , as shown in Figure 23. The soil behavior type index does not apply to zones 1, 8 and 9. Profiles of I_c provide a simple guide to the continuous variation of soil behavior type in each soil profile based on CPT results.

Independent studies have shown that the normalized SBT_n chart shown in Figure 23 typically has greater than 80% reliability when compared with samples. Differences are often due to the presence of soil microstructure (such as aging and bonding).

Schneider et al (2008) proposed a CPT-based soil type chart based on normalized cone resistance (Q_t) and normalized excess pore pressure ($U_2 = \Delta u_2 / \sigma'_{vo}$). Application of the Schneider et al chart can be problematic for some onshore projects where the CPTu pore pressure results may not always be reliable, due to loss of saturation. However, for offshore projects, where CPTu sensor saturation is more reliable, and onshore projects in soft fine-grained soils with high groundwater, the chart can be very helpful. The Schneider et al chart is focused primarily on contractive fine-grained soils where positive excess pore pressures are recorded, and Q_t is often small.

Robertson (2016) updated the SBT_n charts to provide descriptions that are more behavior based as well as a method to estimate if soils have significant microstructure. The resulting charts are shown in Figure 25. The $Q_{tn} - F_r$ chart (shown in more detail in Fig. 25b) includes a line that separates soils that are either dilative or contractive at large strains. This boundary applies to soils that have little or no microstructure (e.g., little or no aging and/or bonding). The pore pressure chart ($\Delta u_2 / \sigma'_{vo}$) is modified slightly from Schneider et al (2008) and also includes a region to identify if soils have significant microstructure. An additional chart that uses $I_G = G_o / q_n$ requires shear wave velocity (V_s) measurements to obtain the small strain shear modulus G_o that can be used to identify soils with significant microstructure. Full details are contained in Robertson (2016).

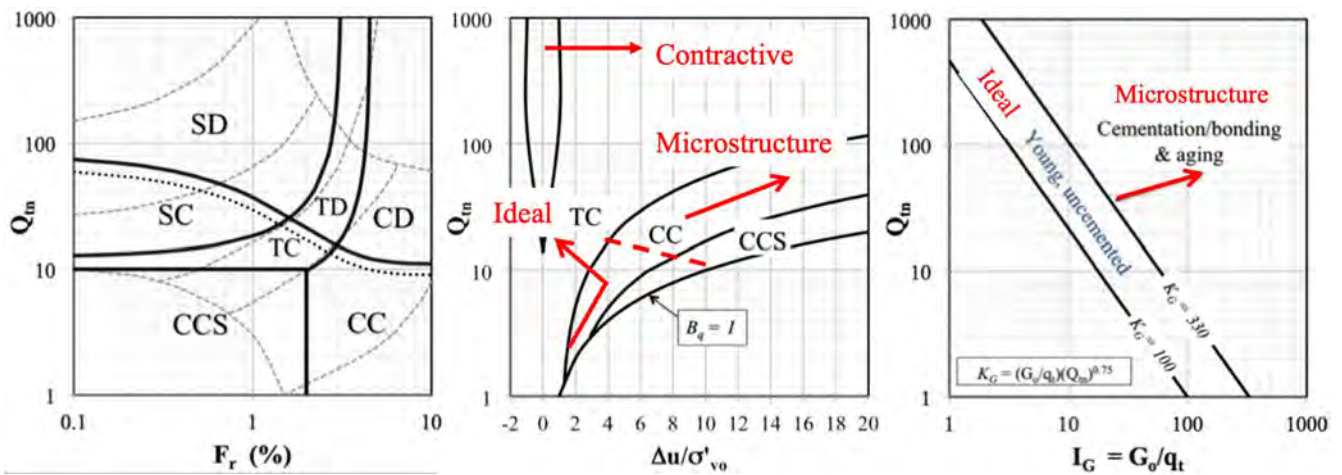


Figure 25 (a). Updated Normalized CPT Soil Behavior Type (SBT_n) charts

(After Robertson, 2016)

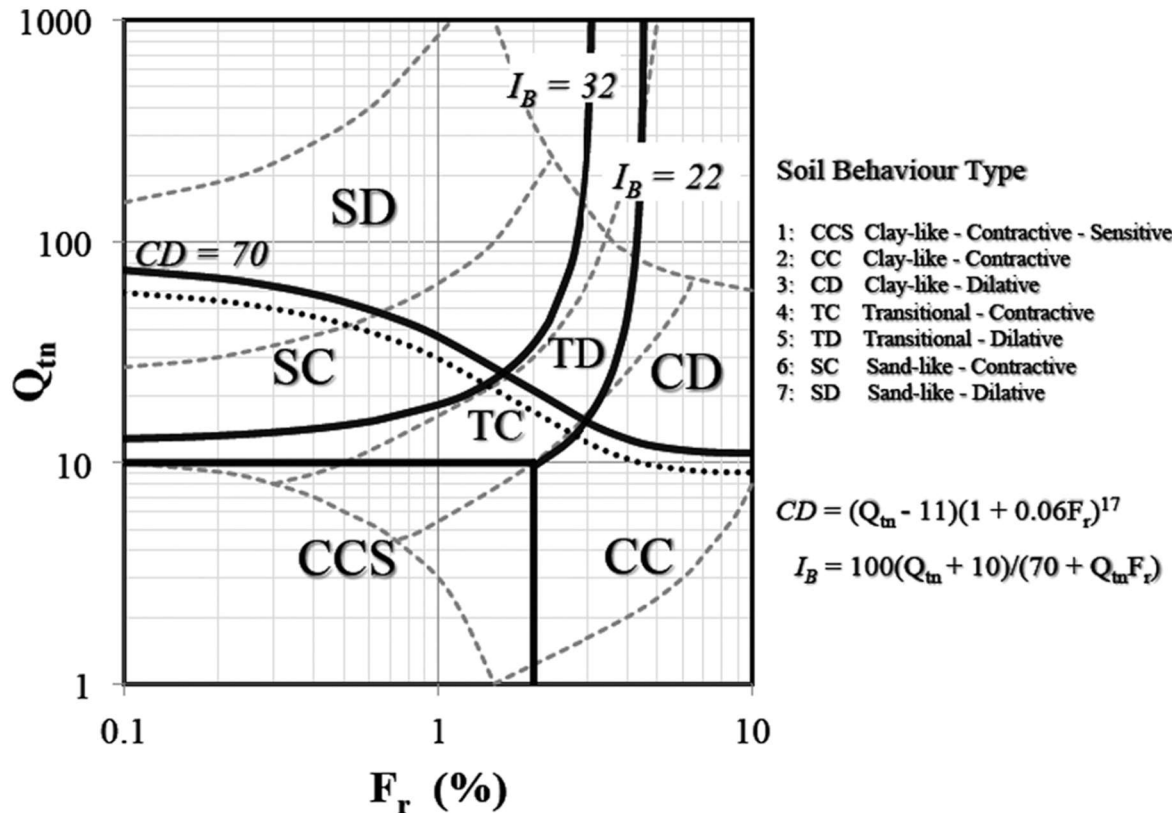


Figure 25 (b). Updated Normalized CPT Soil Behavior Type (SBT_n)
Q_{tn}-F_r chart (After Robertson, 2016)

The boundary between contractive and dilative behavior at large strains on the Q_{tn}-F_r chart in Figure 25b, for soils with little or no microstructure, is defined by:

$$CD = 70 = (Q_{tn} - 11)(1 + 0.06F_r)^{17}$$

Robertson (2016) also suggested a modified Soil Behavior Type Index, I_B:

$$I_B = 100(Q_{tn} + 10) / (70 + Q_{tn}F_r)$$

The modified SBT I_B capture the SBT boundaries better than the original circular I_c. Throughout this Guide use will be made of the normalized soil behavior type (SBT) chart using normalized CPT parameters (e.g., Figure 25b). Hence, accuracy in both q_t and f_s are important, particularly in soft fine-grained soil. Accuracy in f_s measurements requires that the CPT be carried out according to the standard (e.g., ASTM D5778) with particular attention to cone design (separate load cells and equal-end area friction sleeves), tolerances, and zero-load readings.

In recent years, the SBT charts have been color coded to aid in the visual presentation of SBT on a CPT profile. An example CPTu profile is shown in Figure 26. The red line on the shear wave velocity plot (Fig. 26b) are the measured values of V_s and the black line shows the estimated values for a soil with little or no microstructure (Robertson, 2009).

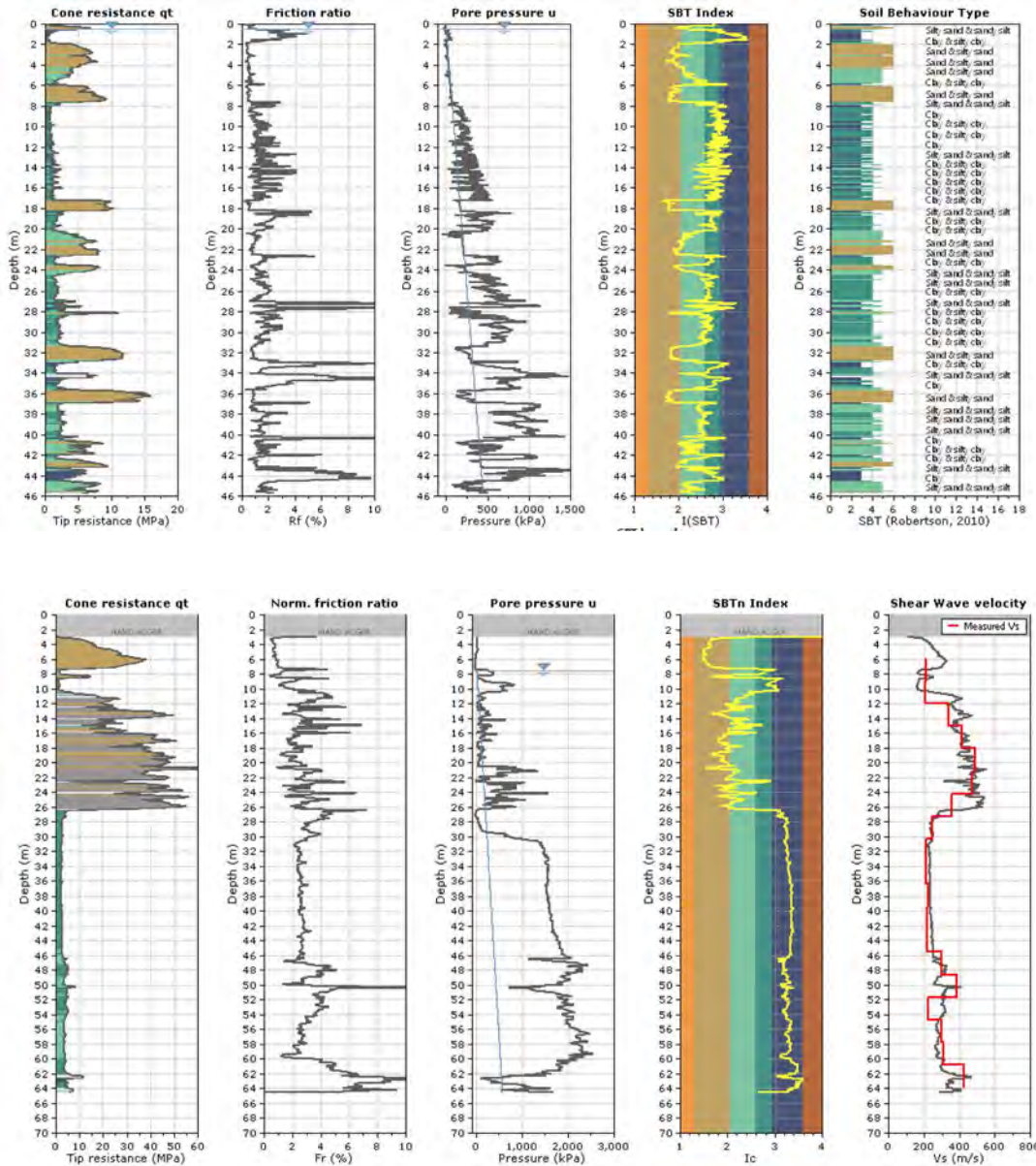


Figure 26(a) and (b). Examples color plots of (a) CPTu (Venice Lagoon) and (b) SCPTu (San Francisco)

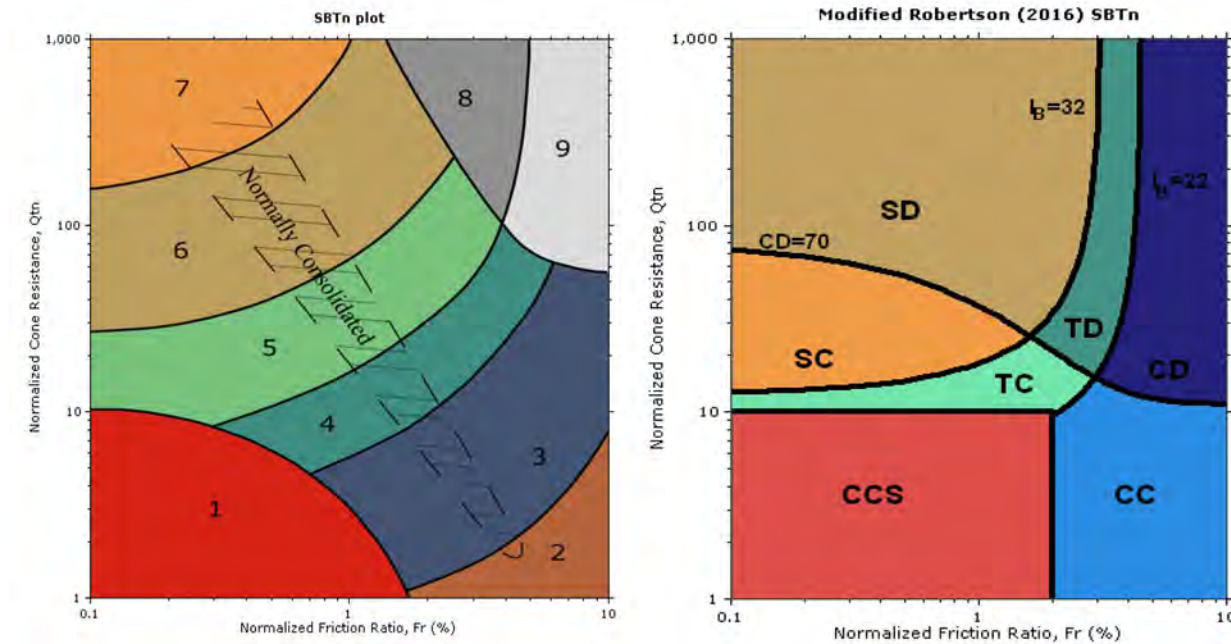


Figure 26(c) Color SBTn charts

Figure 26c shows the color SBT charts. When using the non-normalized SBT chart, the associated colors are used and when using the normalized SBTn chart, the alternate colors apply. This provides a visual presentation of estimated SBT type on the CPT profile, either color added under the cone resistance plot or on the I_c or I_B plot.

Equivalent SPT N_{60} Profiles

The Standard Penetration Test (SPT) was one of the most common in-situ tests in many parts of the world, especially in North and South America. Despite continued efforts to standardize the SPT procedure and equipment there are still problems associated with its repeatability and reliability. However, some geotechnical engineers have developed considerable experience with design methods based on local SPT correlations. When these engineers are first introduced to the CPT, they initially prefer to see CPT results in the form of equivalent SPT N -values. Hence, there is a need for reliable CPT/SPT correlations so that CPT data can be used in existing SPT-based design approaches.

There are many factors affecting the SPT results, such as borehole preparation and size, sampler details, rod length and energy efficiency of the hammer-anvil-operator system. One of the most significant factors is the energy efficiency of

the SPT system. This is normally expressed in terms of the rod energy ratio (ER_r). An energy ratio of about 60% has generally been accepted as the reference value that represents the approximate historical average SPT energy.

Several studies have been presented over the years to relate the SPT N value to the CPT cone penetration resistance, q_c . Robertson et al. (1983) reviewed these correlations and presented the relationship shown in Figure 27 relating the ratio $(q_c/p_a)/N_{60}$ with mean grain size, D_{50} (varying between 0.001mm to 1mm). Values of q_c are made dimensionless when dividing by the atmospheric pressure (p_a) in the same units as q_c . It is observed that the ratio increases with increasing grain size. The values of N used correspond to an average energy ratio of about 60%. Hence, the ratio applies to N_{60} , as shown on Figure 27. Other studies have linked the ratio between the CPT and SPT with fines content for sandy soils.

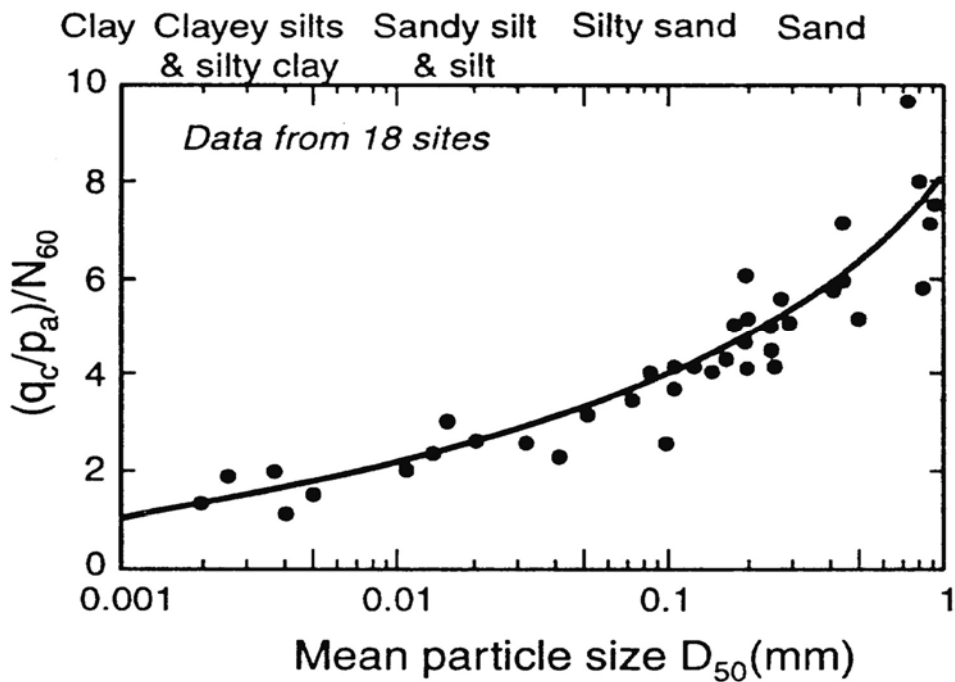


Figure 27. CPT-SPT correlations with mean grain size
(Robertson et al., 1983)

The above correlations require the soil grain size information to determine the mean grain size (or fines content). Grain characteristics can be estimated directly from CPT results using soil behavior type (SBT) charts. The CPT SBT charts show a clear trend of increasing friction ratio with increasing fines content and decreasing grain size. Robertson et al. (1986) suggested $(q_c/p_a)/N_{60}$ ratios for each

soil behavior type zone using the non-normalized CPT chart and the suggested $(q_c/p_a)/N_{60}$ ratio for each soil behavior type is given in Table 5.

These values provide a reasonable estimate of SPT N_{60} values from CPT data. For simplicity the above correlations are given in terms of q_c . For fine grained soft soils, the correlations should be applied to total cone resistance, q_t . Note that in sandy soils $q_c = q_t$.

One disadvantage of this simplified approach is the somewhat discontinuous nature of the conversion. Often a soil will have CPT data that cover different SBT zones and hence produces discontinuous changes in predicted SPT N_{60} values.

Zone	Soil Behavior Type (SBT)	$\frac{(q_c/p_a)}{N_{60}}$
1	<i>Sensitive fine grained</i>	2.0
2	<i>Organic soils – clay</i>	1.0
3	<i>Clays: clay to silty clay</i>	1.5
4	<i>Silt mixtures: clayey silt & silty clay</i>	2.0
5	<i>Sand mixtures: silty sand to sandy silt</i>	3.0
6	<i>Sands: clean sands to silty sands</i>	5.0
7	<i>Dense sand to gravelly sand</i>	6.0
8	<i>Very stiff sand to clayey sand*</i>	5.0
9	<i>Very stiff fine-grained*</i>	1.0

Table 5 Suggested $(q_c/p_a)/N_{60}$ ratios

Jefferies and Davies (1993) suggested the application of the soil behavior type index, I_c to link with the CPT-SPT correlation. The soil behavior type index, I_c , can be combined with the CPT-SPT ratios to give the following simple and continuous relationship:

$$\frac{(q_t/p_a)}{N_{60}} = 8.5 \left(1 - \frac{I_c}{4.6} \right)$$

Robertson (2012) suggested an update of the above relationship that provides improved estimates of N_{60} for insensitive clays:

$$\frac{(q_t/p_a)}{N_{60}} = 10^{(1.1268 - 0.2817Ic)}$$

Jefferies and Davies (1993) suggested that the above approach can provide better estimates of the SPT N_{60} -values than the actual SPT test due to the poor repeatability of the SPT. In fine-grained soils with high sensitivity, the above relationship may overestimate the equivalent N_{60} .

In very loose soils with $(N_1)_{60} < 10$, the weight of the rods and hammer can dominate the SPT penetration resistance and produce very low N-values, which can result in high $(q_t/p_a)/N_{60}$ ratios due to the low SPT N-values measured.

Soil Unit Weight (γ)

Soil total unit weights (γ) are best obtained by obtaining relatively undisturbed samples (e.g., thin-walled Shelby tubes; piston samples) and weighing a known volume of soil. When this is not feasible, the total unit weight can be estimated from CPT results, such as Figure 28 and the following relationship (Robertson and Cabal, 2010):

$$\gamma/\gamma_w = [0.27 [\log R_f] + 0.36 [\log(q_t/p_a)] + 1.236] G_s / 2.65$$

where R_f = friction ratio = $(f_s/q_t)100\%$

γ_w = unit weight of water in same units as γ

p_a = atmospheric pressure in same units as q_t

G_s = specific gravity of soil

The above correlation attempts to adjust the correlation for soils with G_s values that are different than the typical about 2.65 for most silica-based soils.

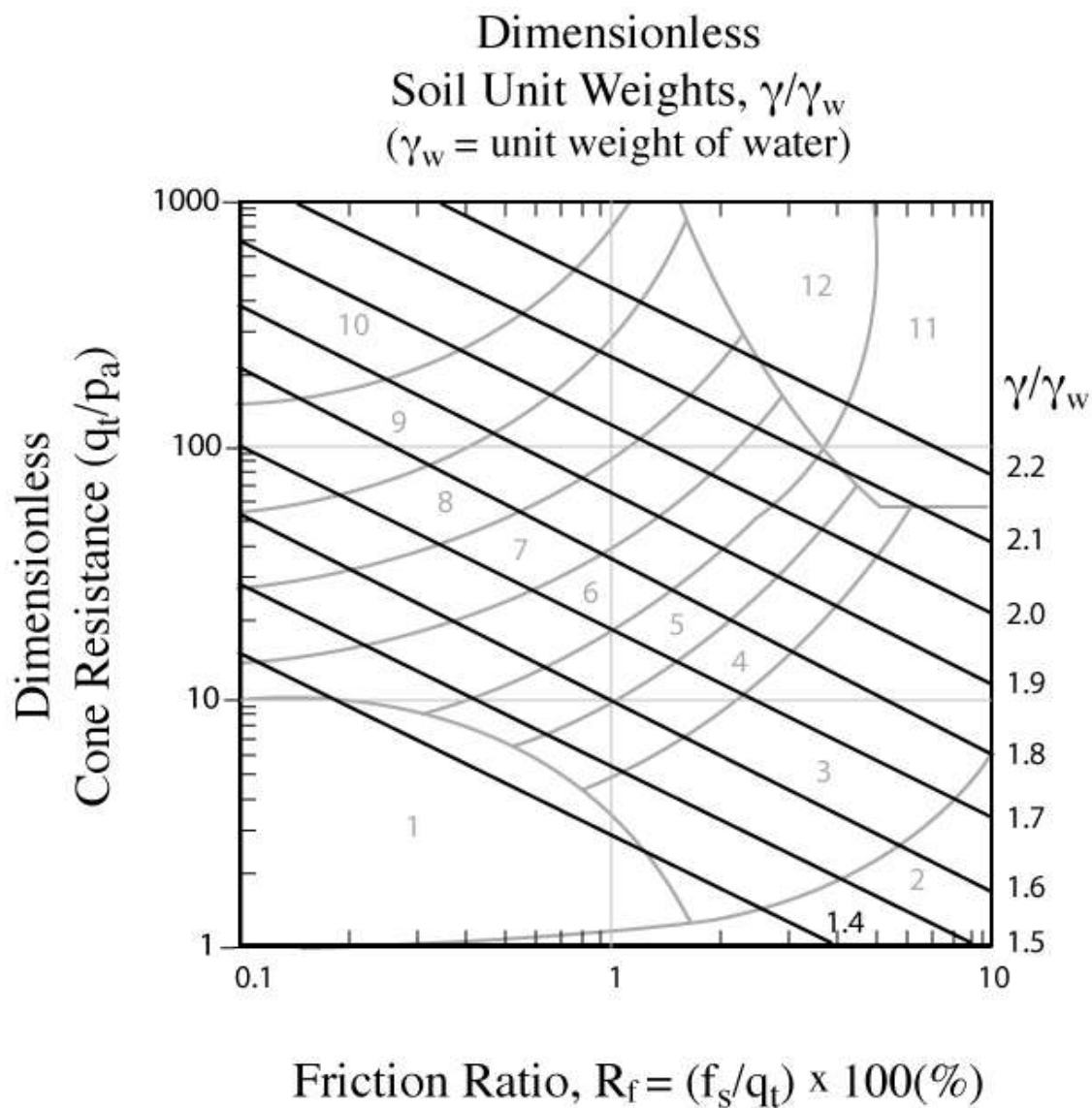


Figure 28. Dimensionless soil unit weight, γ/γ_w based on CPT
($G_s \sim 2.65$)

Alternate methods to estimate soil unit weights from CPT data have been suggested (e.g., Mayne et al, 2010; Lengkeek et al, 2018) as well as methods based on machine learning. The method by Lengkeek et al (2018) was based primarily on soft organic soils in the Netherlands.

Undrained Shear Strength (s_u)

No single value of undrained shear strength, s_u , exists, since the undrained response of soil depends on the direction of loading, soil anisotropy, strain rate, and stress history. Typically, the undrained strength in tri-axial compression is larger than in simple shear that is larger than tri-axial extension ($s_{uTC} > s_{uSS} > s_{uTE}$) where the difference is larger in low plastic soils. The value of s_u to be used in analysis therefore depends on the design problem. In general, the simple shear direction of loading often represents the average undrained strength ($s_{uSS} \sim s_{u(ave)}$). Hence, there is always some uncertainty in estimating and applying undrained shear strength.

Since anisotropy and strain rate will inevitably influence the results of all in-situ tests, their interpretation will necessarily require some empirical content to account for these factors, as well as possible effects of sample disturbance.

Theoretical solutions have provided valuable insight into the form of the relationship between cone resistance and s_u . Most theories result in a relationship between corrected cone resistance, q_t , and s_u of the form:

$$s_u = \frac{q_t - \sigma_v}{N_{kt}}$$

Typically, N_{kt} varies from 10 to 18, with 14 as an average for $s_{u(ave)}$. N_{kt} tends to increase with increasing plasticity and decrease with increasing soil sensitivity. Since N_{kt} is strongly influenced by sensitivity, Robertson (2012) suggested the following method to estimate N_{kt} from friction ratio, F_r using:

$$N_{kt} = 10.5 + 7 \log (F_r)$$

Lunne et al., (1997) and Mayne and Peuchen (2022) showed that N_{kt} decreases as B_q increases. In very sensitive fine-grained soil, where $B_q \sim 1.0$, N_{kt} can be less than 10. Mayne and Peuchen (2022) suggest the following relationship based on data from 70 clay deposits:

$$N_{kt} = 10.5 - 4.6 \ln (B_q + 0.1)$$

This approach requires reliable pore pressure data to determine B_q .

For deposits where little experience is available, estimate s_u using the corrected cone resistance (q_t) and preliminary cone factor values (N_{kt}) from 14 to 16. For a more conservative estimate, select a value close to the upper limit.

In very soft clays, where there may be some uncertainty with the accuracy in q_t , estimates of s_u can be made from the excess pore pressure (Δu) measured behind the cone (u_2) using the following:

$$s_u = \frac{\Delta u}{N_{\Delta u}}$$

Where $N_{\Delta u}$ varies from 2 to 10. For a more conservative estimate, select a value close to the upper limit. Note that $N_{\Delta u}$ is linked to N_{kt} , via B_q , where:

$$N_{\Delta u} = B_q N_{kt}$$

$$\text{Hence, } N_{\Delta u} = B_q [10.5 - 4.6 \ln (B_q + 0.1)]$$

If previous experience is available in the same deposit, the values suggested above should be adjusted to reflect this experience.

For larger, moderate to high-risk projects, where high quality field and laboratory data may be available, site-specific correlations should be developed based on appropriate and reliable values of s_u .

Soil Sensitivity (S_t)

The sensitivity (S_t) of clay is defined as the ratio of undisturbed peak undrained shear strength to totally remolded undrained shear strength.

Based on experience, the remolded undrained shear strength, $s_{u(Rem)}$, can be assumed equal to the sleeve resistance, f_s (during undrained CPT penetration) since both occur at large strains under undrained conditions. Therefore, the sensitivity of a clay can be estimated by calculating the peak s_u from either site specific or general correlations with q_t or Δu and $s_{u(Rem)}$ from f_s , and can be approximated using the following:

$$S_t = \frac{s_u}{s_{u(Rem)}} = \frac{q_t - \sigma_v}{N_{kt}} (1 / f_s) \sim 7 / F_r \text{ (based on typical } N_{kt} = 14)$$

For relatively sensitive clays ($S_t > 10$), the value of f_s can be very low with inherent difficulties in accuracy. Hence, the estimate of sensitivity (and remolded strength) from the CPT should be used as a guide.

Undrained Shear Strength Ratio (s_u/σ'_{vo})

It is often useful to estimate the peak undrained shear strength ratio from the CPT, since this often relates directly to overconsolidation ratio (OCR). Critical State Soil Mechanics presents a relationship between the peak undrained shear strength ratio for normally consolidated (NC) clays under different directions of loading and the effective stress friction angle, ϕ' . Hence, a better estimate of undrained shear strength ratio can be obtained with knowledge of the friction angle [e.g., $(s_u/\sigma'_{vo})_{NC}$ increases with increasing ϕ']. For normally consolidated clays (with little or no microstructure):

$$(s_u/\sigma'_{vo})_{NC} \sim 0.22 \text{ in direct simple shear } (\phi' \sim 26^\circ)$$

From the CPT:

$$(s_u/\sigma'_{vo}) = \left(\frac{q_t - \sigma_{vo}}{\sigma'_{vo}} \right) (1/N_{kt}) = Q_t / N_{kt}$$

Since $N_{kt} \sim 14$

$$(s_u/\sigma'_{vo}) \sim Q_t / 14$$

Hence, for a normally consolidated clay where $(s_u/\sigma'_{vo})_{NC} \sim 0.22$ the expected values of Q_t are:

$$Q_t = 3 \text{ to } 4 \text{ for NC insensitive clay (with no microstructure)}$$

Based on the assumption that the sleeve resistance, f_s , is a direct measure of the remolded shear strength, $s_{u(Rem)} = f_s$. Therefore, the remolded undrained strength ratio $(s_{u(Rem)}/\sigma'_{vo})$ is:

$$s_{u(Rem)}/\sigma'_{vo} = f_s / \sigma'_{vo} = (F \cdot Q_t) / 100$$

Hence, it is possible to represent $(s_u(\text{Rem})/\sigma'_{vo} = f_s / \sigma'_{vo})$ as linear contours on the normalized SBT_n chart (Robertson, 2009 – see Figure 23) when $I_c > \sim 2.6$.

Overconsolidation Ratio (OCR) and Yield Stress (σ'_y)

Overconsolidation ratio (OCR) is often defined as the ratio of the maximum past effective consolidation stress and the present effective overburden stress:

$$\text{OCR} = \frac{\sigma'_p}{\sigma'_{vo}}$$

For mechanically overconsolidated soils where the only change has been the removal of overburden stress, this definition is appropriate. However, for soils with some microstructure (e.g., cemented and/or aged soils) the OCR may represent the ratio of the yield stress (σ'_y) and the present effective overburden stress (σ'_{vo}) and is referred to as the Yield Stress Ratio (YSR). The YSR will also depend on the direction and type of loading. For overconsolidated clays:

$$(s_u/\sigma'_{vo})_{OC} = (s_u/\sigma'_{vo})_{NC} (\text{OCR})^{0.8}$$

Based on this, Robertson (2009) suggested:

$$\text{OCR} = 0.25 (Q_t)^{1.25}$$

This compares very closely to the form suggested by Karlsrud et al (2005) based on high quality block samples from Norway (when soil sensitivity, $S_t < 15$) and that resulting from CSSM:

$$\text{OCR} = 0.25 (Q_t)^{1.2}$$

Kulhawy and Mayne (1990) suggested a simpler method:

$$\text{OCR} = k \left(\frac{q_t - \sigma_{vo}}{\sigma'_{vo}} \right) = k Q_t \quad \text{or} \quad \sigma'_p = k (q_t - \sigma_{vo})$$

An average value of $k = 0.33$ can be assumed, with an expected range of 0.2 to 0.5. Higher values of k are recommended in aged, heavily overconsolidated clays.

If previous experience is available in the same deposit, the value of k should be adjusted to reflect this experience and to provide a more reliable profile of OCR. The simpler Kulhawy and Mayne approach is valid for $Q_t < 20$.

For larger, moderate to high-risk projects, where additional high-quality field and laboratory data may be available, site-specific correlations should be developed based on consistent and relevant values of OCR (or YSR).

Agaiby and Mayne (2019) suggested an extension of this approach that can be applied to all soils based on the following:

$$\sigma'_p = 0.33(q_t - \sigma_{vo})^{m'} (p_a/100)^{1-m'}$$

where m' is a function of SBT I_c ($m' \sim 0.72$ in young, uncemented silica sand and $m' \sim 1.0$ in intact clay).

YSR can be a useful method to define the in-situ state of a clay, like state parameter (ψ) is for sand. For a clay-like soil, the boundary between contractive and dilative behavior at large strain is approximately YSR = 5, just like $\psi = -0.05$ is the boundary for sand-like soils.

A modification to the Agaiby and Mayne approach can provide a simplified method to link YSR and ψ , using the following:

$$YSR = 0.33 (Q_{tn})^{m'}$$

Where Q_{tn} was defined by Robertson (2009) and m' is modified to become:

$$m' = 1 - [0.28 / (1 + (I_c/2.6)^{15})]$$

When $I_c > 2.8$, $m' = 1.0$.

The above simplified method can produce similar values of in-situ state (YSR) for both clay-like and sand-like soils, provided there is little or no microstructure.

Consistency between values of k (for OCR) and N_{kt} (for s_u)

Been et al (2010) correctly suggested that there should be some consistency between the factors used to estimate OCR (i.e., k) and s_u (i.e., N_{kt}).

Based on the concept SHANSEP, Been et al (2010) suggested the following:

$$(Q_t)^{1-m} = S N_{kt} (k)^m$$

Where:

$$OCR = k (Q_t) \quad \text{when } Q_t < 20$$

$$s_u/\sigma'_{vo} = Q_t/N_{kt} = S (OCR)^m$$

$$S = (s_u/\sigma'_{vo})_{OCR=1}$$

For most sedimentary clays, silts and organics fine-grained soil, S ~ 0.25 for average direction of loading and $\phi' \sim 26$, and m ~ 0.8. Hence, the constant to estimate OCR can be automatically estimated based on CPT results using:

$$k = [(Q_t)^{0.2} / (0.25 (10.5 + 7 \log F_r))]^{1.25}$$

Then,

$$OCR = (2.625 + 1.75 \log F_r)^{-1.25} (Q_t)^{1.25}$$

This represents a method to automatically estimate the in-situ state (OCR) in fine-grained soils based on measured CPT results, in a consistent manner.

This compares very closely to the form suggested by Karlsrud et al (2005) based on high quality block samples from Norway (when soil sensitivity, S_t < 15) and that resulting from CSSM:

$$OCR = 0.25 (Q_t)^{1.2}$$

When Fr ~2% the two approaches give essentially the same result.

In-Situ Stress Ratio (K_o)

There is no reliable method to determine K_o from CPT. However, an estimate can be made in fine-grained soils based on an estimate of OCR, as shown in Figure 29. Kulhawy and Mayne (1990) suggested a simpler approach, using:

$$K_o = (1 - \sin\phi') (\text{OCR})^{\sin\phi'}$$

That can be approximated (for low plastic fine-grained soils) to:

$$K_o \sim 0.5 (\text{OCR})^{0.5}$$

These approaches are limited to mechanically overconsolidated, fine-grained soils (i.e., soils with little or no microstructure). Considerable scatter exists in the database used for these correlations and therefore they must be considered only as a guide.

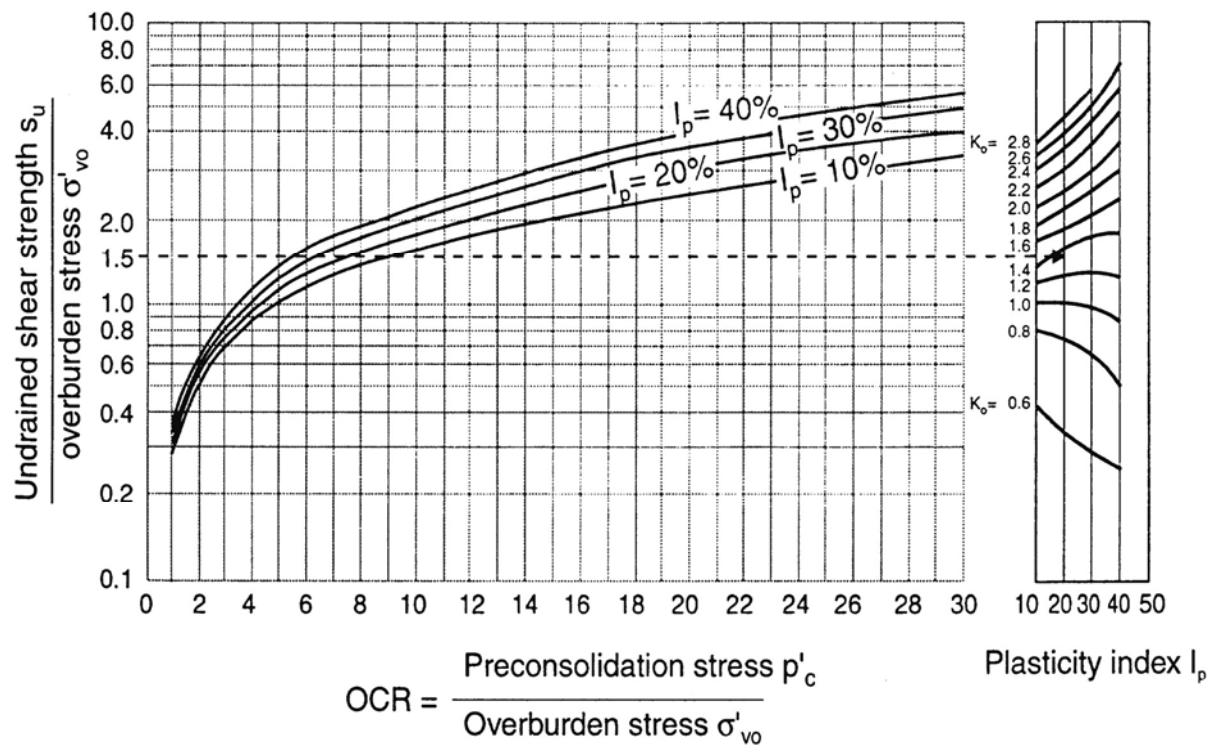


Figure 29. OCR and K_o from s_u/σ'_vo and Plasticity Index, I_p
(after Andresen et al., 1979)

Relative Density (Dr)

For coarse-grained soils, the density, or more commonly, the relative density or density index, is often used as an intermediate soil parameter. Relative density, D_r , or density index, I_D , is defined as:

$$I_D = D_r = \frac{e_{\max} - e}{e_{\max} - e_{\min}}$$

where:

e_{\max} and e_{\min} are the maximum and minimum void ratios and e is the in-situ void ratio.

The problems associated with the determination of e_{\max} and e_{\min} are well known. Also, research has shown that the stress strain and strength behavior of coarse-grained soils is too complicated to be represented by only the relative density of the soil. However, for many years relative density has been used by engineers as a parameter to describe the in-situ state of sand deposits.

Research using large calibration chambers has provided numerous correlations between CPT penetration resistance and relative density for clean, predominantly quartz (silica-based) sands. The calibration chamber studies have shown that the CPT resistance is controlled by sand density, in-situ vertical and horizontal effective stresses, and sand compressibility. Sand compressibility is controlled by grain characteristics, such as grain size, shape, and mineralogy. Angular sands tend to be more compressible than rounded sands as do sands with high mica and/or carbonate compared with clean quartz (silica) sands. More compressible sands give a lower penetration resistance for a given relative density than less compressible sands.

Kulhawy and Mayne (1990) suggested a simple relationship for estimating relative density:

$$D_r^2 = \frac{Q_{cn}}{305 Q_C Q_{OCR} Q_A}$$

where:

Q_{cn} (or Q_{tn}) is the normalized tip resistance, as defined above

Q_C = Compressibility factor ranges from 0.90 (low compress.) to 1.10 (high compress.)

$$\begin{aligned} Q_{OCR} &= \text{Overconsolidation factor} = OCR^{0.18} \\ Q_A &= \text{Aging factor} = 1.2 + 0.05 \log(t/100) \end{aligned}$$

A constant of 350 is reasonable for medium, clean, uncemented, unaged quartz sands that are about 1,000 years old (see Fig. 30). The constant is close to 300 for finer and younger sands and can be closer to 400 for some coarse or older sands. The constant increases with age and increases significantly when age exceeds 10,000 years. The relationship can then be simplified for most young, uncemented clean sands (where $I_c < 1.6$) to:

$$D_r^2 = Q_{tn} / 350$$

The approach can be extended to silty sands ($I_c < 2.6$), where the CPT penetration process is drained, by using the normalized clean sand equivalent, $Q_{tn,cs}$ (see Figure 48 for details).

$$D_r^2 = Q_{tn,cs} / 350$$

Bray and Olaya (2022) suggested an updated simplified version based on non-plastic silty sands:

$$D_r^2 = (Q_{tn} I_c^{3.5}) / 1500$$

The above correlations apply only to soils that have little to no microstructure.

Figure 30 shows data from the CANLEX research project (Fear et al., 2000) that illustrates the variation of the correlation with age. The data points were from sites where high quality undisturbed frozen samples were obtained to determine D_r .

Since the cone resistance is also influenced by the horizontal effective stress, research has shown that it would be better to normalize q_t using the mean effective stress (p'). However, this requires knowledge of either the horizontal effective stress or K_o , which are rarely known with any accuracy. Hence, it has become common practice to normalize the cone resistance using the vertical effective stress, since this can be estimated with reasonable accuracy. For most young sand-like soils with little stress history and little or no microstructure, the simple normalization using σ'_{vo} can be equally effective. For older soils and soils with some stress history (i.e., $OCR > 1$), any potential errors in the normalization are

mostly compensated using semi-empirical correlations that are based on well-documented case histories, where the in-situ K_o is incorporated within the correlation.

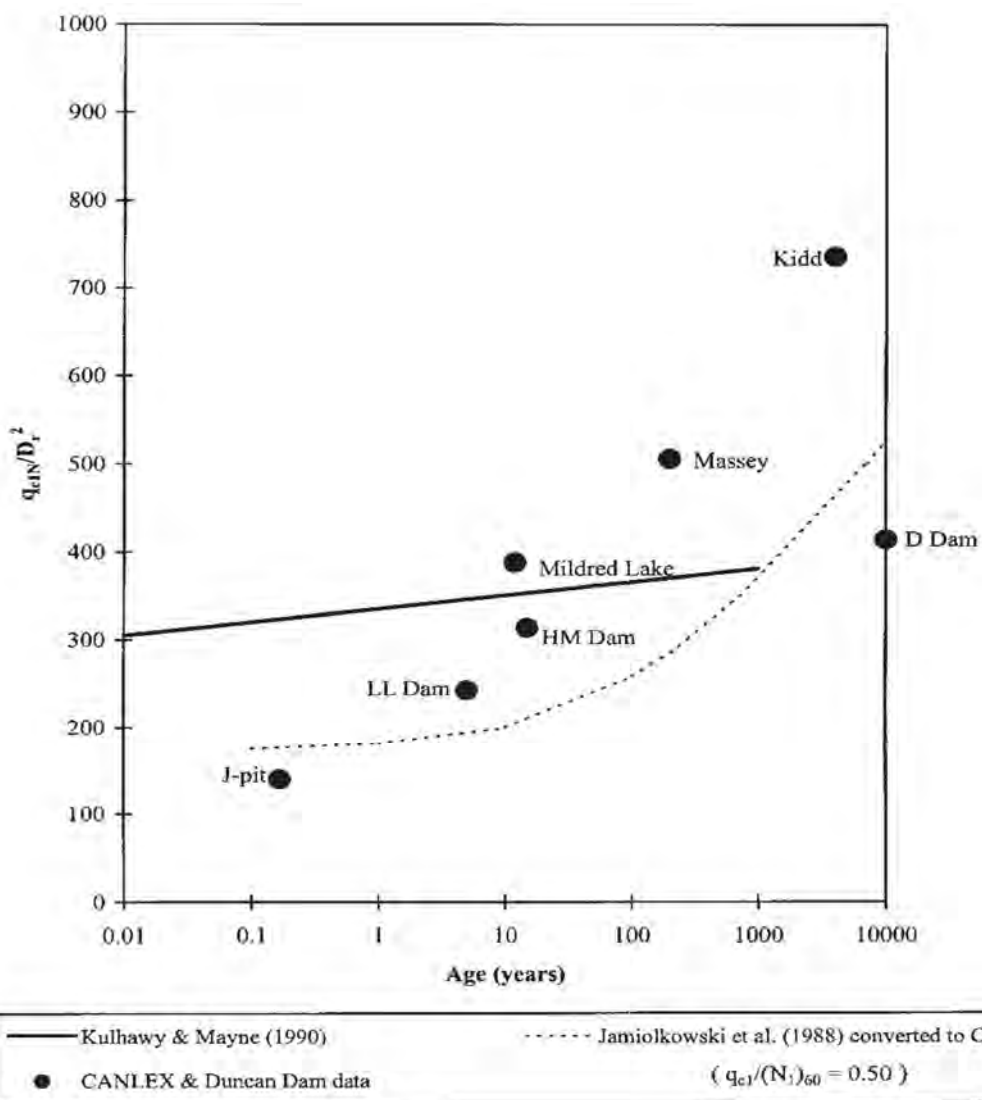


Figure 30. Effects of soil age on CPT penetration resistance in sands
(note: $q_{c1N} = Q_{tn}$) (After Fear et al. 2000)

State Parameter (ψ)

The state parameter (ψ) is defined as the difference between the current void ratio, e and the void ratio at critical state e_{cs} , at the same mean effective stress for coarse-grained (sandy) soils. Since the Critical State Line is very flat, in terms of $e - \log p'$, at low to moderate effective stress ($p' < 3$ atm.), there is little difference between defining in-situ state using either D_r or ψ . Using critical state concepts, Jefferies and Been (2006) provided a detailed description of the evaluation of soil state using the CPT. They describe in detail that the problem of evaluating state from CPT response is complex and depends on several soil parameters. The main parameters are essentially the shear stiffness, shear strength, compressibility, and plastic hardening. Jefferies and Been (2006) provided a description of how state can be evaluated using a combination of laboratory and in-situ tests. They stress the importance of determining the in-situ horizontal effective stress and shear modulus using in-situ tests and determining the shear strength, compressibility, and plastic hardening parameters from laboratory testing on reconstituted samples. They also show how the problem can be assisted using numerical modeling. For high-risk projects a detailed interpretation of CPT results using laboratory results and numerical modeling may be appropriate (e.g., Shuttle and Cunning, 2007), although soil variability can complicate the interpretation procedure. Some unresolved concerns with the Jefferies and Been (2006) approach relate to the stress normalization using $n = 1.0$ for all soils, and the influence of soil fabric in sands with high fines content.

For low-risk projects and in the initial screening for high-risk projects there is a need for a simple estimate of in-situ soil state. Plewes et al (1992) provided a means to estimate soil state using the normalized soil behavior type (SBT_n) chart suggested by Jefferies and Davies (1991). Jefferies and Been (2006) updated this approach using their normalized SBT_n chart based on the parameter $Q_t(1-B_q) + 1$. Robertson (2009) expressed concerns about the accuracy and precision of the Jefferies and Been (2006) normalized parameter in soft soils, where B_q is close to 1.0. In sands, where $B_q \sim 0$, the normalization suggested by Jefferies and Been (2006) is essentially the same as that used by Robertson (1990).

Based on the data presented by Jefferies and Been (2006) and Shuttle and Cunning (2007) as well the measurements from the CANLEX project (Wride et al, 2000) for predominantly, uncemented young (i.e., little or no microstructure) sands, combined with the link between OCR and state parameter in fine-grained soil, Robertson (2009) developed contours of state parameter (ψ) on the updated SBT_n $Q_{tn} - F$ chart for uncemented, Holocene-age soils. The contours of ψ , shown on

Figure 31, are approximate since in-situ stress state and plastic hardening will also influence the estimate of in-situ soil state in the coarse-grained region of the chart (i.e., when $I_c < 2.60$) and soil sensitivity for fine-grained soils. Jefferies and Been (2006) suggested that soils with a state parameter less than -0.05 (i.e., $\psi < -0.05$) are dilative at large strains.

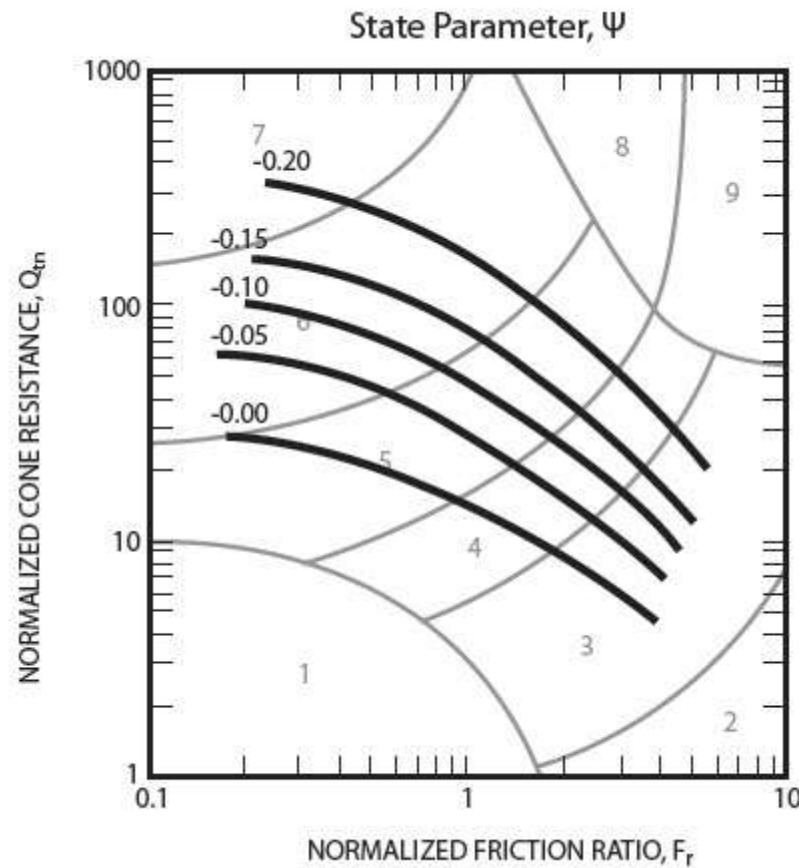


Figure 31. Contours of estimated state parameter, ψ (thick lines), on normalized SBT_n Q_{tn} – F_r chart for uncemented Holocene-age soils
(After Robertson, 2009)

Robertson (2010) suggested a simplified and approximate relationship between ψ and the clean sand equivalent normalized cone resistance, $Q_{tn,cs}$, as follows:

$$\psi = 0.56 - 0.33 \log Q_{tn,cs}$$

The clean sand equivalent normalized cone resistance, $Q_{tn,cs}$ evolved from the study of liquefaction case histories and details are provided in a later section on “*Liquefaction*” (see Figure 48).

Peak Friction Angle (ϕ')

The shear strength of uncemented, coarse-grained soils is usually expressed in terms of a peak secant friction angle, ϕ' .

Significant advances have been made in the development of theories to model the cone penetration process in sands (e.g., Yu and Mitchell, 1998). Cavity expansion models are popular since they are relatively simple and can incorporate many of the important features of soil response. However, empirical correlations based on calibration chamber test results and field results are still the most used.

Robertson and Campanella (1983) suggested a correlation to estimate the peak friction angle (ϕ') for uncemented, unaged, moderately compressible, predominately quartz sands based on calibration chamber test results. For sands of higher compressibility (i.e., carbonate sands or sands with high mica content), the method will tend to predict friction angles values that are too low.

$$\tan \phi' = \frac{1}{2.68} \left[\log \left(\frac{q_c}{\sigma'_{vo}} \right) + 0.29 \right]$$

Kulhawy and Mayne (1990) suggested an alternate relationship for clean, rounded, uncemented quartz sands, and evaluated the relationship using high quality field data.

$$\phi' = 17.6 + 11 \log (Q_{tn})$$

Jefferies and Been (2006) showed a strong link between state parameter (ψ) and the peak friction angle (ϕ') for a wide range of sands. Using this link, it is possible to link $Q_{tn,cs}$ with ϕ' , using:

$$\phi' = \phi'_{cv} - 48 \psi$$

Where ϕ'_{cv} = constant volume (or critical state) friction angle depending on mineralogy (Bolton, 1986), typically about 33 degrees for sub-rounded quartz sands but can be as high as 40 degrees for felspathic and carbonate sands.

Hence, the relationship between normalized clean sand equivalent cone resistance, $Q_{tn,cs}$ and ϕ' becomes:

$$\phi' = \phi'_{cv} + 15.84 [\log Q_{tn,cs}] - 26.88$$

The above relationship produces estimates of peak friction angle for clean quartz sands that are like those by Kulhawy and Mayne (1990). However, the above relationship based on state parameter has the advantage that it includes the importance of grain characteristics and mineralogy that are reflected in both ϕ'_{cv} , as well as soil type through $Q_{tn,cs}$. The above relationship also tends to predict ϕ' values closer to measured values in calcareous sands where the CPT tip resistance can be low for high values of ϕ' , due to a high value for ϕ'_{cv} .

For fine-grained soils, the best means for defining the effective stress peak friction angle is from laboratory on high quality undisturbed samples. An assumed value of $\phi' = 26^\circ$ for clays and 30° for silts is often sufficient for many low-risk projects. Alternatively, an effective stress limit plasticity solution for undrained cone penetration developed at the Norwegian Institute of Technology (NTH: Senneset et al., 1989) allows the approximate evaluation of effective stress parameters (c' and ϕ') from piezocene (u_2) measurements. In a simplified approach for normally-to lightly-overconsolidated clays and silts ($c' = 0$), the NTH solution can be approximated for the following ranges of parameters: $20^\circ \leq \phi' \leq 40^\circ$ and $0.1 \leq B_q \leq 1.0$ (Mayne 2006):

$$\phi' (\text{deg}) = 29.5^\circ \cdot B_q^{0.121} [0.256 + 0.336 \cdot B_q + \log Q_t]$$

For heavily overconsolidated soils, fissured geomaterials, and highly cemented or structured clays, the above will not provide reliable results and ϕ' should be determined by laboratory testing on high quality undisturbed samples. The above approach is only valid when positive (u_2) pore pressures are recorded (i.e., $B_q > 0.1$).

Stiffness and Modulus

CPT data can be used to estimate modulus in soils for subsequent use in elastic or semi-empirical settlement prediction methods. However, correlations between q_c and Young's moduli (E) are sensitive to stress and strain history, aging, soil mineralogy and microstructure.

A useful guide for estimating Young's moduli for young, uncemented predominantly silica sands is given in Figure 32. The modulus has been defined as that mobilized at about 0.1% strain. For more heavily loaded conditions (i.e., larger strain) the modulus would decrease (see "Applications" section).

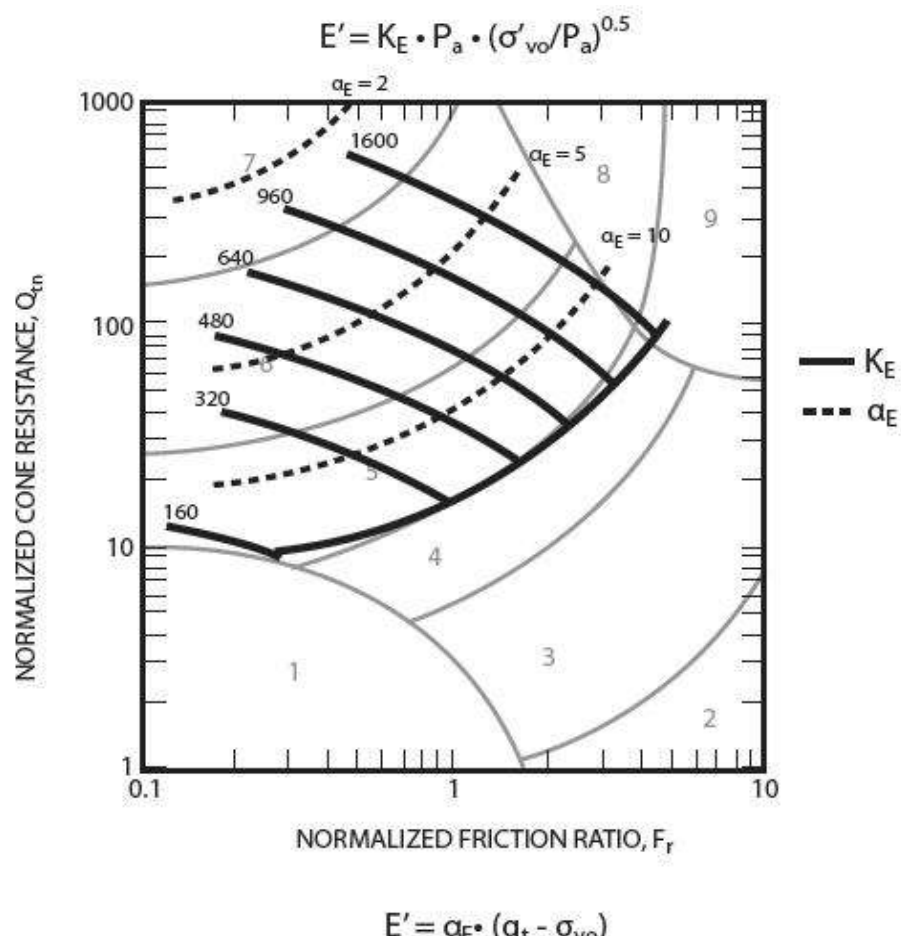


Figure 32. Evaluation of drained Young's modulus (at ~ 0.1% strain) from CPT for young, uncemented silica sands, $E = \alpha_E (q_t - \sigma_{vo})$
where: $\alpha_E = 0.015 [10^{(0.55I_c + 1.68)}]$

Modulus from Shear Wave Velocity

A major advantage of the seismic CPT (SCPT) is the additional measurement of the shear wave velocity, V_s . The shear wave velocity is measured using a downhole technique during pauses in the CPT resulting in a continuous profile of V_s . Elastic theory states that the small strain shear modulus, G_o can be determined from:

$$G_o = \rho V_s^2$$

Where: ρ is the mass density of the soil ($\rho = \gamma/g$) and G_o is the small strain shear modulus (shear strain, $\gamma < 10^{-4}$ %). Hence, the addition of shear wave velocity during the CPT provides a direct measure of small strain soil stiffness.

The small strain shear modulus represents the elastic stiffness of the soil at shear strains (γ) less than 10^{-4} percent. Elastic theory also states that the small strain Young's modulus, E_o is linked to G_o , as follows:

$$E_o = 2(1 + \nu) G_o$$

where: ν is Poisson's ratio, which ranges from 0.1 to 0.3 for most soils.

Application to engineering problems requires that the small strain modulus be softened/reduced to the appropriate strain level. For most well-designed structures, where the average shear strain is relatively small, the degree of softening is often close to a factor of about 2.5. Hence, for many applications the equivalent Young's modulus (E') can be estimated from:

$$E' \sim \rho V_s^2$$

Further details regarding appropriate use of soil modulus for design is given in the section on *Applications of CPT Results*.

V_s can also be used directly for the evaluation of liquefaction potential. Hence, the SCPT can provide two independent methods to evaluate liquefaction potential in soils with little or no microstructure.

Estimating Shear Wave Velocity (V_s) from CPT

Shear wave velocity (V_s) can be correlated to CPT cone resistance as a function of soil type and SBT I_c . However, shear wave velocity is sensitive to age and cementation, where older deposits of the same soil have higher V_s (i.e., higher stiffness) than younger deposits and likewise for cemented soils. Based on extensive SCPT data (Robertson, 2009), Figure 33 shows a relationship between normalized CPT data (Q_{tn} and F_r) and normalized shear wave velocity, V_{s1} , for uncemented Holocene and Pleistocene age soils, where:

$$V_{s1} = V_s \cdot (p_a / \sigma'_{vo})^{0.25}$$

V_{s1} is in the same units as V_s (e.g., either m/s or ft/s). Younger Holocene age soils tend to plot toward the center and lower left of the SBT_n chart whereas older Pleistocene age soil tend to plot toward the upper right part of the chart.

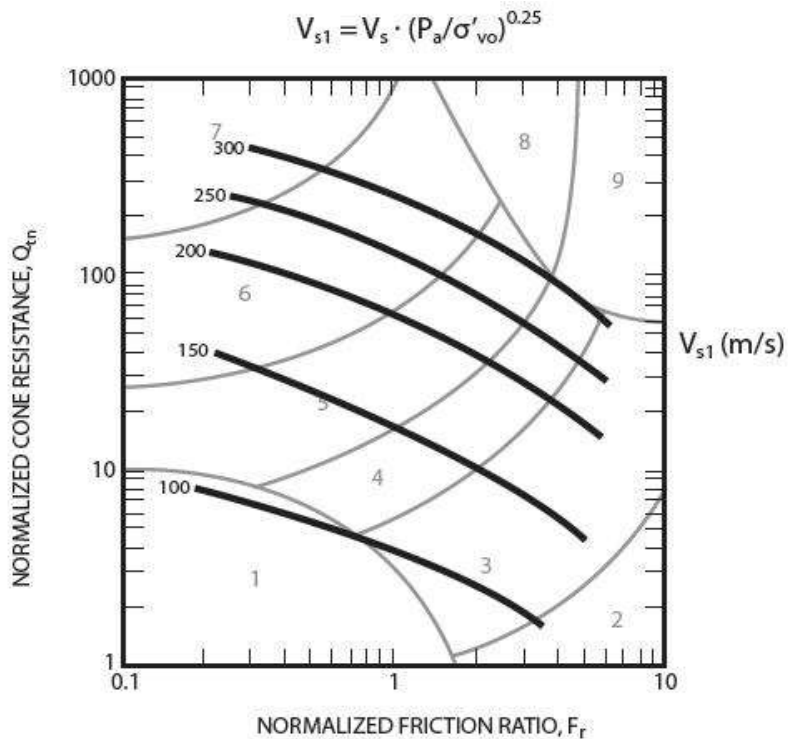


Figure 33. Evaluation of normalized shear wave velocity, V_{s1} , from CPT for uncemented Holocene and Pleistocene age soils (1m/s = 3.28 ft/sec)

$$V_s = [\alpha_{vs} (q_t - \sigma_v)/p_a]^{0.5} \text{ (m/s); where } \alpha_{vs} = 10^{(0.55 I_c + 1.68)}$$

Identification of soils with microstructure

Almost all available empirical correlations to interpret in-situ tests assume that the soil is '*ideal*' with little or no microstructure, i.e., like soils in which the correlation was based. The most common forms of microstructure are due to aging and bonding (e.g., cementation) but can also be caused by unusual mineralogy, stress history and suction hardening in unsaturated soils with clay minerals. Most existing correlations apply to silica-based soils that are young and uncemented (i.e., no bonding). Application of existing empirical correlations in soils that are older and/or bonded can produce incorrect interpretations. Hence, it is important to be able to identify soils with '*unusual*' characteristics (i.e., soils with significant microstructure). The cone resistance (q_t) is a measure of large strain soil strength, and the shear wave velocity (V_s) is a measure of small strain soil stiffness (G_o). Robertson (2016) showed that combining measured V_s with CPT data can be used to identify soils that have significant microstructure, as shown in Figure 34.

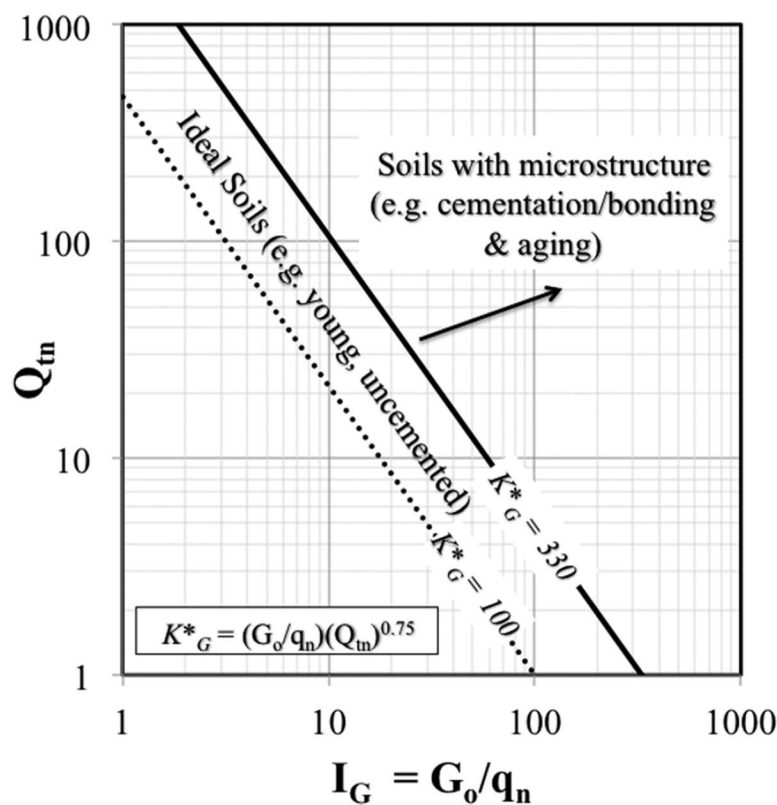


Figure 34. Chart to estimate if soils have significant microstructure

(After Robertson 2016)

Note: $q_n = (q_t - \sigma_{vo})$

The parameter K^*_G (i.e., G_o/q_n when $Q_{tn} = 1.0$) can be defined as a normalized rigidity index:

$$K^*_G = [G_o/q_n] Q_{tn}^{0.75}$$

K^*_G can be used to estimate the magnitude of microstructure. Experience suggests that when $K^*_G < 330$, empirical correlations that are based on soils with little or no microstructure tend to provide reasonable estimates of soil behavior. However, when $K^*_G > 330$ some correlations may require modification to account for microstructure.

Microstructure covers a wide spectrum from none (e.g., freshly deposited soils such as mine tailings, where K^*_G can be close to 100) to extensive (heavily cemented soils such as soft rock, where K^*_G can be as high as 5,000). The average value for uncemented Holocene age soils, that represent most liquefaction case histories, is approximately 200.

K^*_G can also be used to estimate the amount of bonding, represented by a cohesion intercept, c' .

The application of Figure 34 and K^*_G is a more reliable method to estimate the possibility of microstructure than comparing estimated V_s (using Figure 33) with measured V_s , since the databased used to develop Figure 33 contained older Pleistocene-age deposits that likely had some microstructure.

The chart shown in Figure 34 can also be used to estimate G_o , and hence V_s , for a range of soils with different microstructure (or age).

For Holocene-age soils with no microstructure, where the average $K^*_G = 200$, then:

$$(V_s)^2 = 200 q_n (g / \gamma) / (Q_{tn})^{0.75}$$

Where q_n , γ , and g are in consistent units (e.g., q_n in kN/m^2 , γ in kN/m^3 and g in m/s^2 to give V_s in m/s).

Hydraulic Conductivity (k)

An approximate estimate of soil hydraulic conductivity or coefficient of permeability, k , can be made from an estimate of soil behavior type using the CPT SBT charts. Table 6 provides estimates based on the CPT-based SBT charts shown in Figures 23. These estimates are approximate at best but can provide a guide to variations of possible permeability.

SBT Zone	SBT	Range of k (m/s)	$SBT_n I_c$
1	Sensitive fine-grained	3×10^{-10} to 3×10^{-8}	NA
2	Organic soils - clay	1×10^{-10} to 1×10^{-8}	$I_c > 3.60$
3	Clay	1×10^{-10} to 1×10^{-9}	$2.95 < I_c < 3.60$
4	Silt mixture	3×10^{-9} to 1×10^{-7}	$2.60 < I_c < 2.95$
5	Sand mixture	1×10^{-7} to 1×10^{-5}	$2.05 < I_c < 2.60$
6	Sand	1×10^{-5} to 1×10^{-3}	$1.31 < I_c < 2.05$
7	Dense sand to gravelly sand	1×10^{-3} to 1	$I_c < 1.31$
8	*Very dense/ stiff soil	1×10^{-8} to 1×10^{-3}	NA
9	*Very stiff fine-grained soil	1×10^{-9} to 1×10^{-7}	NA

*Overconsolidated and/or cemented

Table 6 Estimated soil permeability (k) based on the CPT SBT chart by Robertson (2010) shown in Figures 23

Robertson (2010) suggested that the average relationship between soil permeability (k) and $SBT_n I_c$, shown in Table 6, can be represented by:

$$\text{When } 1.0 < I_c \leq 3.27 \quad k = 10^{(0.952 - 3.04 I_c)} \quad \text{m/s}$$

$$\text{When } 3.27 < I_c < 4.0 \quad k = 10^{(-4.52 - 1.37 I_c)} \quad \text{m/s}$$

The above relationships can be used to provide an approximate estimate of soil permeability (k) and to show the likely variation of soil permeability with depth from a CPT sounding. Since the normalized CPT parameters (Q_{tn} and F_r) respond to the mechanical behavior of the soil and depend on many soil variables, the suggested relationship between k and I_c is approximate and should only be used as a guide.

Robertson et al. (1992) presented a summary of available data to estimate the horizontal coefficient of permeability (k_h) from dissipation tests using t_{50} . Since the relationship is also a function of the soil stiffness, Robertson (2010) updated the relationship as shown in Figure 35.

Jamiolkowski et al. (1985) suggested a range of possible values of k_h/k_v for soft clays as shown in Table 7.

Nature of clay	k_h/k_v
No macrofabric, or only slightly developed macrofabric, essentially homogeneous deposits	1 to 1.5
From fairly well- to well-developed macrofabric, e.g. sedimentary clays with discontinuous lenses and layers of more permeable material	2 to 4
Varved clays and other deposits containing embedded and more or less continuous permeable layers	3 to 10

Table 7 Range of possible field values of k_h/k_v for soft clays
(Modified from Jamiolkowski et al., 1985)

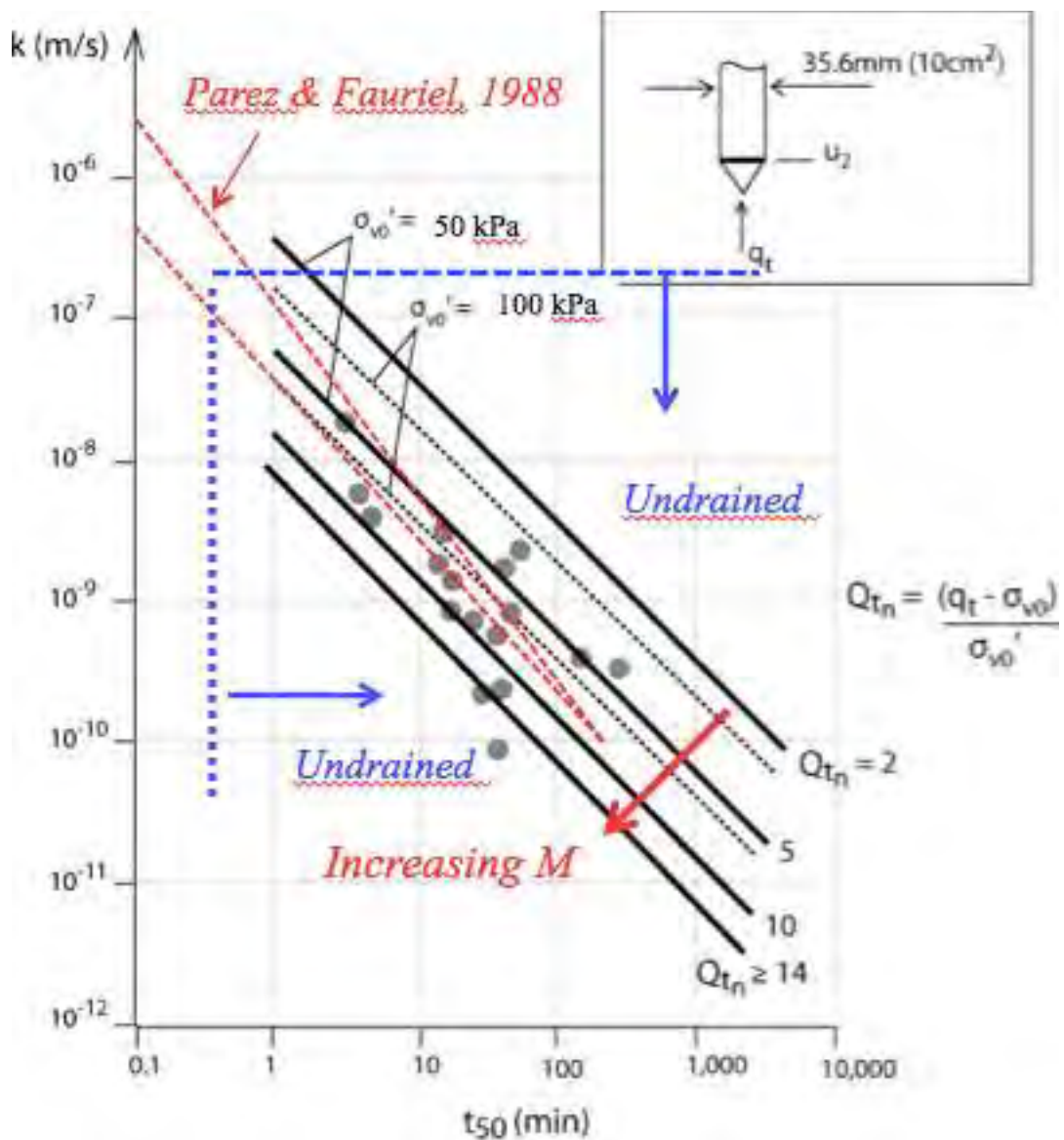


Figure 35. Relationship between CPTu t_{50} (in minutes), based on u_2 pore pressure sensor location and 10cm^2 cone, and soil permeability (k_h) as a function of normalized cone resistance, Q_{tn} (after Robertson 2010)

Consolidation Characteristics

Flow and consolidation characteristics of a soil are normally expressed in terms of the coefficient of consolidation, c , and hydraulic conductivity, k . They are inter-linked through the formula:

$$c = \frac{k M}{\gamma_w}$$

Where: M is the 1-D constrained modulus relevant to the problem (i.e., unloading, reloading, virgin loading).

The parameters c and k vary over many orders of magnitude and are some of the most difficult parameters to measure in geotechnical engineering. It is often considered that an accuracy within one order of magnitude is acceptable. Due to soil anisotropy, both c and k have different values in the horizontal (c_h , k_h) and vertical (c_v , k_v) direction. The relevant design values depend on drainage and loading direction.

Details on how to estimate k from CPT soil behavior type charts are given in the previous section.

The coefficient of consolidation can be estimated by measuring the dissipation or rate of change of pore pressure with time after a stop in CPT penetration, as illustrated in Figure 19. Many theoretical solutions have been developed for deriving the coefficient of consolidation from CPT pore pressure dissipation data. The coefficient of consolidation can be interpreted at 50% dissipation, using the following basic formula:

$$c = \left(\frac{T_{50}}{t_{50}} \right) r_o^2 (I_r)^{0.5}$$

where:

- T_{50} = theoretical time factor
- t_{50} = measured time for 50% dissipation
- r_o = penetrometer radius
- I_r = soil rigidity index = G/s_u

It is clear from this formula that the dissipation time is inversely proportional to the radius of the probe. Hence, in soils of very low permeability, the time for dissipation can be decreased by using smaller diameter probes. Robertson et al. (1992) reviewed dissipation data from around the world and compared the results with the leading theoretical solution by Teh and Housby (1991), as shown in Figure 36.

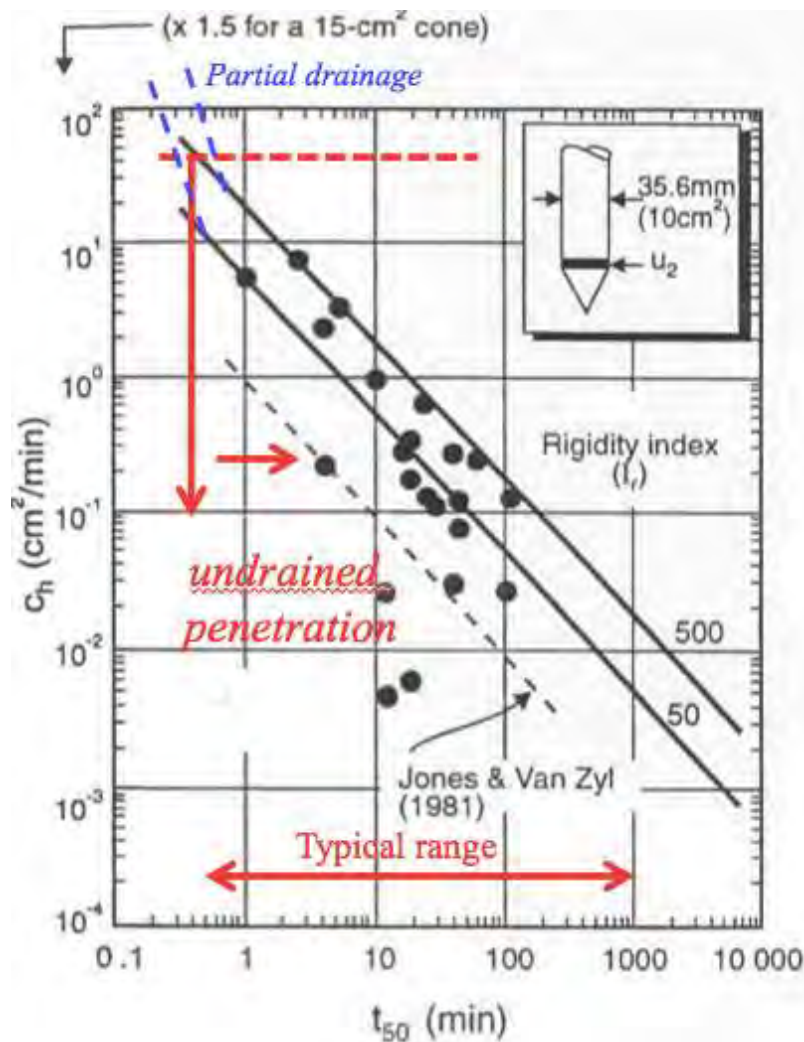


Figure 36. Average laboratory c_h values and CPTU results
(after Robertson et al., 1992, Teh and Housby theory shown as solid lines for $I_r = 50$ and 500).

The review showed that the theoretical solution provided reasonable estimates of c_h . The solution and data shown in Figure 36 apply to a pore pressure sensor located just behind the cone tip (i.e., u_2)

The Teh and Houlsby solution (with t_{50} in mins) can be approximated to (for $I_r \sim 200$):

$$c_h = (1.67 \times 10^{-6}) 10^{(1 - \log t_{50})} \quad \text{m}^2/\text{s}$$

The pore pressures around an advancing cone are complex and depend on soil stress history, sensitivity, anisotropy, dilatancy and structure, as illustrated in Figure 37.

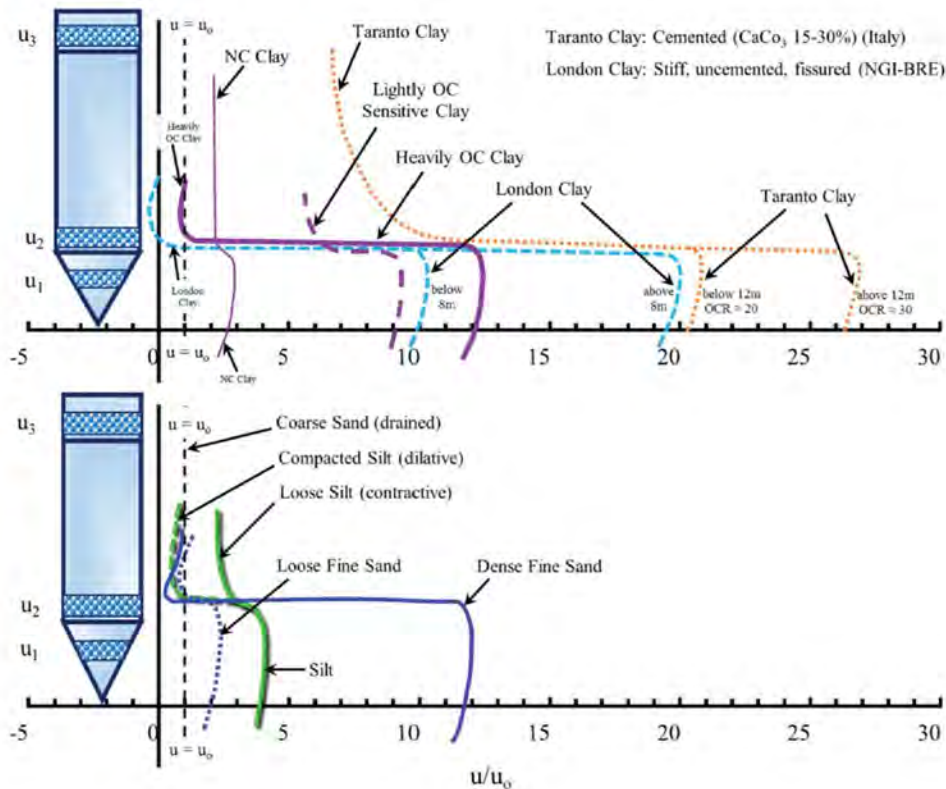


Figure 37. Example variation in pore pressures around an advancing cone
(After Robertson et al., 1986)

Figure 37 shows that in fine-grained soils (where the penetration process is undrained) that are dilative at large strains (e.g., overconsolidated clay with $OCR > 5$), the pore pressures at the u_2 location can be negative of the equilibrium pressure (u_0). At shallow depths onshore, this can result in negative pore pressures up to a maximum of about -100kPa (-15psi), after which the pore pressure element will become unsaturated due to air bubbles caused by cavitation. The large difference between the pore pressures on the face of the cone (u_1) and behind the cone (u_2) can result in an initial increase in the u_2 pore pressures during a

dissipation test due to the local redistribution or pore pressures around the cone before radial dissipation dominates. Care is required to ensure that the dissipation is continued to the correct equilibrium (u_o) and not stopped prematurely after the initial rise. In these cases, the pore pressure sensor can be moved to the face of the cone (u_1) or the t_{50} time can be estimated using the maximum pore pressure as the initial value.

Based on available experience, the CPT dissipation method should provide estimates of c_h to within \pm half an order of magnitude. However, the technique is repeatable and provides an accurate measure of changes in consolidation characteristics within a given soil profile. Rates of dissipation can also be influenced by adjacent soil layers of different permeability.

An approximate estimate of the coefficient of consolidation in the vertical direction can be obtained using the ratios of permeability in the horizontal and vertical direction given in the section on hydraulic conductivity, since:

$$c_v = c_h \left(\frac{k_v}{k_h} \right)$$

Table 7 can be used to provide an estimate of the ratio of hydraulic conductivities.

For relatively short dissipations, the dissipation results can be plotted on a square-root time scale. The gradient of the initial straight line is m , where:

$$c_h = (m/M_T)^2 r^2 (I_r)^{0.5}$$

$M_T = 1.15$ for u_2 position and 10cm^2 cone (i.e., $r = 1.78\text{ cm}$).

Constrained Modulus

Consolidation settlements can be estimated using the 1-D Constrained Modulus, M, where:

$$M = 1/m_v = \delta\sigma_v / \delta\varepsilon = 2.3 (1+e_0) \sigma'_{vo} / C_c$$

Where m_v = equivalent oedometer coefficient of compressibility.

Constrained modulus can be estimated from CPT results using the following empirical relationship:

$$M = \alpha_M (q_t - \sigma_{vo})$$

Sangrelat (1970) suggested that α_M varies with soil plasticity and natural water content for a wide range of fine-grained soils and organic soils, although the data were based on q_c . Meigh (1987) suggested that α_M lies in the range 2 – 8, whereas Mayne (2001) suggested a general value of 5. Robertson (2009) suggested that α_M varies with Q_t , such that:

When $I_c > 2.2$ (fine-grained soils) use:

$$\alpha_M = Q_t \quad \text{when } Q_t < 14$$

$$\alpha_M = 14 \quad \text{when } Q_t > 14$$

When $I_c < 2.2$ (coarse-grained soils) use:

$$\alpha_M = 0.0188 [10^{(0.55I_c + 1.68)}]$$

Robertson (2009) suggested a factor $\alpha_m = 0.03$, but experience shows that a factor of 0.0188 provides a slightly more conservative estimate of M when $I_c < 2.2$ and is consistent with the observation by Mayne (2001) that $M \sim G_o$ in sands. Estimates of drained 1-D constrained modulus from undrained cone penetration will always be approximate. Estimates can be improved with additional information about the soil, such as plasticity index, natural water content and shear wave velocity. Also α_M can be lower in organic soils and soils with high water content.

Applications of CPT Results

The previous sections have described how CPT results can be used to estimate geotechnical parameters that can be used as input in analyses. An alternate approach is to apply the in-situ test results directly to an engineering problem. A typical example of this approach is the evaluation of pile capacity directly from CPT results without the need for soil parameters.

As a guide, Table 8 shows a summary of the applicability of the CPT for direct design applications. The ratings shown in the table have been assigned based on current experience and represent a qualitative evaluation of the confidence level assessed to each design problem and general soil type. Details of ground conditions and project requirements can influence these ratings.

In the following sections several direct applications of CPT/CPTu results are described. These sections are not intended to provide full details of geotechnical design, since this is beyond the scope of this guide. However, they do provide some guidelines on how the CPT can be applied to many geotechnical engineering applications. A good reference for foundation design is the Canadian Foundation Engineering Manual (CFEM, 2006, <https://www.karma-link.ca/shop>). Dr. Bengt Fellenius also has a good book on Basics of Foundation Design that can be downloaded from <https://www.fellenius.net/papers.html>.

Type of soil	Pile design	Bearing capacity	Settlement*	Compaction control	Liquefaction
Sand	1 – 2	1 – 2	2 – 3	1 – 2	1 – 2
Clay	1 – 2	1 – 2	2 – 3	3 – 4	1 – 2
Intermediate soils	1 – 2	2 – 3	2 – 4	2 – 3	1 – 2

Reliability rating: 1=High; 2=High to moderate; 3=Moderate; 4=Moderate to low; 5=low

* improves with SCPT data

Table 8 Perceived applicability of the CPT/CPTU for various direct design problems

Shallow Foundation Design

General Design Principles

Typical Design Sequence:

1. Select minimum depth to protect against:
 - external agents: e.g., frost, erosion, trees
 - poor soil: e.g., fill, organic soils, etc.
2. Define minimum area necessary to protect against soil failure:
 - perform bearing capacity analyses
2. Compute settlement and check if acceptable
3. Modify selected foundation if required.

Typical Shallow Foundation Problems

Study of 1200 cases of foundation problems in Europe showed that the problems could be attributed to the following causes:

- 25% footings on recent fill (mainly poor engineering judgment)
- 20% differential settlement (50% could have been avoided with good design)
- 20% effect of groundwater
- 10% failure in weak layer
- 10% nearby work (excavations, tunnels, etc.)
- 15% miscellaneous causes (earthquake, blasting, etc.)

In design, ***settlement*** is generally the ***critical*** issue. Bearing capacity is generally not of prime importance.

Construction

Construction details can significantly alter the conditions assumed in the design.

Examples are provided in the following list:

- During Excavation
 - bottom heave
 - slaking, swelling, and softening of expansive clays or rock

- piping in sands and silts
- remolding of silts and sensitive clays
- disturbance of granular soils
- Adjacent construction activity
 - groundwater lowering
 - excavation
 - pile driving
 - blasting
- Other effects during or following construction
 - reversal of bottom heave
 - scour, erosion, and flooding
 - frost action

Shallow Foundation - Bearing Capacity

General Principles

Load-settlement relationships for typical footings (Vesic, 1972):

1. Approximate elastic response
2. Progressive development of local shear failure
3. General shear failure

In dense coarse-grained soils failure typically occurs along a well-defined failure surface. In loose coarse-grained soils, volumetric compression dominates and punching failures are common. Increased depth of overburden can change a dense (dilative) sand to behave more like loose (contractive) sand. In (homogeneous) fine-grained cohesive soils, failure occurs along an approximately circular surface.

Significant parameters are:

- nature of soils
- density and resistance of soils
- width and shape of footing
- depth of footing
- position of load.

A given soil does not have a unique bearing capacity; the bearing capacity is a function of the footing shape, depth, and width as well as load eccentricity.

General Bearing Capacity Theory

Initially developed by Terzaghi (1936); there are now over 30 theories with the same general form, as follows:

Ultimate bearing capacity, (q_f):

$$q_f = 0.5 \gamma B N_\gamma s_\gamma i_\gamma + c N_c s_c i_c + \gamma D N_q s_q i_q$$

where:

- $N_\gamma N_c N_q$ = bearing capacity coefficients (function of ϕ')
- $s_\gamma s_c s_q$ = shape factors (function of B/L)
- $i_\gamma i_c i_q$ = load inclination factors
- B = width of footing
- D = depth of footing
- L = length of footing

Complete rigorous solutions are impossible since stress fields are unknown. All theories differ in simplifying assumptions made to write the equations of equilibrium. No single solution is correct for all cases.

Shape Factors

Shape factors are applied to account for 3-D effects. Based on limited theoretical ideas and some model tests, recommended factors are as follows:

$$s_c = s_q = 1 + \left(\frac{B}{L} \right) \left(\frac{N_q}{N_c} \right)$$

$$s_\gamma = 1 - 0.4 \left(\frac{B}{L} \right)$$

Load Inclination Factors

When load is inclined (δ), the shape of a failure surface changes and reduces the area of failure, and hence, a reduced resistance. At the limit of inclination, $\delta = \phi$, $q_f = 0$, since slippage can occur along the footing-soil interface.

In general:

$$i_c = i_q = \left(1 - \frac{\delta}{90^\circ}\right)^2$$

$$i_\gamma = \left(1 - \frac{\delta}{\phi}\right)^2$$

For an eccentric load, Terzaghi proposed a simplified concept of an equivalent footing width, B' .

$$B' = B - 2e$$

where 'e' is the eccentricity. For combined inclined and eccentric load, use B' and relevant values of shape factors. For footings near a slope, use modified bearing capacity factors (e.g., Bowles, 1982). They will be small for clay but large for granular soils.

Effect of Groundwater

The bearing capacity is based on effective stress analysis hence position of the groundwater table affects the value of the soil unit weight.

- If depth to the water table, $d_w = 0$, use γ' in both terms
- If $d_w = D$ (depth of footing), use γ' in width term and γ in depth term.

In general, install drainage to keep $d_w > D$.

Indirect Methods Based on Soil Parameters

Granular, coarse-grained soils

Bearing capacity is generally not calculated, since settlements control, except for very narrow footings.

Cohesive, fine-grained soils

Short-term stability generally controls, hence application of undrained shear strength, s_u .

$$q_f = N_c s_u + \gamma D$$

where:

N_c = function of footing width and shape; for strip footings at the ground surface, $N_c = (\pi + 2)$.

s_u = apply Bjerrum's correction, based on past experience, to field vane shear strength or from CPT.

Allowable bearing capacity:

$$q_{all} = (q_f - \gamma D) / FS$$

$$\text{Hence, } q_{all} = \frac{N_c s_u}{FS}$$

Where: FS is Factor of Safety, typically > 3.0 .

Use a high FS to account for limitations in theory, underestimation of loads, overestimation of soil strength, avoid local yield in soil and keep settlements small.

Direct Approach to estimate Bearing Capacity (In-Situ Tests)

Based on in-situ tests, theory, model tests and past foundation performance.

SPT

- Empirical direct methods
- Limited to granular soils, however, sometimes applied to very stiff clays
- Often linked to allowable settlement of 25mm (Terzaghi & Peck)
- SPT of poor reliability, hence, empirical methods tend to be very conservative

CPT

Empirical direct methods:

Granular, coarse-grained soils:

$$q_f = K_\phi q_{c(av)}$$

where:

$q_{c(av)}$ = average CPT penetration resistance below depth of footing, $z = B$

Eslaamizaad & Robertson (1996) suggested $K_\phi = 0.16$ to 0.30 depending on B/D and shape. In general, assume $K_\phi = 0.16$ for settlement ratio of $s/B = 0.1$. Lehane (2019) also suggested $K_\phi = 0.16$ for assessing foundation capacity at $s/B = 0.1$ (see Figure 38). In general, settlement will control design.

Cohesive, fine-grained soils:

$$q_f = K_{su} q_{c(av)} + \gamma D$$

$K_{su} = 0.30$ to 0.60 depending on footing B/D and shape and soil OCR and sensitivity for $s/B = 0.1$ (Figure 38). In general, assume $K_{su} = 0.30$ in clay for a conservative estimate.

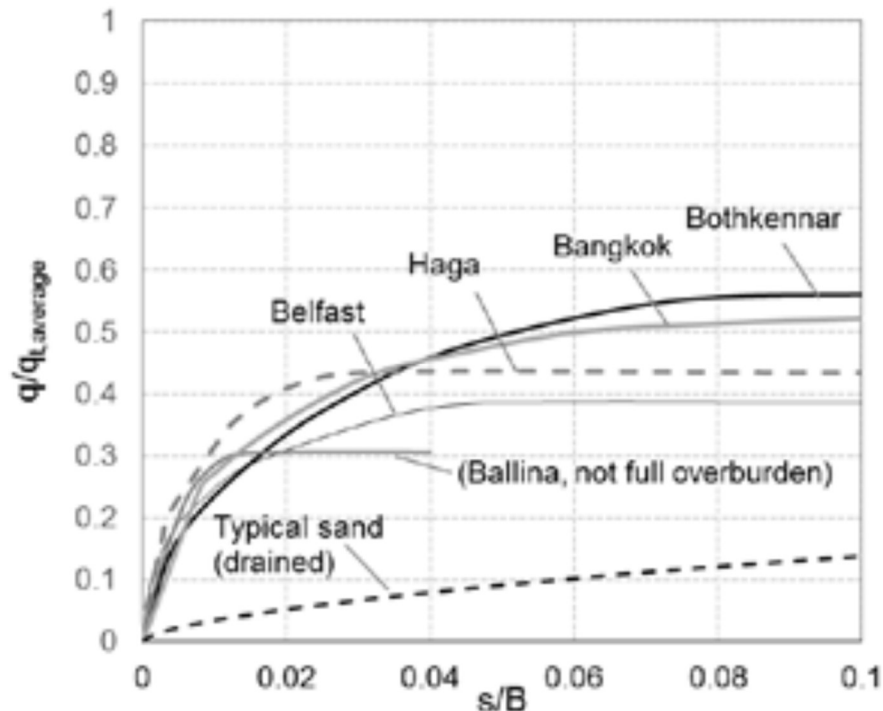


Figure 38. Field data for mobilized bearing stress vs settlement ratio (s/B) for footing on clay (Lehane (2017))

Shallow Foundation Design – Settlement

General Design Principles

Requires:

- magnitude of settlement
- rate of settlement
- compatibility with acceptable behavior of building

For well-designed foundations, the magnitude of strains in the ground is generally very small ($\varepsilon < 10^{-1} \%$). Hence, ground response is approximately elastic (non-linear elastic).

Granular coarse-grained soils

Coarse-grained soils have high permeability, thus immediate settlements. However, long term settlements can occur due to submergence, change in water level, blasting, machine vibration or earthquake loading.

Cohesive fine-grained soils

Fine-grained soils have very low permeability, thus the need to consider magnitude and duration of settlement.

In soft, normally to lightly overconsolidated clays, 80% to 90% of settlement is due to primary consolidation. Secondary settlement also can be large. In stiff, overconsolidated clays ($OCR > 4$), approximately 50% of settlement can be due to immediate distortion settlement and secondary settlement is generally small.

Methods for granular coarse-grained soils

Due to difficulty in sampling, most methods are based on in-situ tests, either direct or via estimate of equivalent elastic modulus (E').

For most tests, the link between test result and modulus is empirical, since it depends on many variables, e.g., mineralogy, stress history, stress state, age, cementation, etc.

CPT

Meyerhof (1974) suggested that the total settlement, s , could be calculated using the following formula:

$$s = \frac{\Delta p B}{2q_{c(av)}}$$

where:

- Δp = net footing pressure
- B = footing width
- $q_c \text{ (av)}$ = average CPT penetration resistance below depth of footing,
- z = B

Schmertmann (1970) recommended using the following equation:

$$s = C_1 C_2 \Delta p \sum \left(\frac{I_z}{C_3 E'} \right) \Delta z$$

where:

C_1 = correction for depth of footing

$$= 1 - 0.5(\sigma'_1 / \Delta p)$$

C_2 = correction for creep and cyclic loading

$$= 1 + 0.2 \log (10 t_{\text{yr}})$$

C_3 = correction for shape of footing

= 1.0 for circular footings

= 1.2 for square footings

= 1.75 for strip footings

σ'_1 = effective overburden pressure at footing depth (see Figure 38)

Δp = net footing pressure

t_{yr} = time in years since load application

I_z = strain influence factor (see Figure 39)

Δz = thickness of sublayer

E' = Equivalent Young's modulus = $\alpha_E q_c$

α_E = function of degree of loading, soil density, stress history, cementation, age, grain shape and mineralogy (e.g. Figure 40)

= 2 to 4 for very young, normally consolidated sands;

= 4 to 10 for aged ($> 1,000$ years), normally consolidated sands;

= 6 to 20 for overconsolidated sands

q_c = average CPT resistance for sublayer

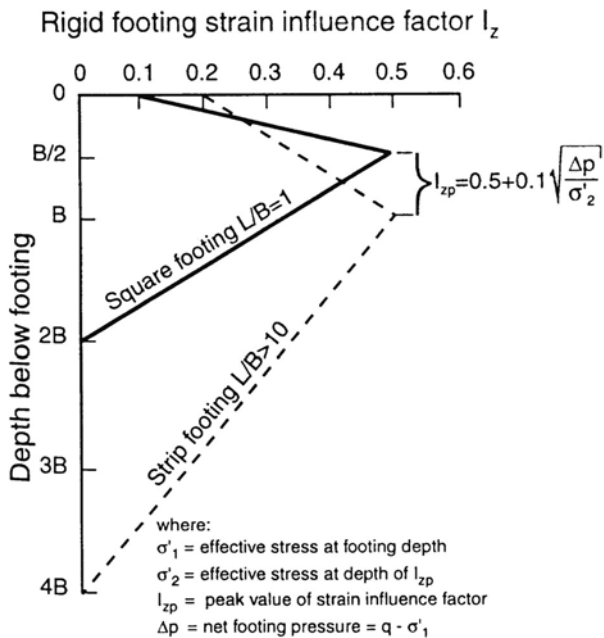
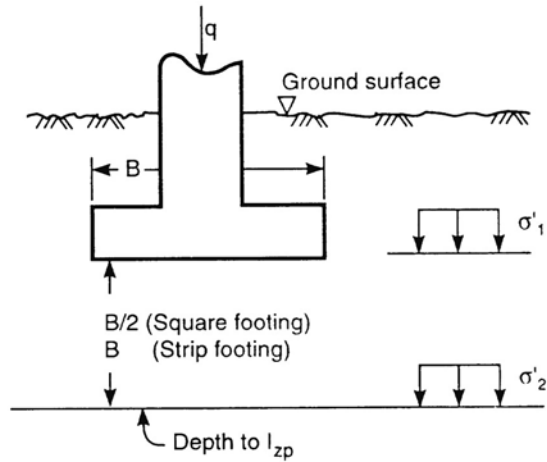
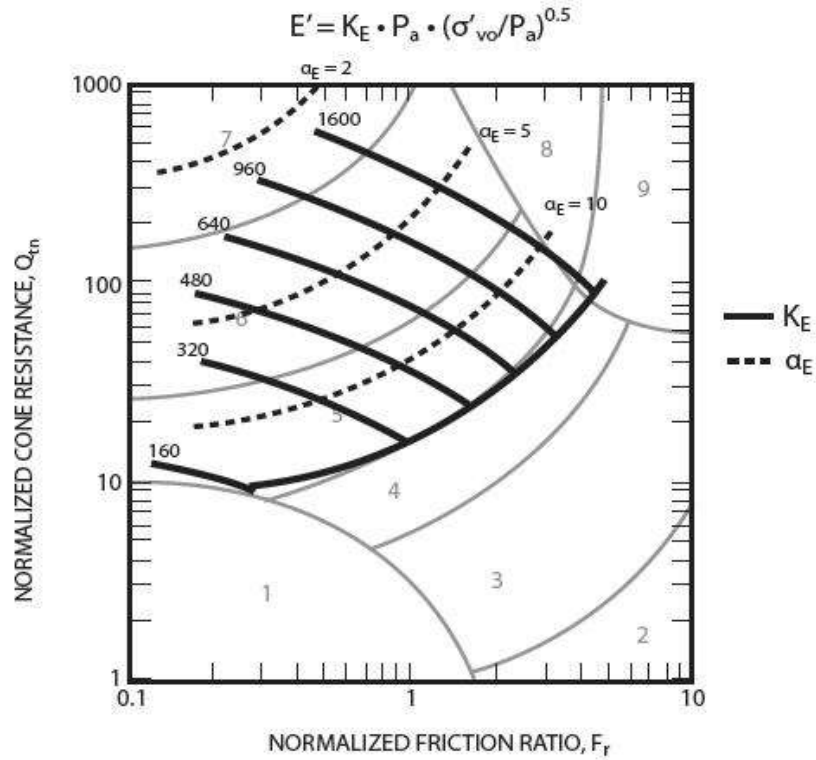


Figure 39. Strain influence method for footings on sand
(Schmertmann, 1970)

In this method, the sand is divided into several layers, n , of thickness, Δz , down to a depth below the base of the footing equal to $2B$ for a square footing and $4B$ for a strip footing (length of footing, $L > 10B$). A value of q_c is assigned to each layer. Note in sandy soils $q_c = q_t$. The method by Schmertmann (1970) only applies to clean sands and is difficult to apply in interlayered deposits.



$$E' = \alpha_E \cdot (q_t - \sigma_{vo})$$

Figure 40. Evaluation of drained Young's modulus from CPT for uncemented sandy soils, $E = \alpha_E (q_t - \sigma_{vo})$

$$\text{Where: } \alpha_E = 0.015 [10^{(0.55l_c + 1.68)}]$$

Based on a review of 30 full-size footing tests on 12 different sands, Mayne and Illingsworth (2010) suggested the following simple relationship (see Figure 38):

$$\frac{q_{\text{applied}}}{q_c} = \frac{3}{5} \cdot \sqrt{\frac{s}{B}}$$

where:

q_{applied} = applied footing stress

q_c = average cone resistance within 1.5B below footing

The method by Mayne and Illingsworth (2010) is simple to apply and provides a reasonable estimate of settlements of footings on sand, provide the sand has little or no microstructure.

Seismic Shear Wave Velocity

For soils that have microstructure, the settlement of footings can be made based on measured shear wave velocity (V_s), since this is a direct measure of soil stiffness. Eslaamizaad and Robertson (1996) suggested using V_s to determine the small strain stiffness (G_o) directly and applying it to settlement calculations, as follows:

$$G_o = \frac{\gamma}{g} (V_s)^2$$

The equivalent Young's modulus (E') can be estimated as follows:

$$E' = 2(1 + \nu)\psi G_o \approx 2.6\psi G_o$$

where:

Ψ = a function of the degree of loading and stress history (see Figure 41).

Fahey, (1998) suggested that the variation of ψ could be defined by:

$$\psi = G/G_o = 1 - f(q/q_{ult})^g$$

Mayne (2005) suggested that values of $f = 1$ and $g = 0.3$ are appropriate for uncemented soils that are not highly structured, and these values agree well with the NC relationship shown in Figure 41. Hence,

$$E' = 0.047 [1 - (q/q_{ult})^{0.3}] [10^{(0.55I_c + 1.68)}] (q_t - \sigma_{vo})$$

Since settlement is a function of degree of loading (q/q_{ult}), it is possible to calculate the load settlement curve, using a range of E' values as function of (q/q_{ult}) :

$$s = \left(\frac{\Delta p B}{E'} \right) i_c$$

where: i_c = influence coefficient

In general, for most well designed shallow foundations, $q/q_{ult} = 0.3$ (i.e., $FS > 3$), then $\Psi \sim 0.3$, hence, $E' \approx G_o$.

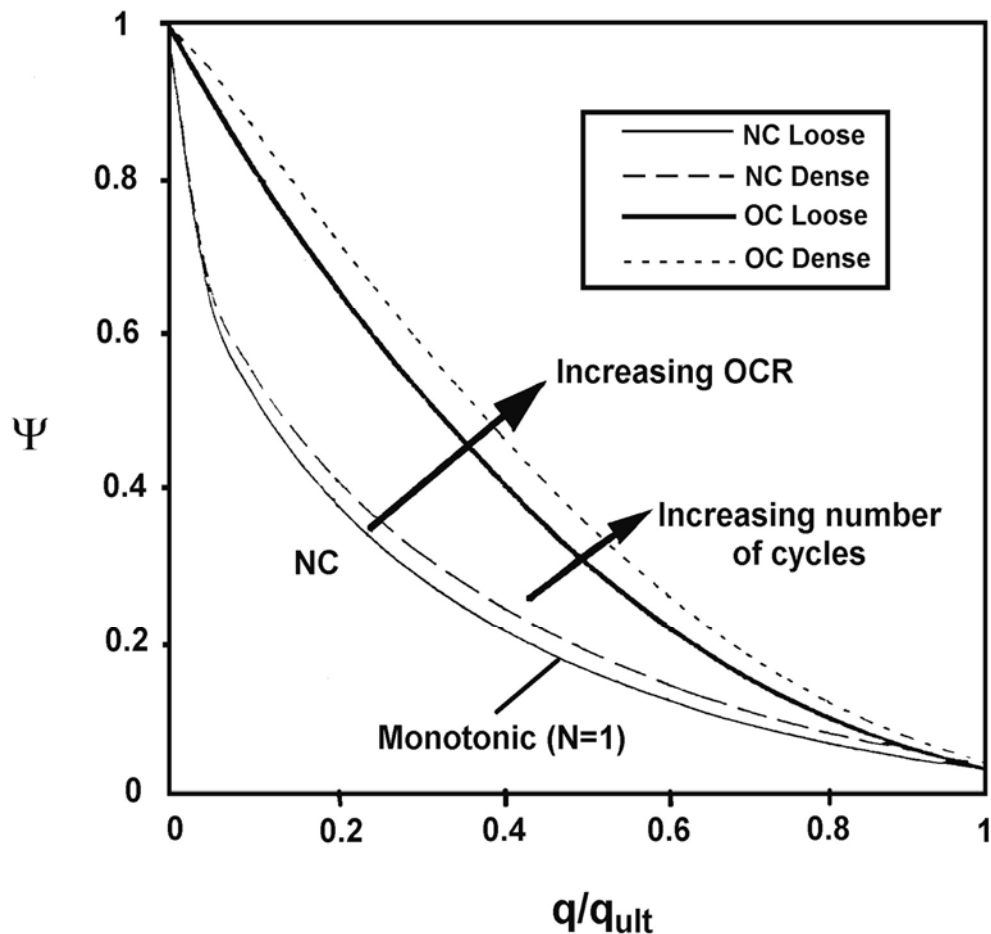


Figure 41. Factor Ψ versus q/q_{ult} for sands with various densities and stress histories

Shear wave velocity has the advantage of providing a direct measure of soil stiffness without an empirical correlation. The only empiricism required is to adjust the small strain modulus for effects of stress level and strain level below the footing. The shear wave velocity approach can also be applied to estimate settlements in very stiff clays where consolidation settlements are very small.

Methods for cohesive fine-grained soils

The key parameter is the preconsolidation pressure, σ'_p , or yield stress (σ'_y). This can be measured in the laboratory on high quality samples. However, OCR and σ'_p profiles can be estimated from the CPT. It is useful to link results from high quality laboratory tests with continuous profiles of the CPT.

In general, to keep settlements small, the applied stress must be $< \sigma'_p$. In soft ground this may require some form of ground improvement.

Components of settlement are:

s_i = immediate (distortion) settlement

s_c = consolidation settlement

s_s = secondary time dependent (creep) settlement

Immediate Settlements

Based on elastic theory, Janbu (1963) proposed:

$$s_i = \left(\frac{\Delta p B}{E_u} \right) \mu_o \mu_l$$

where:

B = footing width

Δp = net pressure

E_u = soil modulus (undrained)

μ_o, μ_l = influence factors for depth of footing and thickness of compressible layer

Undrained modulus can be estimated from undrained shear strength (s_u) from either field vane tests and/or the CPT but requires knowledge of soil plasticity.

$$E_u = n \cdot s_u$$

Where: n varies from 40 to 1000, depending on degree of loading and plasticity of soil (see Figure 42).

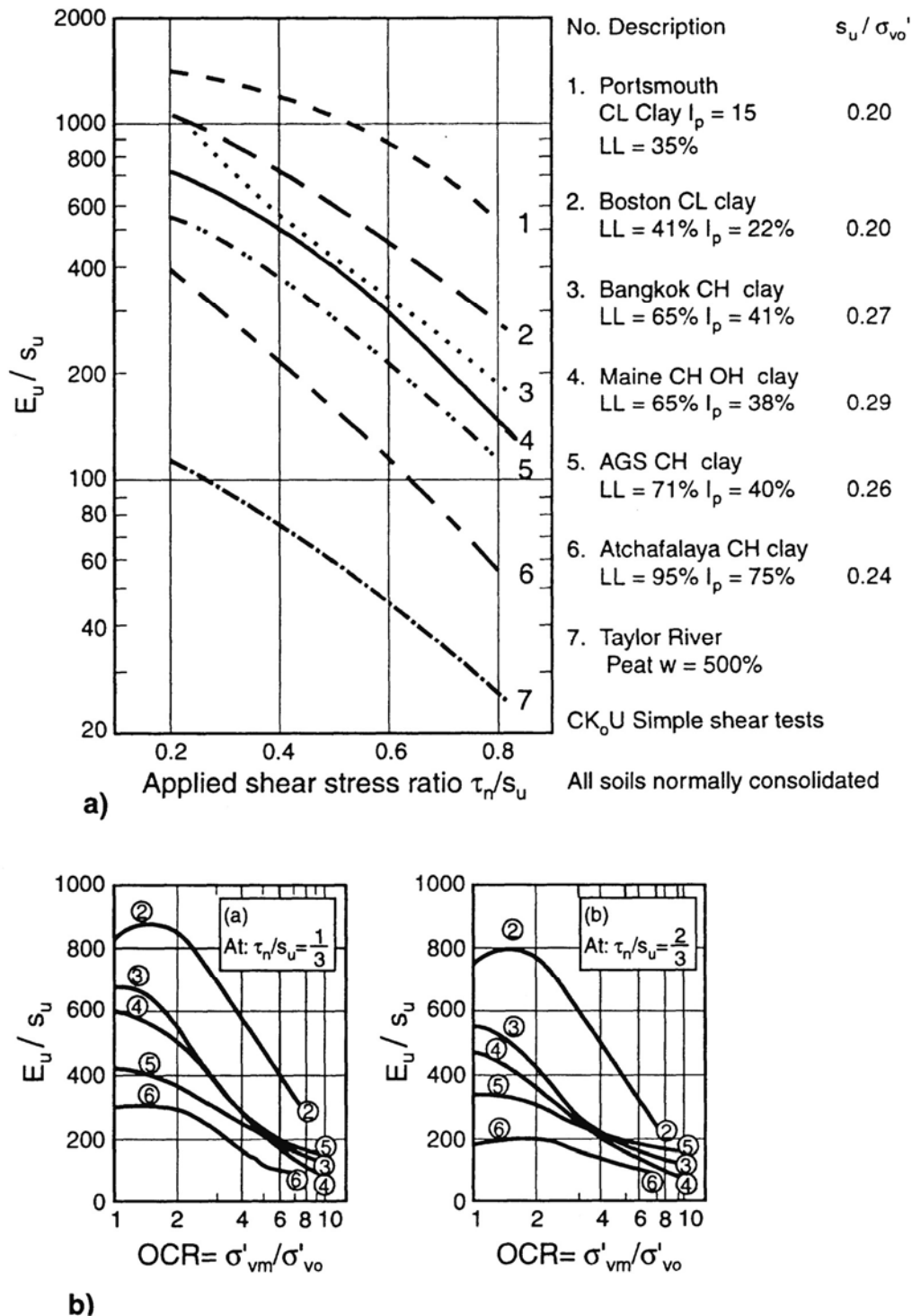


Figure 42. Selection of soil stiffness ratio for clays
(after Ladd et al., 1977)

Consolidation Settlements

Terzaghi's 1-D theory of consolidation often applies, since 2- and 3-D effects are often small. Settlement for a wide range of footings and soils can be calculated using the 1-D constrained modulus, M, using:

$$\varepsilon_{\text{vol}} = (\Delta\sigma'_v / M)$$

Hence, $s = (\Delta\sigma'_v / M) H$

The 1-D Constrained Modulus (M) can be estimated from the CPT using:

$$M = \alpha_M (q_t - \sigma_{vo})$$

When $I_c > 2.2$ (fine-grained soils) use:

$$\alpha_M = Q_t \quad \text{when } Q_t < 14$$

$$\alpha_M = 14 \quad \text{when } Q_t > 14$$

When $I_c < 2.2$ (coarse-grained soils) use:

$$\alpha_M = 0.0188 [10^{(0.55I_c + 1.68)}]$$

The above approach can be applied to all soils, since M can be estimated for a wide range of soils. The above approach is simpler than the Schmertmann (1970) approach that is limited to sands. When using CPT results, the settlement can be calculated over each depth increment and the total settlement becomes the summation over the full depth. The above approach, based on 1-D constrained modulus, M, is often suitable for many projects. Care is required when applying the above approach to lightly overconsolidated soils if loading will significantly exceed σ'_p .

Rate of settlement is important, hence, the need for coefficient of consolidation, c_v . Experience shows that c_v can be highly variable due to non-linearity of the stress-strain relationship as well as change in permeability as soils compress. Values of c_v can be best estimated either:

1. Separately from 1-D constrained modulus, M (or m_v , since $M = 1/m_v$) from oedometer tests on high quality samples and permeability, k from in-situ tests, using:

$$c_v = \frac{k M}{\gamma_w}$$

or

2. Directly from CPTu dissipation tests.

c_v values vary by orders of magnitude, hence, accuracy of the calculation is generally very poor. Drainage conditions play a major role yet are difficult to identify. The CPTu can provide an excellent picture of the drainage conditions. Avoid a design that *depends* on the time-settlement relationship. For settlement sensitive structures, try to minimize differential settlements (e.g., Osaka Airport - mechanical adjustments due to very large long-term settlements).

Secondary Settlements

Time dependent settlements depend on soil mineralogy and degree of loading. Organic soils can have high secondary settlement. In general, avoid soils with high secondary settlements. Mesri, (1994) suggested a simplified approach that links coefficient of secondary consolidation (C_α) and compression index, C_c , for inorganic clays and silts, as follows:

$$C_\alpha = 0.04 \left(\frac{C_c}{1 + e_o} \right) \sim 0.1 (\sigma'_v / M)$$

Long term secondary (creep) settlement, s_s is then:

$$s_s = C_\alpha \Delta z \log(t/t_p)$$

where t_p is duration of primary consolidation.

Provided that the applied stress is less than 80% of σ'_p , secondary consolidation is generally small. The 1D constrained modulus, M can be estimated from the CPT (see earlier section).

Allowable Settlements

Loads considered in settlement analyses depend on the nature of soil and time-dependence of settlement. Differential settlements generally control.

Sands

- Load: maximum possible load due to immediate settlement
- Differential settlement: can be up to 100% of maximum settlement due to natural variability of sand. Typically, less than or equal to 25mm (1 inch)

Clays

- Load: dead load plus % of live load (LL) depending on duration of live load
 - 50% of LL for buildings
 - 30% of LL for bridges
 - 75% of LL for reservoirs
- Settlements: are more uniform and can be larger than 25mm (1 inch)

Typical Design Sequence

1. Check for possible isolated footing design
2. Check for possible raft foundation
3. Ground improvement
4. Deep foundations

Raft Foundations

Consider a raft when:

- Area of footing > 50% of building area
- Need to provide underground space in location of high groundwater
- Need to reduce magnitude of total settlements (i.e. floating foundation)
- Need to reduce differential settlements

A raft is an inverted slab, designed to distribute structural loads from columns and walls, while keeping deformations within acceptable limits.

The structural characteristics of a raft foundation can be optimized by accounting for the interaction between the raft and supporting ground. Structural engineers usually perform an elastic analysis using elastic (Winkler) springs. Hence, they would like the spring constant, k_s .

k_s = coefficient of subgrade reaction (kN/m^3)

$$k_s = \frac{p}{s}$$

where:

p = net applied stress

s = settlement resulting from applied stress, p

The process is governed by the relative stiffness of the structure and the ground. The coefficient of subgrade reaction is not a soil parameter since it depends on the size of the footing and degree of loading. Often estimates are made from global tables (e.g., Terzaghi; see Table 9). However, it is best to obtain estimates based on in-situ testing.

Soil type	Subgrade reaction (kN/m^3)
Loose sand	5,000 – 16,000
Medium dense sand	10,000 – 80,000
Dense sand	60,000 – 125,000
Clayey sand	30,000 – 80,000
Silty sand	20,000 – 50,000
Clayey soil: $s_u < 50 \text{ kPa}$	10,000 – 20,000
$50 \text{ kPa} < s_u < 100 \text{ kPa}$	20,000 – 50,000
$100 \text{ kPa} < s_u$	>50,000

Table 9 Recommended coefficient of subgrade reaction (k_s) for different soil types (Terzaghi, 1955)

Plate Load Tests (PLT)

Plate load tests can provide a direct measure of the relationship between p and s , but size effects can dominate results. Terzaghi (1955) suggested a link between a 1-foot square plate (k_{s1}) and the width of footing B , as follows:

$$k_s = k_{s1} \left(\frac{B + 1}{2B} \right)^2$$

However, there is very large scatter in the results, due to variability in ground stiffness with depth.

Shear Wave Velocity (V_s)

Based on work by Vesic (1961) and elastic theory, the modulus of subgrade reaction is:

$$k'_s = 0.65 \sqrt[12]{\frac{E B^4}{E_f I_f}} \left(\frac{E}{1 - v^2} \right)$$

where:

- E = modulus of elasticity of soil
- E_f = modulus of elasticity of footing
- B = footing width
- I_f = moment of inertia
- v = Poisson's ratio for soil
- k'_s = modulus of subgrade reaction:

$$k'_s = k_s B$$

For most values of E_s and E_f , the expression simplifies to:

$$k'_s \approx \left(\frac{E}{1 - v^2} \right)$$

Bowles (1974) suggested:

$$k_s = 120 q_{all}$$

where q_{all} is in kPa and k_s is in kN/m³.

It is possible to estimate E from shear wave velocity, V_s . The small strain shear modulus is given by the following:

$$G_o = \frac{\gamma}{g} (V_s)^2$$

In addition:

$$G_{eq} = \Psi G_o$$

and

$$E = 2(1 + v) G_{eq}$$

Since $v \approx 0.2$ to 0.3 ,

$$k'_s = k_s B \approx 2.9 \Psi G_o$$

Hence:

$$k_s \approx 2.9 \Psi \frac{\frac{\gamma}{g} (V_s)^2}{B}$$

where:

Ψ = a function of the degree of loading and stress history (see Figure 40).

Fahey, (1998) suggested that the variation of ψ could be defined by:

$$\psi = G/G_o = 1 - f(q/q_{ult})^g$$

Mayne (2005) suggested that values of $f = 1$ and $g = 0.3$ are appropriate for most uncemented soils that are not highly structured, and these values agree well with the NC relationship shown in Figure 41. The value of g increases toward a value of 1.0 when the soil is overconsolidated or under increasing number of load cycles.

For most well-designed foundations, $q/q_{ult} = 0.3$ (i.e., $FS > 3$) and hence, $\Psi = 0.3$, then:

$$k_s \approx G_o / B$$

Deep Foundation Design

Piles

Piles can be used to:

- Transfer high surface loads, through soft layers down to stronger layers
- Transfer loads by friction over significant length of soil
- Resist lateral loads
- Protect against scour, etc.
- Protect against swelling soils, etc.

Piles are generally much more expensive than shallow footings.

Types of Piles

Generally classified based on installation method (Weltman & Little, 1977):

- Displacement
 - Preformed
 - Driven Cast-in-place
 - High pressure grouted
- Non/low displacement
 - Mud bored
 - Cased bored
 - Cast-in-place screwed (auger)
 - Helical (screw)

Contractors are developing new pile types and installation techniques constantly to achieve increased capacity and improved cost effectiveness for different ground conditions. Hence, it is difficult to predict capacity and load-settlement response for all piles using simple analytical techniques, since the capacity and load response characteristics can be dominated by the method of installation.

Selection of Pile Type

1. Assess foundation loads
2. Assess ground conditions

3. Are piles necessary?

4. Technical considerations:

- Ground conditions
- Loading conditions
- Environmental considerations
- Site and equipment constraints
- Safety

5. List all technically feasible pile types and rank in order of suitability based on technical considerations

6. Assess cost of each suitable pile type and rank based on cost considerations

7. Assess construction program for each suitable pile type and rank

8. Make overall ranking based on technical, cost and program considerations

General Design Principles

Axial Capacity

The total ultimate pile axial capacity, Q_{ult} , consists of two components: end bearing load (or point resistance), Q_b , and side friction load (sometimes referred to as the shaft or skin friction), Q_s , as follows:

$$Q_{ult} = Q_s + Q_b$$

In sands, the end bearing, Q_b , tends to dominate, whereas in soft clays, the side friction, Q_s , tends to dominate. The end bearing, Q_b , is calculated as the product between the pile end area, A_p , and the unit end bearing, q_p . The friction load, Q_s , is the product between the outer pile shaft area, A_s , by the unit side friction, f_p .

$$Q_{ult} = f_p A_s + q_p A_p$$

Obviously, different f_p values are mobilized along different parts of the pile, so that, in practice, the calculation is performed as a summation of small components. For open-ended piles, some consideration should be made regarding whether the pile is plugged or unplugged (de Ruiter and Beringen, 1979), but the procedure is essentially as outlined above. In general, most pipe piles behave plugged (closed-ended) at working loads but become unplugged (open-ended) at failure. The allowable or design pile load, Q_{all} will be then given by the total ultimate axial capacity divided by a factor of safety. Sometimes separate factors of safety are applied to Q_b and Q_s .

Like shallow footings, capacity is a function of displacement. For piles that derive significant end bearing, axial capacity is often unclear and depends on displacement. Factor of safety applied to an estimated axial capacity has often been used to limit displacements. Ideally deep foundations, like footing, should be designed based on allowable settlement, not capacity.

However, basic approaches to estimate capacity are:

- Static Methods
- Pile Dynamics
- Pile Load Tests

Static Methods

Pseudo-theoretical Approach

Pseudo-theoretical methods are based on shear strength parameters.

Like bearing capacity calculations for shallow foundations - there are over 20 different bearing capacity theories. No single solution is applicable to all piles, and most cannot account for installation technique. Hence, there has been extensive application of in-situ test techniques applied via empirical direct design methods.

The most notable is the application of the CPT, since the CPT is a close model of the pile process. Detailed analysis is generally limited to high-risk pile design, such as large offshore piles.

Effective Stress Approach (β)

The effective stress (β) approach (Burland, 1973), has been very useful in providing insight of pile performance.

Unit side friction, $f_p = \beta \sigma_v'$

Unit end bearing, $q_p = N_t \sigma_b'$

Soil Type	Cast-in-place Piles	Driven Piles
Silt	0.2 - 0.3	0.3 - 0.5
Loose sand	0.2 - 0.4	0.3 - 0.8
Medium sand	0.3 - 0.5	0.6 - 1.0
Dense sand	0.4 - 0.6	0.8 - 1.2
Gravel	0.4 - 0.7	0.8 - 1.5

Table 10 Range of β coefficients: cohesionless soils

Soil Type	Cast-in-place Piles	Driven Piles
Silt	10 - 30	20 - 40
Loose sand	20 - 30	30 - 80
Medium sand	30 - 60	50 - 120
Dense sand	50 - 100	100 - 120
Gravel	80 - 150	150 - 300

Table 11 Range of N_t factors: cohesionless soils

The above coefficients are approximate since they depend on ground characteristics and pile installation details. In the absence of pile load tests assume FS = 3.

Randolph and Wroth (1982) related β to the overconsolidation ratio (OCR) for cohesive soils and produced tentative design charts. In general, for cohesive soils:

$$\beta = 0.25 - 0.32, \text{ and } N_t = 3 - 10$$

Effective stress concepts may not radically change empirical based design rules but can increase confidence in these rules and allow extrapolation to new situations.

Total Stress Approach (α)

It has been common to design piles in cohesive soils based on total stress and undrained shear strength, s_u .

$$\text{Unit side friction, } f_p = \alpha s_u$$

$$\text{Unit end bearing, } q_p = N_t s_u$$

Where α varies from 0.5 - 1.0 depending on OCR and N_t varies from 6 to 9 depending on depth of embedment and pile size.

Empirical Approach

CPT Method

Research has shown (Robertson et al., 1988; Briaud and Tucker, 1988; Tand and Funegard, 1989; Sharp et al., 1988) that CPT methods generally give superior predictions of axial pile capacity compared to most conventional methods. The main reason for this is that the CPT provides a continuous profile of soil response. Almost all CPT methods use reduction factors to measured CPT values. The need for such reduction factors is due to a combination of the following influences: scale effect, rate of loading effects, difference of insertion technique, position of the CPT friction sleeve and differences in horizontal soil displacements. The early work by DeBeer (1963) identified the importance of scale effects. Despite these differences, the CPT is still the test that gives the closest simulation of a pile. Superiority of CPT methods over non-CPT methods has been confirmed in other studies (e.g., O'Neill, 1986).

Many CPT-based pile design methods are available. Many are based on only one pile type (e.g., steel pipe piles) and do not apply to other pile types. Since there are many different pile types available, it is preferred to use a method that is based on full-scale pile load tests on a wide range of pile types and in a wide range of soil conditions. The main CPT method by Bustamante and GIANESELLI (1982 - LCPC Method) is outlined below. The LCPC CPT method is recommended since it provides simple guidance to account for many different pile installation methods and generally provides good estimates of axial capacity of single piles.

LCPC CPT Method (Bustamante and GIANESELLI, 1982)

The method by Bustamante and GIANESELLI was based on the analysis of 197 pile load (and extraction) tests with a wide range of pile and soil types, which may partly explain the good results obtained with the method. The method, also known

as the LCPC method, is summarized in Table 12 and Table 13. The LCPC method was updated with small changes by Bustamante and Frank, (1997)

Nature of soil	q_c (MPa)	Factors k_c	
		Group I	Group II
Soft clay and mud	< 1	0.4	0.5
Moderately compact clay	1 to 5	0.35	0.45
Silt and loose sand	≤ 5	0.4	0.5
Compact to stiff clay and compact silt	> 5	0.45	0.55
Soft chalk	≤ 5	0.2	0.3
Moderately compact sand and gravel	5 to 12	0.4	0.5
Weathered to fragmented chalk	> 5	0.2	0.4
Compact to very compact sand and gravel	> 12	0.3	0.4

Group I: plain bored piles; mud bored piles; micro piles (grouted under low pressure); cased bored piles; hollow auger bored piles; piers; barrettes.

Group II: cast screwed piles; driven precast piles; prestressed tubular piles; driven cast piles; jacked metal piles; micropiles (small diameter piles grouted under high pressure with diameter < 250 mm); driven grouted piles (low pressure grouting); driven metal piles; driven rammed piles; jacket concrete piles; high pressure grouted piles of large diameter.

Table 12 Bearing capacity factors, k_c
(Bustamante and Ganeselli, 1982)

The pile unit end bearing, q_p , is calculated from the calculated equivalent average cone resistance, q_{ca} , multiplied by an end bearing coefficient, k_c (Table 12). The pile unit side friction, f_p , is calculated from measured q_c values divided by a friction coefficient, α_{LCPC} (Table 13).

$$q_p = k_c q_{ca}$$

$$f_p = \frac{q_c}{\alpha_{LCPC}}$$

Maximum f_p values are also recommended based on pile and soil type. Only the measured CPT q_c is used for the calculation of both side friction and pile end bearing resistance. This is considered an advantage by many due to the difficulties associated in interpreting sleeve friction (f_s) in CPT data.

Nature of soil	q_c (MPa)	Category											
		Coefficients, α				Maximum limit of f_p (MPa)							
		I		II		I		II		I		II	
		A	B	A	B	A	B	A	B	A	B	A	B
Soft clay and mud	< 1	30	30	30	30	0.015	0.015	0.015	0.015	0.035	0.035	–	–
Moderately compact clay	1 to 5	40	80	40	80	0.035	0.035	0.035	0.035	0.08	0.08	≥ 0.12	≥ 0.12
Silt and loose sand	≤ 5	60	150	60	120	0.035	0.035	0.035	0.035	0.08	0.08	–	–
Compact to stiff clay and compact silt	> 5	60	120	60	120	0.035	0.035	0.035	0.035	0.08	0.08	≥ 0.20	≥ 0.20
Soft chalk	≤ 5	100	120	100	120	0.035	0.035	0.035	0.035	0.08	0.08	–	–
Moderately compact sand and gravel	5 to 12	100	200	100	200	0.08	0.035	0.08	0.08	0.12	0.12	≥ 0.20	≥ 0.20
Weathered to fragmented chalk	> 5	60	80	60	80	0.12	0.08	0.12	0.12	0.15	0.15	≥ 0.20	≥ 0.20
Compact to very compact sand and gravel	> 12	150	300	150	200	0.12	0.08	0.12	0.12	0.15	0.15	≥ 0.20	≥ 0.20

Category – IA: plain bored piles; mud bored piles; hollow auger bored piles; micropiles (grouted under low pressure); cast screwed piles; piers; barrettes. IB: cased bored piles; driven cast piles. IIA: driven precast piles; prestressed tubular piles; jacket concrete piles. IIB: driven metal piles; jacked metal piles. IIIA: driven grouted piles; driven rammed piles. IIIB: high pressure grouted piles of large diameter > 250 mm; micropiles (grouted under high pressure).

Note: Maximum limit unit skin friction, f_p : bracket values apply to careful execution and minimum disturbance of soil due to construction.

Table 13 Friction coefficient, α
(Bustamante and Ganeselli, 1982)

The equivalent average cone resistance, q_{ca} , at the base of the pile used to compute the pile unit end bearing, q_p , is the mean q_c value measured along two fixed distances, a , ($a = 1.5D$, where D is the pile diameter) above (-a) and below (+a) the pile tip. The authors suggest that q_{ca} be calculated in three steps, as shown in Figure 43. The first step is to calculate q'_{ca} , the mean q_c between -a and +a. The second step is to eliminate values higher than $1.3q'_{ca}$ along the length -a to +a, and the values lower than $0.7q'_{ca}$ along the length -a, which generates the thick curve shown in Figure 43. The third step is to calculate q_{ca} , the mean value of the thick curve.

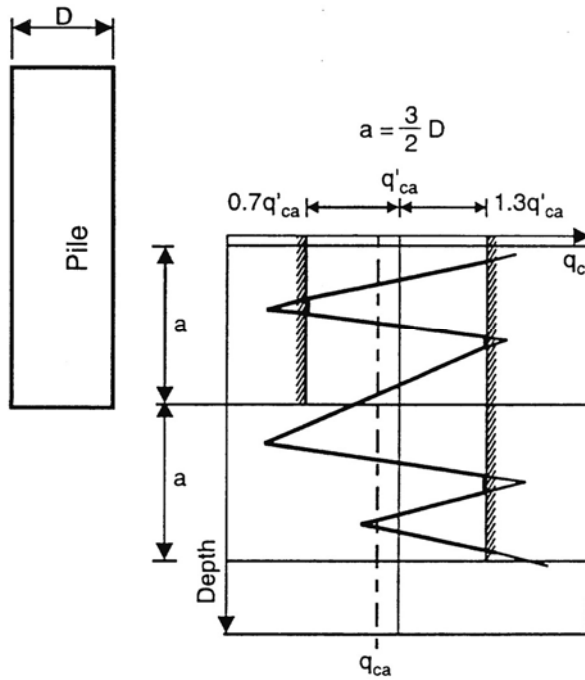


Figure 43. Calculation of equivalent average cone resistance (Bustamante and GIANESELLI, 1982).

More recently, newer methods have been developed to estimate the axial capacity of piles (e.g., Niazi, F.S. and Mayne P.W., 2016 and Lehane et al., 2022). Fellenius (2022) describes a unified design approach based on designing foundations considering actual and acceptable settlements, as opposed to basing the design on a pile "capacity" reduced by various factors of safety or resistance factors. The unified method is a logical method because it considers actual loads, deformations, and movements, whereas the conventional design means calculating forces for an ultimate condition that hopefully will never develop. A complete description is beyond the scope of this Guide and the reader is encouraged to read Basics of Foundation Design (Fellenius, 2022): <https://www.fellenius.net/papers.html>

Other Design Considerations

Factor of Safety

To obtain the design load, factors of safety are applied to the ultimate load and a deterministic approach is usually adopted to define these values. The selection of an appropriate factor of safety depends on many factors, such as reliability and sufficiency of the site investigation data, confidence in the method of calculation,

previous experience with similar piles in similar soils and whether pile load test results are available.

Factors of safety are generally of the order of 2, although real values are sometimes greater, as partial factors of safety are sometimes applied during calculations (particularly to soil strengths) before arriving to the ultimate pile capacity.

Recommended factors of safety for calculating the axial capacity of piles from the CPT are given in Table 14.

Method	Factor of safety (FS)
Bustamante and GIANESELLI (1982)	2.0 (Q_s) 3.0 (Q_b)
de Ruiter and Beringen (1979)	2.0 (static loads) 1.5 (static + storm loads)

Table 14 Recommended factors of safety for axial capacity of piles from CPT

The design of high-capacity large diameter bored piles in stiff clay or dense sand can be difficult since settlement criteria usually control rather than capacity. Hence, high factors of safety are often applied to limit settlement.

Pile Dynamics

The objective of methods that rely on pile dynamics is to relate the dynamic pile behavior to the ultimate static pile resistance. Hence, pile dynamics can work well in drained soils (sands, gravels, etc.) but can be difficult in undrained soils (silts, clays, etc.).

The early approach was to use simple pile driving equations (Hiley, Engineering News, etc.) based on equating the available energy of the hammer to the work performed by the pile. However, these were based on a rigid pile concept, which is fundamentally incorrect. Current approaches are based on 1-D wave-equation analyses (Goble et al., 1970). This method considers the characteristics of the hammer, driving cap, pile, and soil. The method is commonly applied using commercial software (i.e., WEAP). This method is good to assist in selection of

hammers and prediction of driving stresses and the choice of driving criteria. It is also useful for dynamic monitoring during construction.

Pile Load Tests

Since there is much uncertainty in the prediction of pile capacity and response, it is common to perform pile load tests on major projects.

For major projects, it is common to apply static methods (i.e., LCPC CPT method) to obtain a first estimate of capacity, apply pile dynamics if driven piles selected (aid in hammer selection, driving stresses, driving criteria) and perform a small number of pile load tests to evaluate pile response and to calibrate the static method. Results from the pile load tests can be used to modify the static prediction (i.e., CPT prediction) of pile capacity and the modified method applied across the site. For low-risk projects, pile load tests may not be warranted, and a slightly conservative prediction should be applied using the static (CPT) method.

Group Capacity

The capacity of a group of piles is influenced by the spacing, pile installation and ground conditions. The group efficiency is defined as the ratio of the group capacity to the sum of the individual pile capacities.

Driven piles in coarse-grained soils develop larger individual capacities when installed as a group since lateral earth pressures and soil density increase due to pile driving. Hence, it is conservative to use the sum of the individual pile capacities.

For bored pile groups, the individual capacity can reduce due to reduced lateral stresses. Meyerhof (1976) suggested a reduction factor of 0.67.

For piles in fine-grained soils the capacity of the pile group should be estimated based on the ‘block’ of piles since the soil between the piles may move with the pile group.

Design of Piles in Rock

Piles can be placed on or socketed into rock to carry high loads. The exact area of contact with rock, depth of penetration into rock and quality of rock are largely unknown, hence, there is much uncertainty. The capacity is often confirmed based on driving or installation details, local experience, and test loading. End bearing capacity can be based on pressuremeter test results or strength from rock cores. Shaft resistance should be estimated with caution, due to possible poor

contact between rock and pile, possible stress concentration and resulting progressive failure.

Pile Settlement

Although the installation of piles changes the deformation and compressibility characteristics of the soil mass governing the behavior of single piles under load, this influence usually extends only a few pile diameters below the pile base. Meyerhof (1976) suggested that the total settlement of a group of piles at working load can generally be estimated assuming an equivalent foundation. For a group of predominately friction piles (i.e., $Q_s > Q_b$), the equivalent foundation is assumed to act on the soil at an effective depth of 2/3 of the pile embedment. For a group of piles that are predominately end bearing (i.e., $Q_b > Q_s$), the equivalent foundation is taken at or close to the base of the piles. The resulting settlement is calculated in a manner similar to that of shallow foundations.

Sometimes large capacity piles are installed and used as single piles and the load settlement response of a single pile is required. The load settlement response of a single pile is controlled by the combined behavior of the side resistance (Q_s) and base resistance (Q_b). The side resistance is usually developed at a small settlement of about 0.5 percent of the shaft diameter and generally between 5 to 10mm. In contrast to the side resistance, the base resistance requires much larger movements to develop fully, usually about 10 to 20 percent of the base diameter. An estimate of the load settlement response of a single pile can be made by combining the two components of resistance according to the above guidelines. In this way, a friction pile (i.e., $Q_s \gg Q_b$), will show a clear plunging failure at a small settlement of about 0.5% of the pile diameter. On the other hand, an end bearing pile (i.e., $Q_b \gg Q_s$), will not show a clear plunging failure until very large settlements have taken place and usually settlement criteria control before failure can occur. In both cases, the side friction is almost fully mobilized at working loads. Hence, it is often important to correctly define the proportions of resistance (Q_b/Q_s).

Methods have been developed to estimate the load-transfer ($t-z$) curves (Verbrugge, 1988, Lehane et al., 2022). However, these methods are approximate and are strongly influenced by pile installation and soil type. The recommended method for estimating load settlement response for single piles is to follow the general guidelines above regarding the development of each component of resistance.

Negative Shaft Friction and Down Drag on Piles

When the ground around a pile settles, the resulting downward movement can induce downward forces on the pile.

The magnitude of the settlement can be very small to develop these downward forces. For end bearing piles, the negative shaft friction plus the dead load can result in structural failure of the pile. For friction piles, the negative shaft friction can result in greater settlements. No pile subject to down drag will settle more than the surrounding ground.

Lateral Response of Piles

Vertical piles can resist lateral loads by deflecting and mobilizing resistance in the surrounding ground. The response depends on the relative stiffness of the pile and the ground. In general, the response is controlled by the stiffness of the ground near the surface, since most long piles are relatively flexible.

A common approach is to simulate the ground by a series of horizontal springs. The spring stiffness can be estimated based on a simple subgrade modulus approach (assumes the ground to be linear and homogeneous) or as non-linear springs (p-y curves) (Matlock, 1970). The p-y curves can be estimated using empirical relationships based on lab results or in-situ tests (e.g., pressuremeter, DMT, SCPT) (Baguelin et al., 1978; Robertson et al., 1986). The initial stiffness of the p-y curves is controlled by the small strain stiffness (G_0) that can be determined by measuring (or estimating) the shear wave velocity (V_s) using the SCPT.

Another approach is to simulate the ground as an elastic continuum. Poulos and Davis, (1980) and Randolph, (1981) suggested design charts that require estimates of equivalent ground modulus for uniform homogeneous ground profiles.

The above approaches apply to single piles. When piles are installed in groups, interaction occurs, and lateral deformations can increase. These can be estimated using simplified theoretical solutions (Poulos and Davis, 1980, Randolph, 1981). The direction of the applied load relative to the group is important for laterally loaded pile groups.

Ground Improvement Compaction Control

Ground improvement can occur in many forms depending on soil type and project requirements. For coarse-grained soils such as sands and silty sands, deep compaction is a common ground improvement technique. Deep compaction can comprise: vibro-compaction, vibro-replacement (stone columns), dynamic compaction, compaction piles, and deep blasting.

The CPT has been found to be one of the best methods to monitor and document the effect of deep compaction due to the continuous, reliable, and repeatable nature of the data. Most deep compaction techniques involve cyclic shear stresses in the form of vibration to induce an increase in soil density. Vibratory compaction is generally more effective in soil deposits with a friction ratio less than 1%. When the friction ratio exceeds about 1.5% vibratory compaction is usually not effective. These recommendations apply to average values in a soil deposit. Local seams or thin layers with higher friction ratio values are often of little practical importance for the overall performance of a project and their effect should be carefully evaluated when compaction specifications are prepared. Soils with an initial cone resistance below about 3 MPa (30 tsf) can be compressible or contain organic matter, silt or clay and will generally not respond well to vibratory compaction. Soils with a high initial cone resistance are normally dense and will not show significant compaction and generally do not need compaction. It is also important to establish the level and variation of the groundwater table before compaction since some compaction methods are less effective in dry or partially saturated soils. The CPTu provides the required information on groundwater conditions.

Often the aim of deep compaction is for one or more of the following:

- increase bearing capacity (i.e., increase shear strength)
- reduce settlements (i.e., increase stiffness)
- increase resistance to liquefaction (i.e., increase density).

The need for deep compaction and geotechnical conditions will be project specific and it is important that design specifications take account of these site-specific requirements. Cone resistance in coarse-grained soils is governed by many factors including soil density, in-situ stresses, stress history, and soil compressibility. Changes in shear strength, stiffness and density can be documented with changes in measured cone resistance.

A common problem in many deep compaction projects is to specify a minimum value of q_c for compaction over a large depth range. This results in a variation of relative density with depth, with the required degree of compaction near the surface being much higher than at depth. For certain projects, a high degree of compaction close to the ground surface may be justified but can be achieved using surface compaction methods. However, this can be very difficult to obtain with certain deep compaction techniques and this decision should be based on engineering judgment related to the geotechnical project requirements. It is generally preferred to specify a minimum normalized value of cone resistance corrected for overburden stress, Q_{tn} . Since, grain characteristics can vary rapidly in many sandy deposits, it is also preferred to specify an acceptance criterion based on *normalized clean sand equivalent* values of cone resistance (Q_{tn}^{cs}), using the methodology shown in Figure 48, especially when compaction is performed to reduce the potential for liquefaction. Specification using $(Q_{tn})_{cs}$ can reduce problems in silty zones, where traditional approaches have often resulted in excessive ground improvement to reach unrealistic criteria.

It is relatively common to have the CPT soil behavior type index (I_c) decrease after compaction (e.g., vibro-compaction). The cause for the decrease is likely due to changes in horizontal effective stresses due to ground improvement. When this has occurred it has been common to use the pre-improvement values of I_c that are less influenced by complex changes in horizontal effective stresses and better represent the correct soil type. Any small change in I_c typically has little influence in the analysis for clean sands (where the initial $I_c < 2.0$).

An important aspect of deep compaction that is not yet fully understood is the increase in cone resistance with time after compaction. This time effect has been observed in different ground conditions and with different compaction methods. Often no measurable change in pore pressure has been observed and the increase takes place without visible ground settlements. Charlie et al. (1992) studied several cases where cone resistance was measured with time after compaction. A range of compaction techniques were used and the results are shown in Figure 44. The cases were representative of a wide range of climates and geologic conditions with average temperatures varying from -10°C (Beaufort Sea) to +27°C (Nigeria). Charlie et al. (1992) suggested that the time effect could be linked to the average air temperature. The possibility of time effects should be evaluated for each project. For very large projects, it may be necessary to perform field trials.

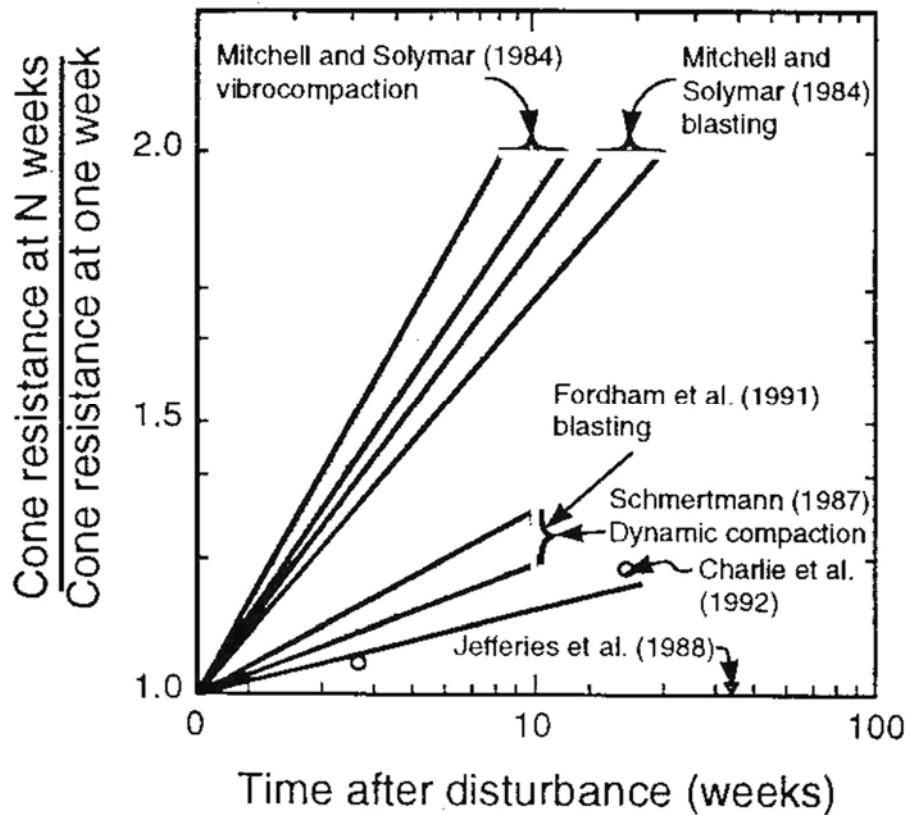


Figure 44 Influence of time after disturbance on CPT results
(after Charlie et al., 1992)

For projects where deep compaction is recommended to either increase resistance to liquefaction or decrease future settlements for shallow foundations, the seismic CPT should be considered, since it provides both penetration resistance and shear wave velocity. The combined values can improve interpretation, especially in silty sands and soils that have some microstructure before improvement.

Ground improvement can also include many other techniques, such as grouting, soil mixing and stone columns as well as pre-loading. The CPT can also be used to evaluate the effectiveness of these other techniques although this will depend on soil conditions and the ground improvement method. The CPT has also found some limited use in monitoring surface compaction. Since surface compaction is often carried out in thin layers with frequent quality control, the CPT has not found extensive application in this area.

Another form of ground improvement is soil mixing, where compounds are mixed with soil to improve their behavior. Sometimes quality control is defined in terms

of a target unconfined compressive strength (q_u). The unconfined compressive strength (q_u) is twice the undrained shear strength (s_u) that can be estimate directly from the CPT. An advantage of the CPT for quality control testing in soil mixing is that the CPT provides a continuous profile and can identify weak zones.

Design of Wick or Sand Drains

Pre-loading is a common form of ground improvement in fine-grained soils where the rate of consolidation is important. Installation of sand drains or wick drains can significantly decrease the time for consolidation settlements. Prior to 1975, vertical sand drains were common to aid consolidation with temporary pre-load. Since 1975, geosynthetics in the form of wick drains have dominated the market. Wick drains are usually fluted or corrugated plastic or cardboard cores within geotextile sheaths that completely encircle those cores. They are usually 100mm wide by 2 to 6mm thick. The wick drain is usually pushed or driven into the ground to the desired depth using a lance or mandrel. The drain then remains in place when the lance or mandrel is removed. Installation can be in the range of 1 to 5 minutes depending on ground conditions, pushing equipment and depth of installation. The design of wick drains is not standardized but most equate the diameter of the particular type of drain to an equivalent sand drain diameter.

The method developed by Barron (1948) and Kjellman (1948), as mentioned by Hansbo (1970), is commonly used, and the relevant design equations are as follows:

$$t = \frac{D^2}{8c_h} [\ln(D/d) - 0.75] \ln \frac{1}{1-U}$$

Where:

- t = consolidation
- c_h = coefficient of consolidation for horizontal flow
- d = equivalent diameter of the wick drain (\approx circumference/ π)
- D = sphere of influence of the wick drain (for a triangular pattern use 1.05 times the spacing, for a square pattern use 1.13 times the spacing).
- U = average degree of consolidation

The key input parameter for the soil is the coefficient of consolidation for horizontal flow, c_h . This parameter can be estimated from dissipation tests using the CPTu. The value derived from the CPTu is particularly useful since, the cone represents a very similar model to the installation and drainage process around the wick drain. Although there is some possible smearing and disturbance to the soil around the CPT, similar smearing and disturbance often exists around the wick, and hence, the calculated value of c_h from the CPTU is usually representative of the soil for wick drain design.

Details on estimation of c_h from dissipation tests were given in the section on (geotechnical parameters) consolidation characteristics. To provide a reasonable estimate of c_h , a sufficient number of dissipation tests should be carried out through the zone of interest. The dissipation tests should be carried out to at least 50% dissipation. Several dissipation tests should be carried out to full dissipation to provide an estimate of the equilibrium groundwater conditions prior to pre-loading.

Liquefaction

Soil liquefaction is a major concern for structures constructed with or on sand or sandy soils. The major earthquakes of Niigata (1964), Kobe (1995) and Christchurch (2010/11) have illustrated the significance and extent of damage caused by soil liquefaction. Recent failures in mine tailings impoundments (e.g., Morgenstern et al., 2016, Robertson et al. 2019) have illustrated that soil liquefaction is also a major design problem for large sand structures such tailings and earth dams.

To evaluate the potential for soil liquefaction, it is important to determine the soil stratigraphy and in-situ state of the deposits. The CPT is an ideal in-situ test to evaluate the potential for soil liquefaction because of its repeatability, reliability, continuous measurements, and cost effectiveness.

Liquefaction Definitions

Several phenomena are described as soil liquefaction; hence, the following definitions are provided to aid in the understanding of the phenomena.

Flow (*static*) Liquefaction

- Applies only to strain softening soils in undrained shear (i.e., soils susceptible to strength loss/reduction in undrained shear).
- Requires in-situ static shear stresses to be greater than the residual or minimum/liquefied undrained shear strength (e.g., sloping ground).
- Either static or cyclic loading can trigger flow liquefaction.
- For failure of a soil structure to occur, such as a slope, a sufficient volume of material must strain soften. The resulting failure can be a slide or a flow depending on the material characteristics and ground geometry. The resulting movements are due to internal causes and often occur after the trigger mechanism.
- Can occur in any strain-softening saturated (or near-saturated) soil, such as very loose non-plastic soil, very sensitive fine-grained (low-plastic clay), and loose non-plastic silt.

Cyclic (seismic) Liquefaction

- Requires undrained cyclic loading during which shear stress reversal occurs.
- Requires sufficient undrained cyclic loading to accumulate pore pressures such that the effective stresses essentially reach zero during cyclic loading.
- Deformations during cyclic loading can accumulate to large values, but generally stabilize shortly after cyclic loading stops. The resulting movements are due to external causes and occur mainly during the cyclic loading.
- Can occur in almost all saturated non-plastic and low-plastic soil (sand, silt) provided that the cyclic loading is sufficiently large in magnitude and duration.
- Plastic (clay) soils can experience some softening during cyclic loading when the applied cyclic shear stress is close to the undrained shear strength. However, deformations are generally small due to the cohesive strength at low effective stress. Rate effects (creep) often control deformations in cohesive soils.

Note that strain softening soils can also experience cyclic liquefaction depending on ground geometry. Figure 45 presents a flow chart to clarify the phenomena and definitions of soil liquefaction.

If a soil is contractive at large strains and strain softening (i.e., can experience strength loss/reduction in undrained shear), flow liquefaction is possible if the soil can be triggered to strain-soften and if the gravitational shear stresses are larger than the minimum undrained shear strength. The trigger can be either monotonic or cyclic. Whether a slope or soil structure will fail, and slide will depend on the amount of strain softening soil relative to strain hardening soil within the structure, the brittleness of the strain softening soil and the geometry of the ground. The resulting deformations of a soil structure with both strain softening and strain hardening soils will depend on many factors, such as distribution of soils, ground geometry, amount and type of trigger mechanism, brittleness of the strain softening soil and drainage conditions. Examples of flow liquefaction failures are Aberfan flow slide (Bishop, 1973), Zealand submarine flow slides (Koppejan et al., 1948), and the recent tailings dam failures in Brazil (Morgenstern et al. 2016; Robertson et al. 2019). In general, flow liquefaction failures are not common, however, when they occur, they typically take place

quickly with little warning and usually have extreme consequences since the failed material can flow rapidly over significant distances. Hence, the design against flow liquefaction should be carried out with caution.

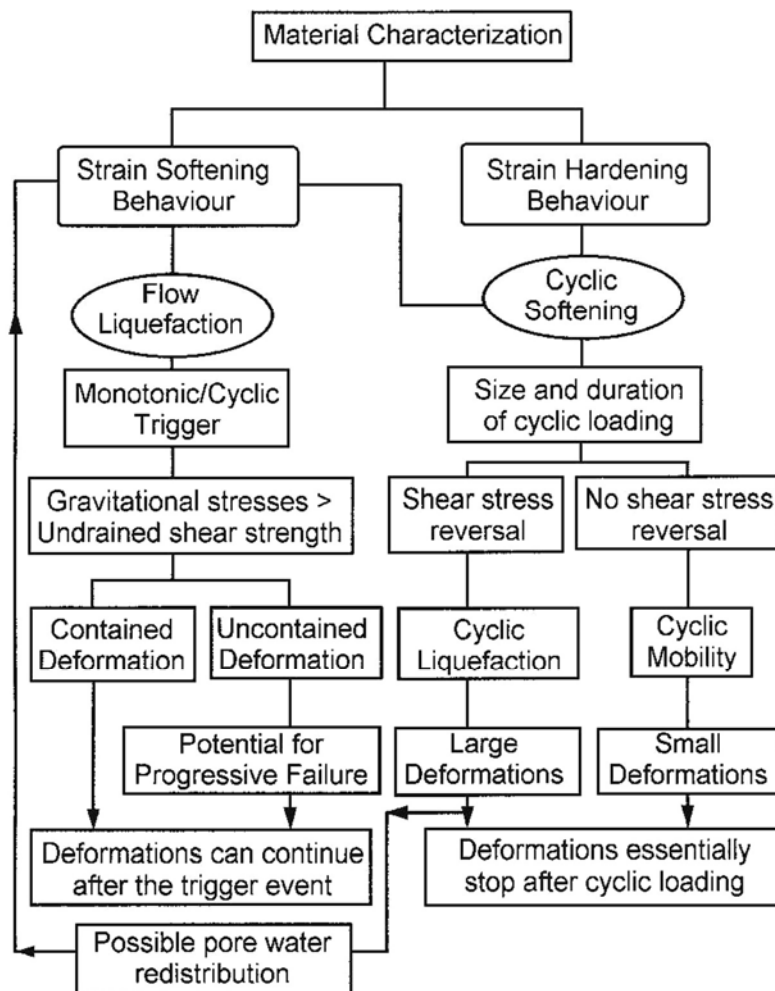


Figure 45. Flow chart to evaluate liquefaction of soils
(After Robertson and Wride, 1998)

If a soil is strain hardening in undrained shear, flow liquefaction will generally not occur. However, cyclic liquefaction can occur due to cyclic undrained loading (e.g., earthquake loading). The amount and extent of deformations during cyclic loading will depend on the state (density/OCR) of the soil, the magnitude and duration of the cyclic loading and the extent to which shear stress reversal occurs. If extensive shear stress reversal occurs and the magnitude and duration of cyclic loading are sufficiently large, it is possible for the effective stresses to essentially

reach zero in sand-like soils, during the cyclic loading, resulting in large deformations. Shear stress reversal is common in level and gently sloping ground during earthquakes where the static shear stresses are small compared to the imposed cyclic shear stresses. Examples of cyclic liquefaction were common in the major earthquakes in Niigata (1964) and Christchurch (2010/11) and manifest in the form of sand boils, damaged lifelines (pipelines, etc.) lateral spreads, slumping of embankments, ground settlements, and ground surface cracks.

If cyclic liquefaction occurs and drainage paths are restricted due to overlying less permeable layers, the sand immediately beneath the less permeable soil can become looser due to pore water redistribution during and after cyclic loading, resulting in possible subsequent flow liquefaction, given the right geometry (see flow chart in Figure 45). In cases where drainage is restricted, caution is required to account for possible void redistribution.

The evaluation of liquefaction (both flow and cyclic) depends on the risk of the project. Risk is defined as the combination of likelihood and consequences as outlined briefly in Table 1. In general, risk is often dominated by the potential consequences. Since flow liquefaction failures are often very rapid and the failed material can flow considerable distance quickly, the consequences of failure are often extreme. For high-risk projects (e.g., potential loss of life, environmental damages, etc.) it is often prudent to assume that flow liquefaction (i.e., strength loss) will be triggered at some time in the life of the project. Given the variables to evaluate liquefaction, it can be helpful to apply a risk-informed approach to design. An example of risk-informed approach for mine tailings can be found at: <https://www.icmm.com/en-gb/guidance/innovation/2021/tailings-management-good-practice>

Cyclic Liquefaction (Level or Gently Sloping Ground Sites)

(Refer to Robertson & Wride, 1998; Zhang et al., 2002 & 2004; Robertson, 2009 for details)

Most of the existing work on cyclic liquefaction has been primarily for earthquakes. The late Prof. H.B. Seed and his co-workers developed a comprehensive methodology to estimate the potential for cyclic liquefaction for level ground sites due to earthquake loading. The methodology requires an estimate of the cyclic stress ratio (CSR) profile caused by the design earthquake and the cyclic resistance ratio (CRR) of the ground. If the CSR is greater than the CRR cyclic liquefaction can occur. The CRR of the soil is estimated based on past case history performance linked to penetration resistance. Alternate methods to estimate CRR based on a mechanics approach have been suggested, but the case history-based methods remain the most popular approach. CSR is usually estimated based on a probability of occurrence for a given earthquake. A site-specific seismicity analysis can be carried out to determine the design CSR profile with depth. A simplified method to estimate CSR was also developed by Seed and Idriss (1971) based on the peak ground surface acceleration (a_{max}) at the site. The simplified approach can be summarized as follows:

$$\text{CSR} = \frac{\tau_{av}}{\sigma'_{vo}} = 0.65 \left[\frac{a_{max}}{g} \right] \left(\frac{\sigma_{vo}}{\sigma'_{vo}} \right) r_d$$

where τ_{av} is the average cyclic shear stress; a_{max} is the maximum (peak) horizontal acceleration at the ground surface; g is the acceleration due to gravity; σ_{vo} and σ'_{vo} are the total and effective vertical overburden stresses at the time of the earthquake, respectively, and r_d is a stress reduction factor which is dependent on depth. The factor r_d can be estimated using the following tri-linear function, which provides a good fit to the average of the suggested range in r_d originally proposed by Seed and Idriss (1971):

$$\begin{aligned} r_d &= 1.0 - 0.00765z && \text{if } z < 9.15 \text{ m} \\ &= 1.174 - 0.0267z && \text{if } z = 9.15 \text{ to } 23 \text{ m} \\ &= 0.744 - 0.008z && \text{if } z = 23 \text{ to } 30 \text{ m} \end{aligned}$$

$$= 0.5 \\ \text{if } z > 30 \text{ m}$$

Where z is the depth in meters. These formulae are approximate at best and represent only average values since r_d shows considerable variation with depth. Idriss and Boulanger (2008) suggested alternate values for r_d , but these are also associated with alternate values of CRR.

The sequence to evaluate cyclic liquefaction for level or gently sloping ground sites is:

1. Evaluate susceptibility of soil to cyclic liquefaction
2. Evaluate triggering of cyclic liquefaction
3. Evaluate post-earthquake deformations.

An overview of the history of evaluation cyclic liquefaction is provided in the recording of the 2015 Seed Lecture by Robertson, that can be viewed at: (<https://www.youtube.com/watch?v=J2-tMdbMvNg>).

1. Evaluate Susceptibility to Cyclic Liquefaction

The response of soil to seismic loading varies with soil type and state (void ratio, effective confining stress, stress history, etc.). Boulanger and Idriss (2004) distinguished between *sand-like* and *clay-like* behavior and showed that cyclic liquefaction occurs primarily in *sand-like* soils. Following criteria can be used to identify soil behavior:

Sand-like Behavior: Sand-like soils are susceptible to cyclic liquefaction when their behavior is typically characterized by Plasticity Index (PI) < 10 and Liquid Limit (LL) < 37 and natural water content (w_c) > 0.85 (LL). More emphasis should be placed on PI, since both LL and w_c tend to be less reliable. Sand-like soils generally have CPT-based SBT index $I_c < 2.8$ (or $I_B > 22$).

- Low risk projects: Assume soils are susceptible to cyclic liquefaction based on above criteria unless previous local experience shows otherwise.
- High risk projects: Either assume soils are susceptible to cyclic liquefaction or obtain high quality samples and evaluate susceptibility based on appropriate laboratory testing, unless previous local experience exists.

Clay-like Behavior: Clay-like soils are generally not susceptible to cyclic liquefaction when their behavior is characterized by $PI > 18$ but they can experience cyclic softening. Clay-like soils generally have CPT-based SBT index $I_c > 2.8$ (or $I_B < 22$).

- Low risk projects: Assume soils are not susceptible to cyclic liquefaction based on above criteria unless previous local experience shows otherwise. Check for cyclic softening.
- High risk projects: Obtain high quality samples and evaluate susceptibility to either cyclic liquefaction and/or cyclic softening based on appropriate laboratory testing, unless previous local experience exists.

Figure 46 shows the index-based criteria suggested by Bray and Sancio (2006) that includes a transition from sand-like to clay-like behavior between $12 < PI < 18$. A similar transition in behavior was suggested by Robertson (2016) based on modified SBT Index $22 < I_B < 32$.

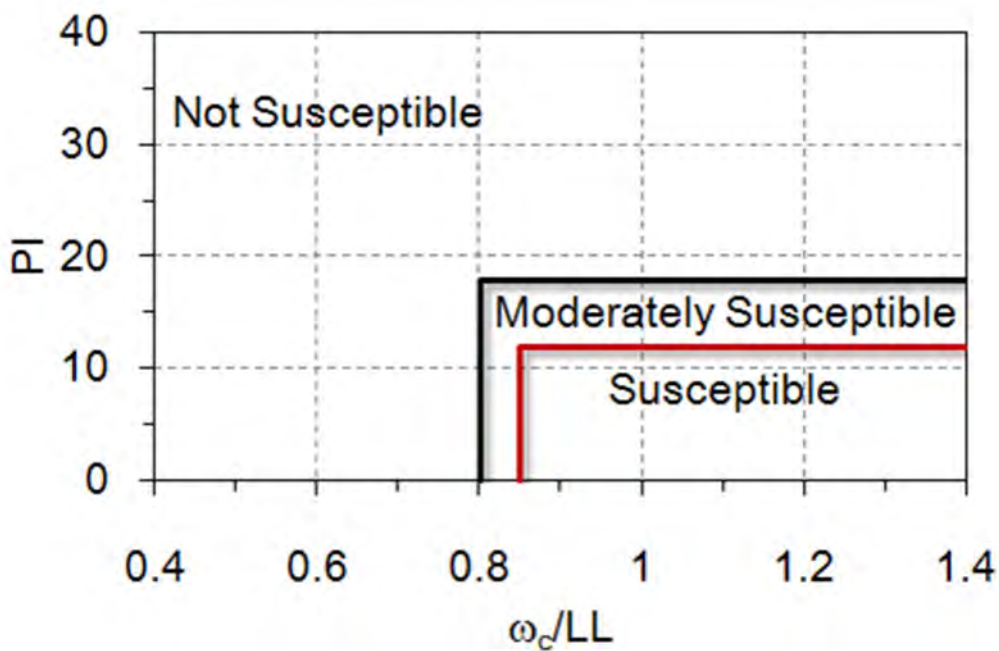


Figure 46. Liquefaction susceptibility criteria (after Bray and Sancio, 2006)

These criteria are generally conservative. Boulanger and Idriss (2004) suggested that sand-like behavior is limited to $PI < 7$. Use the criteria shown in Figure 46, unless local experience in the same geologic unit shows that a lower PI is more appropriate.

Fine-grained soils transition from a behavior that is more fundamentally like sands to behavior that is more fundamentally like clays over a range of Atterberg Limits and moisture contents, as shown in Figure 46. The transition from more sand-like to more clay-like behavior has a direct correspondence to the types of engineering procedures that are best suited to evaluate their seismic behavior. The transition from sand-like to clay-like behavior generally occurs when the modified SBT_n $22 < I_B < 32$ (approx. $2.5 < I_c < 2.8$), as illustrated in Figures 23 and 25(b). For soils that plot in or close to this transition region samples should be obtained to verify behavior.

2. Evaluate Triggering of Cyclic Liquefaction

Sand-like Materials

Seed et al., (1985) developed a method to estimate the cyclic resistance ratio (CRR) for clean sand with level ground conditions based on the Standard Penetration Test (SPT). The CPT has become more popular to estimate CRR, due to the continuous, reliable, and repeatable nature of the data (Youd et al., 2001; Robertson, 2009) and now a larger cyclic liquefaction case history database.

Apply the simplified (NCEER) approach as described by Youd et al (2001) using generally conservative assumptions. The simplified approach should be used for low- to medium-risk projects and for preliminary screening for high-risk projects. For low-risk projects, where the simplified approach is the only method applied, conservative criteria should be used. The recommended CPT trigger correlation for sand-like soils can be estimated using the following simplified equations suggested by Robertson and Wride, (1998):

$$\text{CRR}_{7.5} = 93 \left[\frac{(Q_{tn,cs})}{1000} \right]^3 + 0.08$$

if $50 \leq Q_{tn,cs} \leq 160$

$$\text{CRR}_{7.5} = 0.833 \left[\frac{(Q_{tn,cs})}{1000} \right] + 0.05$$

if $Q_{tn,cs} < 50$

The field observations were based primarily on the following conditions:

- Holocene-age, uncemented silica-based sand deposits with $K_o < 0.7$
- Level or gently sloping ground
- Cyclic stress ratio (CSR)_{7.5} adjusted to magnitude M = 7.5 earthquake
- Depth ranges from 1 to 12 m (3 to 40 ft), 85% for depths < 10 m (30 ft)
- Earthquakes with magnitude mostly between 6 < M < 8
- Representative average CPT values for the layer considered to have experienced cyclic liquefaction.

A summary of the CPT-based cyclic liquefaction database is shown in Figure 47.

Caution should be exercised when extrapolating the CPT correlation to conditions outside the above range. An important feature to recognize is that the correlation is based primarily on average values for the inferred liquefied layers. However, the correlation is often applied to all measured CPT values, which include low values below the average. Therefore, the correlation can be conservative in variable deposits where a small part of the CPT data can indicate possible liquefaction. The data base is constantly expanding but is still dominated by similar earthquake and soil variables (e.g., predominately $6 < M_w < 8$; $0.1 < a_{max} < 0.6$; $0.1 < CSR < 0.6$; $z < 10m$; fines content (FC) < 40%; $I_c < 2.6$). Differences often occur when the design earthquake is outside of the database (e.g., $M > 8$ or $CSR > 0.6$).

It has been recognized for some time that the correlation to estimate CRR_{7.5} for silty sands is different than that for clean sands. Typically, a correction is made to determine an *equivalent clean sand normalized penetration resistance* ($Q_{tn,cs}$) based on grain characteristics, such as fines content, although the corrections are due to more than just fines content and are influenced by the plasticity (mineralogy) of the fines.

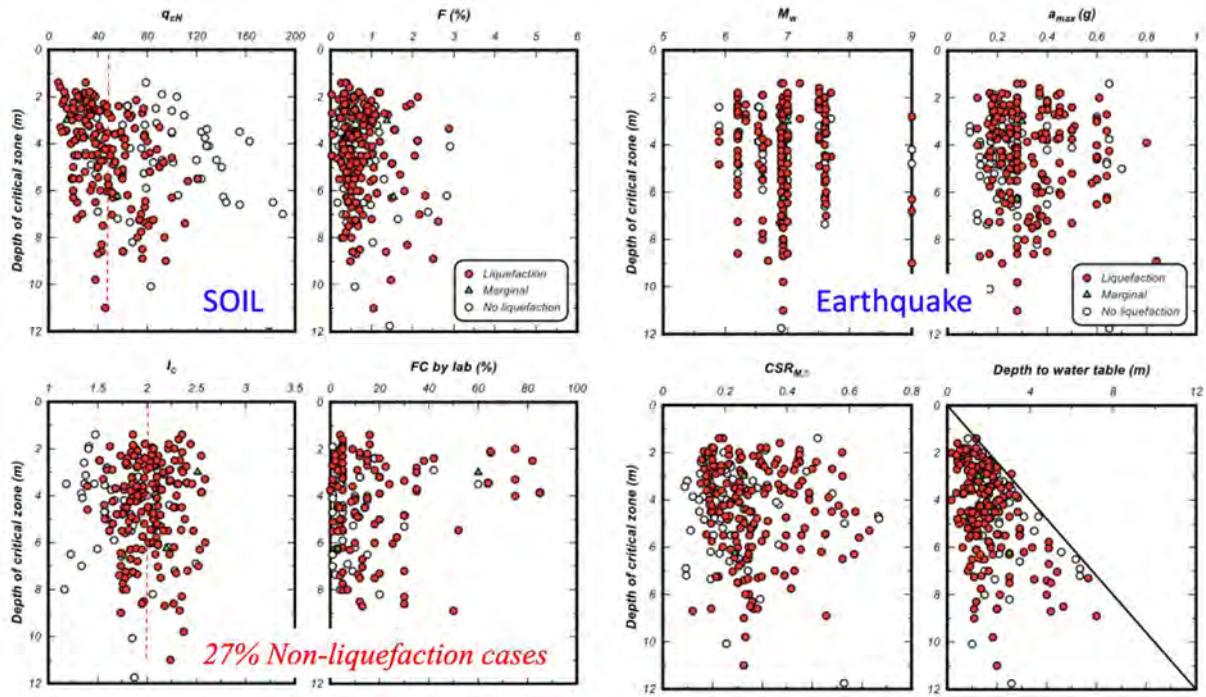


Figure 47. Summary of Cyclic Liquefaction case history database
(Modified from Boulanger and Idriss, 2008)

One reason for the continued use of the SPT has been the need to obtain a soil sample to determine the fines content of the soil. However, this has been offset by the poor repeatability of the SPT data and the weak link between the physical characteristic of fines content to the in-situ mechanical behavior of the soil. Robertson and Wride (1998) suggested that it was better to estimate the in-situ mechanical behavior of the soil directly from the CPT by estimating $Q_{tn,cs}$ using the following direct approach:

$$Q_{tn,cs} = K_c Q_{tn}$$

Where K_c is a correction factor that is a function of behavior characteristics (e.g., compressibility) of the soil.

Robertson and Wride (R&W, 1998) suggested estimating behavior characteristics using the normalized soil behavior chart (SBT_n) by Robertson (1990) and the soil behavior type index, I_c , where:

$$I_c = \left[(3.47 - \log Q_{tn})^2 + (\log F + 1.22)^2 \right]^{0.5}$$

and

$$Q_{tn} = \left(\frac{q_t - \sigma_{vo}}{P_{a2}} \right) \left(\frac{P_a}{\sigma'_{vo}} \right)^n$$

Q_{tn} is the normalized CPT penetration resistance (dimensionless); n = stress exponent; $F = f_s / [(q_c - \sigma_{vo})] \times 100\%$ is the normalized friction ratio (in percent); f_s is the CPT sleeve friction stress; σ_{vo} and σ'_{vo} are the total effective overburden stresses respectively; P_a is a reference pressure in the same units as σ'_{vo} (i.e., $P_a = 100$ kPa if σ'_{vo} is in kPa) and P_{a2} is a reference pressure in the same units as q_c and σ_{vo} (i.e., $P_{a2} = 0.1$ MPa if q_c and σ_{vo} are in MPa). Note, 1 tsf ~ 0.1 MPa.

The soil behavior type chart by Robertson (1990) used a normalized cone penetration resistance (Q_t) based on a simple linear stress exponent of $n = 1.0$, whereas the recommended chart for estimating $CRR_{7.5}$ is based on a normalized cone penetration resistance (Q_{tn}) based on a variable stress exponent. Robertson (2009) updated the stress normalization to allow for a variation of the stress exponent with both SBTn I_c and effective overburden stress using:

$$n = 0.381 (I_c) + 0.05 (\sigma'_{vo}/p_a) - 0.15$$

where $n \leq 1.0$ (see Figure 48 for flow chart).

Robertson and Wride (1998) suggested a correction factor (K_c) to correct the measured normalized cone resistance (Q_{tn}) to an equivalent normalized clean sand resistance ($Q_{tn,cs}$) and Robertson (2021) updated the correction factor to the following simplified version:

$$K_c = 1.0 \quad \text{if } I_c \leq 1.7$$

$$K_c \approx 15 - \frac{14}{1 + (I_c/2.95)^{11}} \quad \text{for } I_c \leq 3.0$$

The correction factor, K_c , is approximate since the CPT responds to many factors such as soil plasticity, fines content, mineralogy, soil sensitivity, age, and stress history. However, in general, these same factors influence the $CRR_{7.5}$ in a similar manner. Caution should be used when applying the relationship to sands that plot in the region defined by $1.64 < I_c < 2.36$ and $F < 0.5\%$ so as not to confuse very

loose clean sands with sands containing fines. In this zone, it is sometimes useful to set $K_c = 1.0$. Soils that fall into the (dilative) clay-like region of the CPT soil behavior chart (e.g., region CD, Figure 25b), in general, are not susceptible to cyclic liquefaction. However, in this SBT region samples should be obtained, and liquefaction potential evaluated using other criteria based primarily on plasticity, e.g., soils with plasticity index greater than about 18 are likely not susceptible to liquefaction. Soils that fall in the lower left region of the CPT SBT chart defined by region CCS (see Figure 25b) can be sensitive and hence, possibly susceptible to both cyclic and flow liquefaction. A flow-chart to estimate $CRR_{7.5}$ from the CPT is summarized in Figure 48.

For low-risk projects and for preliminary screening in high-risk projects, soils in region CC and CD (Figure 25b) would have clay-like behavior and would likely not be susceptible to cyclic liquefaction. Youd et al (2001) recommends that soils be sampled using simple push-in (disturbed) samplers when $I_c > 2.4$ ($I_B < 32$) to verify the behavior type based on simple index testing (e.g., grain size distribution, Atterberg limits and water content) to confirm susceptibility to cyclic liquefaction using the criteria in Figure 46. Selective soil sampling based on I_c (or I_B) should be carried out adjacent to some CPT soundings. Disturbed samples can be obtained using either direct push samplers (e.g., Figure 1) or conventional drilling/sampling techniques close to the CPT sounding.

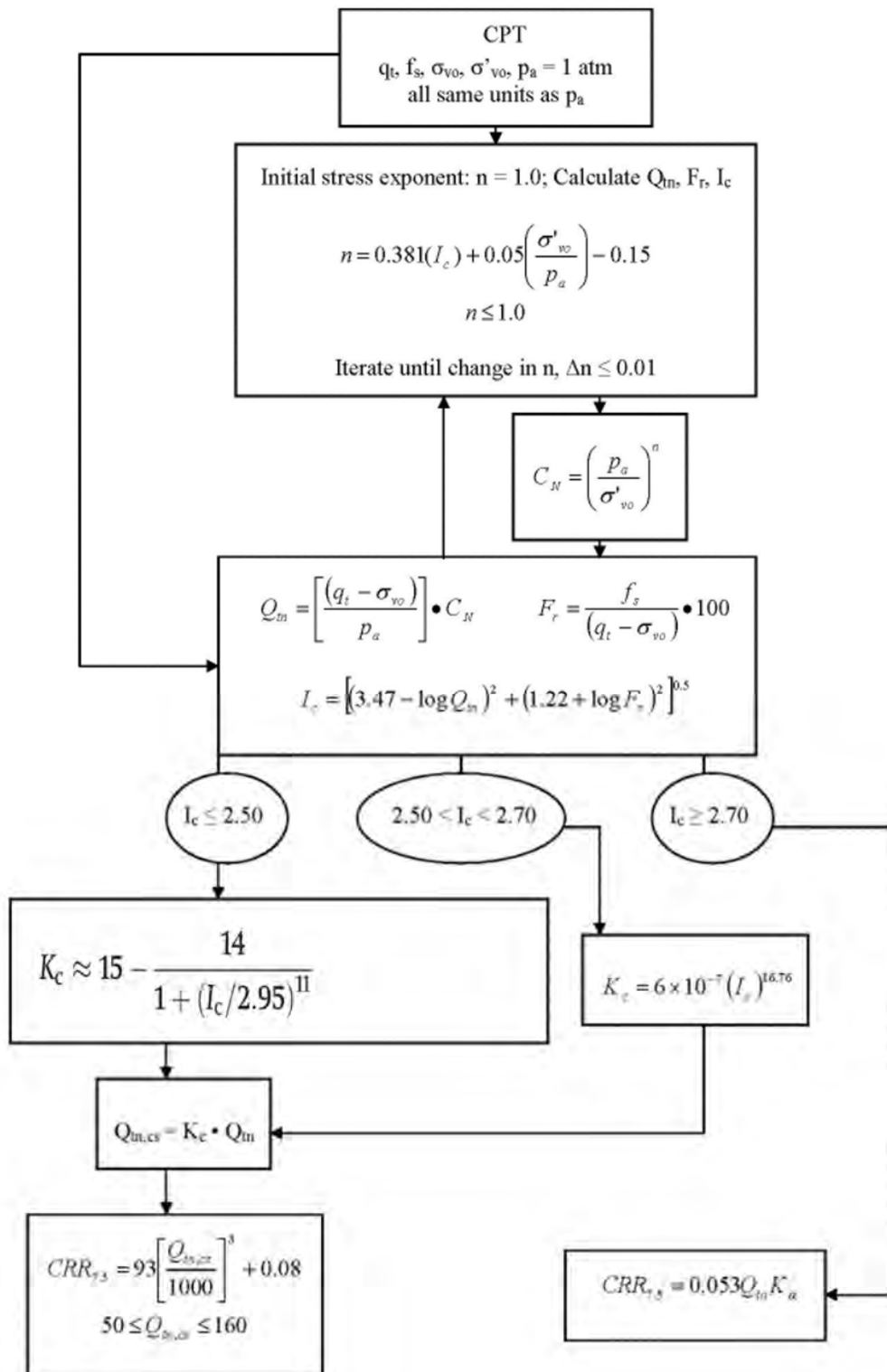


Figure 48. Flow chart to evaluate cyclic resistance ratio (CRR_{7.5}) from CPT

The factor of safety against cyclic liquefaction is defined as:

$$\text{Factor of Safety, } FS = \frac{CRR_{7.5}}{CSR} MSF$$

Where MSF is the Magnitude Scaling Factor to convert the $CRR_{7.5}$ for $M = 7.5$ to the equivalent CRR for the design earthquake.

The NCEER recommended MSF is given by:

$$MSF = \frac{174}{M^{2.56}}$$

The above recommendations are based on the NCEER Workshops in 1996/97 (Youd et al., 2001) and updated by Robertson (2009).

Juang et al., (2006) and Ku et al (2012) related Factor of Safety (FS) to the probability of liquefaction (P_L) for the R&W CPT-based method using:

$$P_L = 1 / (1 + (FS/0.9)^{6.3})$$

After the NCEER workshops in 1996-97, there have been several alternate updated CPT-based methods to estimate the resistance to cyclic liquefaction (e.g., Moss et al. 2006; Idriss and Boulanger, 2008; Boulanger and Idriss, 2014). Each method involves a re-evaluation and expansion of the case history database that includes alternate assessments of past case history CSR values and different methods to correct the measured cone resistance to obtain an equivalent normalized clean sand resistance. These alternate values of CSR and $Q_{tn,cs}$ (or $q_{c1n,cs}$) result in alternate trigger relationships for estimating the CRR. Hence, each method is a package in that the specified method to calculate CSR must be applied along with the specified method to calculate $Q_{tn,cs}$ (or $q_{c1n,cs}$) to estimate CRR. This means that you should not mix methods (i.e., calculate CSR using one method and estimate CRR using another method). This also applies to the various ‘correction factors’ used within each method.

$CRR_{7.5}$ can also be estimated using normalized shear wave velocity V_{s1} (Kayen et al, 2013). The combination of both CPT and V_s to evaluate the potential for soil liquefaction is very useful and can be accomplished in a cost-effective manner using the seismic CPT (SCPT). V_s is a small strain measurement of soil stiffness and is sensitive to the resistance to cyclic loading (CRR), as shown in Figure 49,

but can be a useful addition to the CPT. V_s is also sensitive to microstructure (e.g., age, bonding).

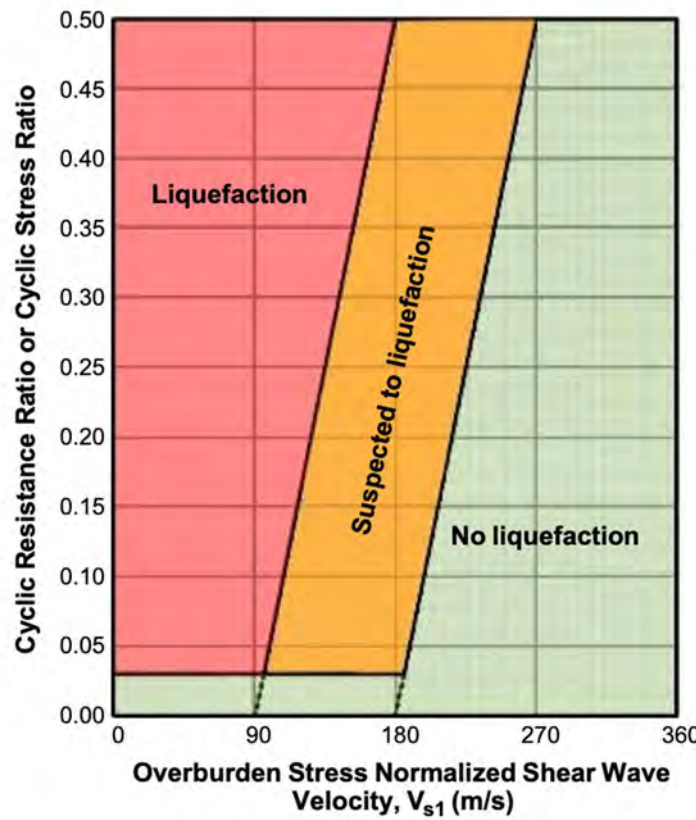


Figure 49. Regions of Liquefaction based on V_{s1}
(After Ahmadi and Paydar, 2014)

Ahmadi and Paydar (2014) suggested that because V_s is influenced by many factors (such as grain characteristics and microstructure) and small changes in V_s can result in large changes in CRR, it is best to apply V_s as a supplement to the CPT-based approach.

The CPT provides near continuous profiles of cone resistance that capture the full detail of soil variability, but large corrections are required based on soil type (compressibility). V_s is measured over a larger depth increment (typically every 1m) and hence provides a more averaged measure but requires smaller corrections for soil type, since it is insensitive to soil compressibility. If the two approaches provide similar results, in terms of $CRR_{7.5}$, there is more confidence in the results. If the two approaches provide different results, further investigation can be warranted to identify the cause (such as soil aging, bonding, etc.). Sometimes the V_s -based approach may predict a higher $CRR_{7.5}$ due to slight soil bonding. In this

case, the amount and cause of bonding should be studied to determine if the earthquake loading is sufficient to destroy the bonds. For example, for small earthquakes, the V_s approach may be correct, but for large earthquakes (that can destroy the benefits of bonding) the CPT approach may be correct.

Stratigraphy – transition zones

Robertson and Campanella (1983) showed that the cone tip resistance is influenced by the soil ahead and behind the cone tip. In strong/stiff soils the zone of influence is large (up to 15 cone diameters) whereas in soft soils the zone of influence is rather small (as small as 1 cone diameter). Ahmadi and Robertson (2005) showed that the size of the zone of influence decreased with increasing stress (e.g., dense sands behave more like loose sand at high values of effective stress).

The zone of influence ahead and behind a cone during penetration will influence the cone resistance at any interface (boundary) between two soil types of significantly different strength and stiffness. Hence, it is often important to identify transitions between different soil types to avoid possible misinterpretation. This issue has become increasingly important with software that provides interpretation of every data point from the CPT. When CPT data are collected at close intervals (typically every 10 to 50mm) several data points are '*in transition*' when the cone passes an interface between two different soil types (e.g., from sand to clay and visa-versa). The CPT data that is in the transition zone can be misleading and indicate the incorrect SBT. It is possible to identify the transition from one soil type to another using the rate of change of I_c (or I_B). When the CPT is in transition from sand to clay the SBT I_c will move from low values in the sand to higher values in the clay. Robertson and Wride (1998) suggested that the approximate boundary between sand-like and clay-like behavior is around $I_c = 2.60$. Hence, when the rate of change of I_c is rapid and is crossing the boundary defined by $I_c = 2.60$, the cone is likely in transition from a sand-like to clay-like soil or vice-versa. Profiles of I_c can provide a simple means to identify and remove these transition zones.

Software, such as *CLiq* (<http://www.geologismiki.gr/Products/CLiq.html>) includes a feature to identify and remove transition zones (see example in Figure 53).

Several methods have been suggested to correct for transition effects (e.g., Boulanger and DeJong, 2018) based on inversion methods. However, these methods are often based on the assumption that the interface between the two soil types is sharp. However, in some cases, the transition may be gradual. Application of these inversion methods to evaluate cyclic liquefaction have generally not been successful and do not match field performance observations. The removal of the transition zones can be considered an extreme case to bracket the likely behavior. Performing analyses for the extreme conditions with and without transition zones can aid in understanding the range of possible soil profile response. Additional comments on liquefaction analyses are provided in a later section.

Clay-like Materials

Clay-like materials tend to develop pore pressures more slowly under undrained cyclic loading, compared to sand-like materials, and generally do not reach zero effective stress under cyclic loading. Hence, clay-like materials are not susceptible to complete cyclic liquefaction (i.e., the condition of zero effective stress). However, when the cyclic stress ratio (CSR) is large relative to the undrained shear strength ratio of clay-like materials, deformations and softening can develop. Boulanger and Idriss (2007) used the term ‘cyclic softening’ to define this build-up of deformations under cyclic loading in clay-like soils and showed that the CRR for cyclic softening in clay-like materials is controlled by the undrained shear strength ratio, which is also controlled by stress history (OCR). Boulanger and Idriss (2007) recommended the following expressions for $CRR_{7.5}$ in natural deposits of clay-like soils:

$$CRR_{7.5} = 0.8 (s_u/\sigma'_{vc}) K_\alpha$$

and

$$CRR_{7.5} = 0.18 (OCR)^{0.8} K_\alpha$$

Where:

s_u/σ'_{vc} is the undrained shear strength ratio for the appropriate direction of loading.

K_α is a correction factor to account to static shear stress. For well-designed structures where the factor of safety for static loading is large, K_α is generally close to 0.9. For heavily loaded soils (e.g., close to foundations) and steeply sloping ground, K_α can be significantly less than 1.0. For seismic loading where $CSR < 0.6$, cyclic softening is possible only in normally to lightly

overconsolidated ($OCR < 4$) clay-like soils. For contractive sand-like soils with a static shear stress bias (e.g., steeply sloping ground), K_α can be smaller than 1.0.

Boulanger and Idriss (2007) recommended three approaches to determine CRR for clay-like materials, which are essentially:

1. Estimate using empirical methods based on stress history.
2. Measure s_u using in-situ tests (e.g., CPT and FVT).
3. Measure CRR on high quality samples using appropriate cyclic laboratory testing.

The third approach provides the highest level of insight and confidence, whereas the first and second approaches use empirical approximations to gain economy. For low-risk projects, the first and second approaches are often adequate. Based on the work of Wijewickreme and Sanin (2007), the $CRR_{7.5}$ for soft low plastic silts can also be estimated using the same approach based on either OCR or s_u (even though $PI < 10$) providing the tests (CPT or FVT) were carried out undrained.

The CPT can be used to estimate both undrained shear strength ratio (s_u/σ'_{vc}) and stress history (OCR). The CPT has the advantage that the results are repeatable and provide a detailed continuous profile of OCR and hence $CRR_{7.5}$.

Robertson (2009) recommended the following CPT-based approach that can be applied to all soils (i.e., no I_c cut-off):

When $I_c \leq 2.50$, assume soils are sand-like and CPT penetration is essentially drained:

Use Robertson and Wride (1998) recommendation based on

$$Q_{tn,cs} = K_c Q_{tn},$$

where K_c is a function of I_c (updated by Robertson, 2022, see Figure 48)

When $I_c > 2.70$, assume soils are clay-like and CPT penetration is essentially undrained, where:

$$CRR_{7.5} = 0.053 Q_{tn} K_\alpha$$

When $2.50 < I_c < 2.70$, transition region:

Use Robertson and Wride (1998) approach based on $Q_{tn,cs}$

$$\text{where: } K_c = 6 \times 10^{-7} (I_c)^{16.76}$$

The recommendations where $2.50 < I_c < 2.70$ represent a transition from essentially drained cone penetration to essentially undrained cone penetration where the soils transition from predominately sand-like to predominately clay-like.

Based on the above approach, the contour of $\text{CRR}_{7.5} = 0.50$ (for $K_\alpha = 1.0$) on the CPT SBT_n chart is shown in Figure 50, compared to case history field observations. For low-risk projects, the $\text{CRR}_{7.5}$ for cyclic softening in clay-like soils can be estimated using generally conservative correlations from the CPT. For medium-risk projects, field vane tests (FVT) can also be used to provide site specific correlations with the CPT. For high-risk projects high quality undisturbed samples should be obtained and appropriate cyclic laboratory testing performed. Since sampling and laboratory testing can be slow and expensive, sample locations should be based on preliminary screening using the CPT.

The approach described above (Robertson, 2009 for all soils) tends to work well in soil profiles that have well defined deposits of either sand-like or clay-like soils. However, the approach can be conservative in profiles where a significant volume of soil plots in the transition region where $2.5 < I_c < 2.7$. In these cases, samples should be obtained to clarify soil behavior. It can be helpful to run analysis using both the NCEER/RW98 method for sand-like soils and Robertson (2009) method for all soils, to evaluate the sensitivity of results to soil type.

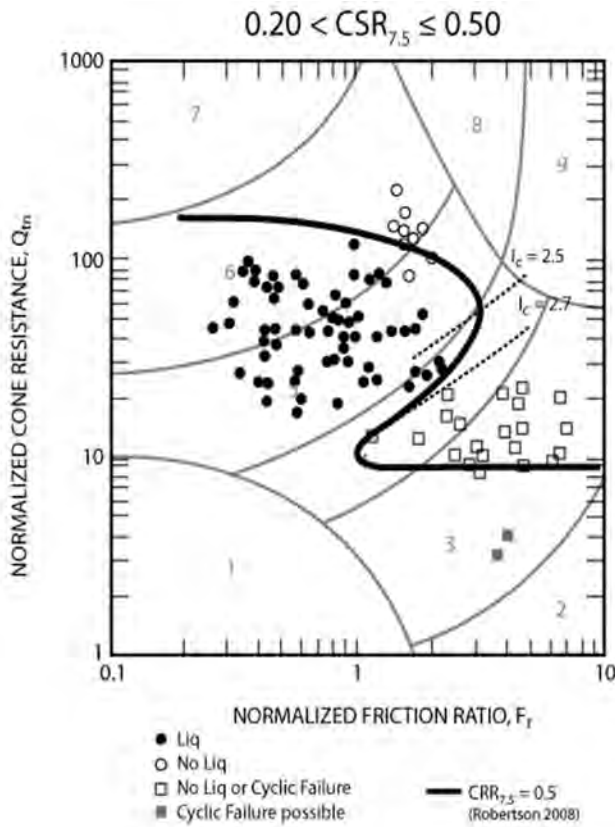


Figure 50. Cyclic Resistance Ratio ($CRR_M = 7.5$) using CPT
(After Robertson, 2009)

3. Evaluate of Post-earthquake Deformations

There have been several simplified indices developed to estimate the level of surface damage due to liquefaction. The first was the Liquefaction Potential Index (LPI) proposed by Iwasaki (1978) that provided a linear weighting to the calculated factor of safety against liquefaction ($1-FS_{liq}$) in the upper 20m of soil and linked the LPI to the severity of surface damage.

After the Christchurch, New Zealand earthquakes of 2010-11, Tonkin and Taylor (2013) developed a Liquefaction Severity Index (LSN) that uses depth weighted calculated volumetric strain within soil layers as a proxy for the severity of liquefaction damage likely at the ground surface. The strain calculation method considers strains that occur when soils have a calculated FS_{liq} below 2.0. This means that the LSN begins to increase smoothly as FS_{liq} decreases, rather than when the FS_{liq} reaches 1.0. One other aspect of LSN is that strains self-limit based

on the initial density as the FS_{liq} decreases, so a given soil profile has a maximum LSN that it tends towards as the PGA increases.

These simplified indices can be a helpful guide to expected surface damages based on past case history performance but ignore the potential post-shaking hydraulic mechanisms that may lead to incorrect estimation of liquefaction-induced ejecta.

Vertical deformations

The primary mechanisms of liquefaction-induced settlement of structures are volumetric-induced, shear-induced (from nearby foundations), and ejecta-induced deformations.

Volumetric-induced 1D settlements are often the most dominate mechanism that produces surface settlements. For low to medium-risk projects and for preliminary estimates for high-risk projects, post-earthquake volumetric-induced 1D settlements can be estimated using various empirical methods to estimate post-earthquake volumetric strains (e.g., Zhang et al., 2002). The method by Zhang et al (2002) uses the FS_{liq} from the Robertson and Wride (1998) method to provide a detailed vertical profile of estimated volumetric strains at each CPT location. The summation of these volumetric strains provides an estimate of the post-earthquake surface settlements. Idriss and Boulanger (2008) suggested a method that is essentially the same approach but uses the FS_{liq} determined from their method. The calculated volumetric strains are also used to determine the LSN.

The CPT-based 1D approach is generally conservative since it is typically applied to all CPT data often using either commercially available software (e.g., *CLiq*) or in-house software. The CPT-based 1D approach captures low (minimum) cone values in soil layers and in transition zones at soil boundaries. These low cone values in transition zones often result in accumulated volumetric strains that tend to increase the estimated settlement. Engineering judgment should be used to remove excessive conservatism in highly inter-bedded deposits where there are frequent transition zones at soil boundaries. Software can remove values in transition zones at soil boundaries (e.g., *CLiq* from <http://www.geologismiki.gr/>).

Robertson and Shao (2010) suggested a simplified CPT-based method to estimate the seismic compression in unsaturated soils. This method includes a factor of 2 to account for multi-directional loading. However, experience suggests that this added factor of 2 is overly conservative.

In clay-like soils the post-earthquake volumetric strains due to cyclic softening will be less than those experienced by sand-like soils due to cyclic liquefaction. A typical value of 0.5% or less is appropriate for most clay-like soils. Robertson (2009) suggested a simplified approach to estimate the post-earthquake volumetric strains in clay-like soils based on CPT results. For high-risk projects, selected high quality sampling and appropriate laboratory testing may be necessary in critical zones identified by the simplified approach.

Engineering judgment is required to evaluate the consequences of the calculated 1D vertical settlements from volumetric-induced strains considering soil variability, depth of the liquefied layers, thickness of non-liquefied soils above liquefied soils and project details (see Zhang et al., 2002). Displacement of buildings located above soils that experience liquefaction will depend on foundation details and depth, thickness, and lateral distribution of liquefied soils. In general, building movements result from a combination of shear-induced and volumetric strains plus possible loss of ground due to ejected soil (sand boils, etc.).

Case histories have shown that shallow foundations with a shallow liquifiable layer can also undergo large shear-induced movements that cannot be estimated using available 1D procedures. Bray and Macedo (2017) suggested a simplified method to estimate the additional settlement that can occur from shear-induced movements below a building. Bray and Macedo (2017) showed that well designed shallow foundations (i.e., high factor of safety against bearing capacity failure) with deep liquifiable layer will largely undergo volumetric reconsolidation that can be estimated using 1D procedures.

Hutabarat and Bray (2022) suggested a simplified method to estimate the severity of liquefaction ejecta-induced deformation. They showed that the severity was a function of the liquefaction demand (L_D), caused by upward seepage pressures that can produce artesian flow from liquefaction induced excess pore pressures, and the crust layer resistance (C_R) based on the strength and thickness of non-liquefiable crust layer. Low L_D values tend to be estimated at stratified soil sites, whereas high L_D values are calculated at sites with thick liquefiable sand deposits. C_R improves the reliability of the procedure by differentiating the performance of sites with or without a competent crust layer overlying a thick liquefiable layer with a high L_D value. The Hutabarat and Bray (2022) chart is shown in Figure 51.

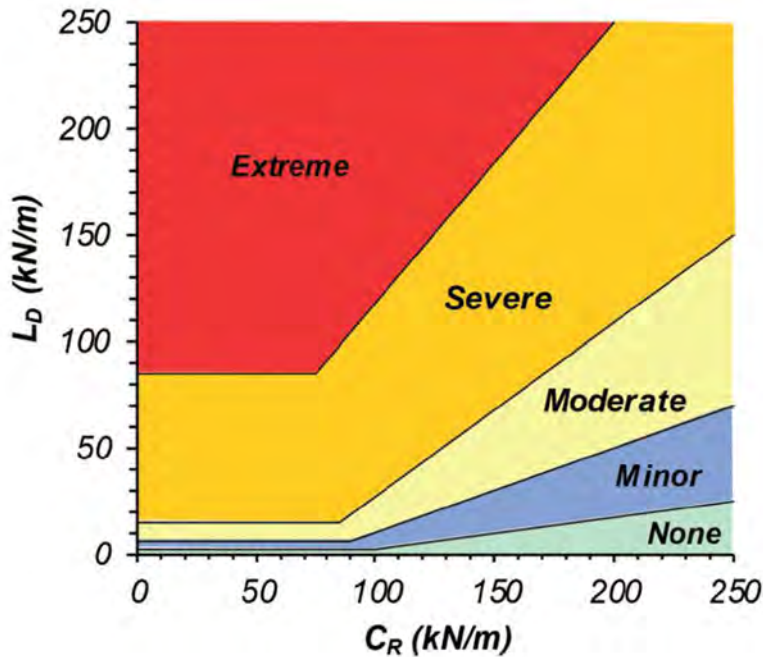


Figure 51. Liquefaction-induced ejecta severity chart
(After Hutabarat and Bray, 2022)

Liquefaction-induced ejecta deformations tend to be higher at sites with thick liquefiable sand layers close to the ground surface combined with a thin weak non-liquefiable crust. This is consistent with the observations made by Ishihara (1985) that linked liquefaction-induced surface damage to the thickness of the liquefiable sand layer and the thickness of overlying surface non-liquefiable crust.

There are some cases in which the $L_D - C_R$ chart has been shown to be less reliable and these cases include:

- A medium-to-dense thick sand may produce more ejecta due to post-shaking upward seepage-induced secondary liquefaction, though liquefaction is only triggered in a limited layer resulting in potential underestimation.
- A deep layer with a low FS_{liq} may reduce the seismic demand at shallow depths, which simplified triggering procedures indicate will liquefy, resulting in potential overestimation. Additionally, a partially stratified site with an intermediate low-permeable layer may not produce ejecta due to reduced upward seepage.

Lateral Deformations

For low to medium-risk projects and for preliminary evaluation for high-risk projects, post-earthquake lateral deformation (lateral spreading) can be estimated using various empirical methods (Youd et al, 2002 and Zhang et al, 2004). The method by Zhang et al (2004) has the advantage that it is based on CPT results and can provide a detailed vertical profile of strains at each CPT location. The Zhang et al (2004) method provides an index of lateral displacement (LDI) using a summation of estimated shear strains and then adjusts this (based on case history performance) to estimate the lateral displacement (LD) for the input ground geometry. Boulanger and Idriss (2008) suggested a similar approach but did not extend the approach beyond the LDI. Hence, it is not possible to compare the Zhang et al (2002) calculated LD with the Boulanger and Idriss (2008) LDI.

The CPT-based approach is generally conservative since it is typically applied to all CPT data and captures low (minimum) cone values in soil layers and in transition zones at soil boundaries. These low cone values in transition zones often result in accumulated shear strains that tend to increase the estimated lateral deformations. Engineering judgment should be used to remove excessive conservatism in highly inter-bedded deposits where there are frequent transition zones at soil boundaries. Software can remove values in transition zones at soil boundaries (e.g., *CLiq* from <http://www.geologismiki.gr/>).

Engineering judgment is required to evaluate the consequences of the calculated lateral displacements considering, soil variability, site geometry, depth of the liquefied layers and project details. In general, assume that any liquefied layer located at a depth more than twice the depth of the free face will have little influence on the lateral deformations. However, engineering judgment is required based on specific site details.

Sites with layered deposits (interbedded sands and clays)

Cubrinovski et al (2019) showed that the performance of a site to earthquake loading and liquefaction is a system response controlled by the complete soil profile. They showed that existing empirical CPT-based liquefaction methods provided generally good predictions of liquefaction and resulting deformations for sites composed mostly of sand-like deposits. However, at sites with interbedded sand-like and clay-like deposits, the existing empirical methods tend to over predict liquefaction and the resulting deformations. The frequent layers of clay-like soils tend to reduce the effects of liquefaction. Cubrinovski et al (2019) and others have suggested that 1-D effective stress dynamic analyses should be

used to evaluate the performance of sites with layered deposits. For high-risk projects, this maybe an appropriate approach. For low to medium-risk projects, the simplified approach can be used but it is important to recognize that the predicted liquefaction and resulting deformations will likely be conservative. The method by Hutabarat and Bray (2022) includes a simplified approach to estimate the amount of earthquake induced pore pressures that can be helpful to understand the likely distribution of high pore pressures and how clay layers may limit the effects of these pore pressures on the overall performance of the site.

When the calculated lateral deformations using the above empirical methods are very large (i.e., shear strains of more than 30%) the soils should also be evaluated for susceptibility for strength loss/reduction (see next section on flow liquefaction in sloping ground) and the overall stability against a flow slide evaluated.

Where appropriate for high-risk projects, dynamic effective stress analyses (ESA) can be carried out to provide some insights, as described by Hutabarat and Bray (2021) and Cubrinovski et al. (2019).

General comments on evaluation of Cyclic Liquefaction

Robertson and Wride (1998) (and updated by Robertson, 2016) suggested zones in which soils are susceptible to liquefaction based on the normalized soil behavior chart. An update of the chart is shown in Figure 52 along with general guidelines related to the evaluation of either cyclic or flow liquefaction.

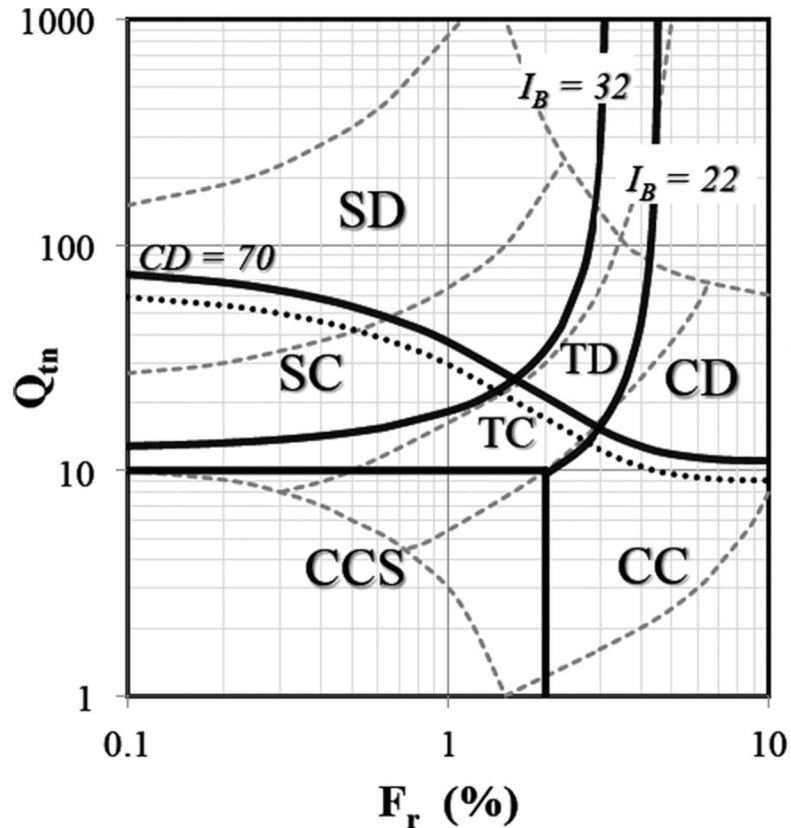


Figure 52 Zones of potential liquefaction/softening based on the CPT
(See Figure 25b for details)

Sand-like soils (SD & SC, $I_B > 32$) - Evaluate potential behavior using CPT-based case-history liquefaction correlations.

- SD Cyclic liquefaction possible depending on level and duration of cyclic loading.
- SC Cyclic liquefaction and (flow-liquefaction) strength loss possible depending on loading and ground geometry.

Clay-like soils (CD & CCS, $I_B < 22$) – Evaluate potential behavior based on in-situ and/or laboratory test measurements.

- CD Cyclic softening possible depending on level and duration of cyclic loading.
- CC/CCS Cyclic softening and (flow-liquefaction) strength loss possible depending on soil sensitivity and plasticity, loading and ground geometry.

Transition soils (TD & TC, $32 > I_B > 22$) – Evaluate potential behavior based on in-situ and/or laboratory test measurements.

- TD Cyclic liquefaction possible depending on level and duration of cyclic loading.
- TC Cyclic softening and (flow-liquefaction) strength loss possible depending on soil sensitivity and plasticity, loading and ground geometry.

The evaluation of liquefaction can be somewhat complex due to the many variables involved. It is common to use commercial software to aid in the analyses. Ideally software, such as *CPeT-IT* should be used first to process the CPT data to ensure quality control and to gain insight into the ground profile and groundwater conditions. After processing using *CPeT-IT*, the CPT data file can be imported into CPT-based liquefaction software such as *CLiq*. In the evaluation of cyclic liquefaction, the ‘correct’ answer is typically not known since the design earthquake is probabilistic in nature with many variables, and most current CPT-based methods are deterministic in nature, also with many variables. However, software can be used to bracket the expected answer in terms of both liquefaction and the resulting deformations. If the current CPT-based methods are applied as published, the results tend to be conservative. *CLiq* allows the user to compare different methods in a simple and efficient manner. Ideally, each method should produce somewhat similar results. If the results differ significantly, they should be evaluated to determine the likely reasons for the differences. Typically, when a site is composed predominately of sand-like soils in the upper 12m and with a high ground water level ($z_w < 4m$) and for a design earthquake with $M_w < 8$ (see database summary in Figure 47), the methods often provide similar results, since they were all based on similar database sites. Differences occur when the site is composed of either interlayered soils (sands and clays) or with input values outside of the range obtained from the case histories.

A detail to remember is that the CRR is based on the in-situ stresses (depth and groundwater conditions) at the time of the CPT to get the correct normalized $Q_{tn,cs}$, but the CSR is based on the estimated in-situ stresses at the time of the earthquake (e.g., the depth and groundwater conditions may differ). It is important to apply comparable return periods for the earthquake and the assumed groundwater conditions at the time of the design earthquake to avoid excess conservatism.

Sensitivity analyses should be carried out changing the major variables (e.g., earthquake loading (e.g., M_w and a_{max}) and soil conditions (e.g., unit weights, groundwater, transition zones) to gain insight into the sensitivity of results.

An example of a CPT-based method to evaluate cyclic liquefaction is shown on Figure 53 for a Moss Landing site that suffered cyclic liquefaction and lateral spreading during the 1989 Loma Prieta earthquake in California (Boulanger et al., 1995). Note that transition zones are identified in red.

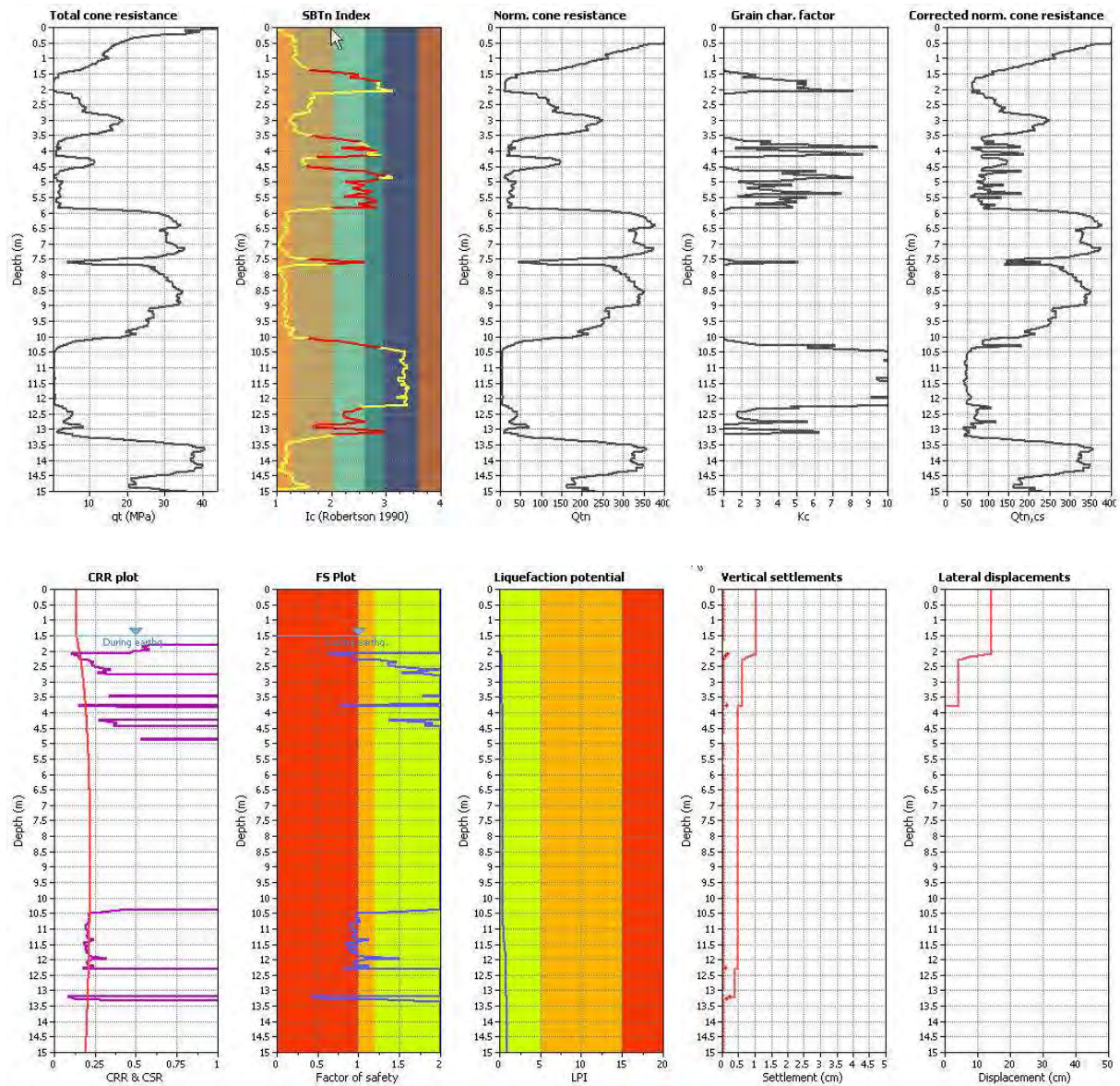


Figure 53. Example of CPT-based approach to evaluate cyclic liquefaction at Moss Landing Site showing (a) intermediate parameters (b) CRR, FS and post-earthquake deformations using '*CLiq*' software (<http://www.geologismiki.gr/>)

CLiq provides option to compare results over a range of earthquake inputs (e.g., range of both M and a_{max} , as shown in Figure 54. The example shows that if the earthquake was larger (e.g., higher a_{max}) the resulting vertical settlements are not overly sensitive, since liquefaction has mostly been triggered. However, if the earthquake was smaller the results become quite sensitive since less of the profile will be triggered and eventually, when a_{max} is below around 0.1 (in this case), very little of the profile will experience liquefaction.

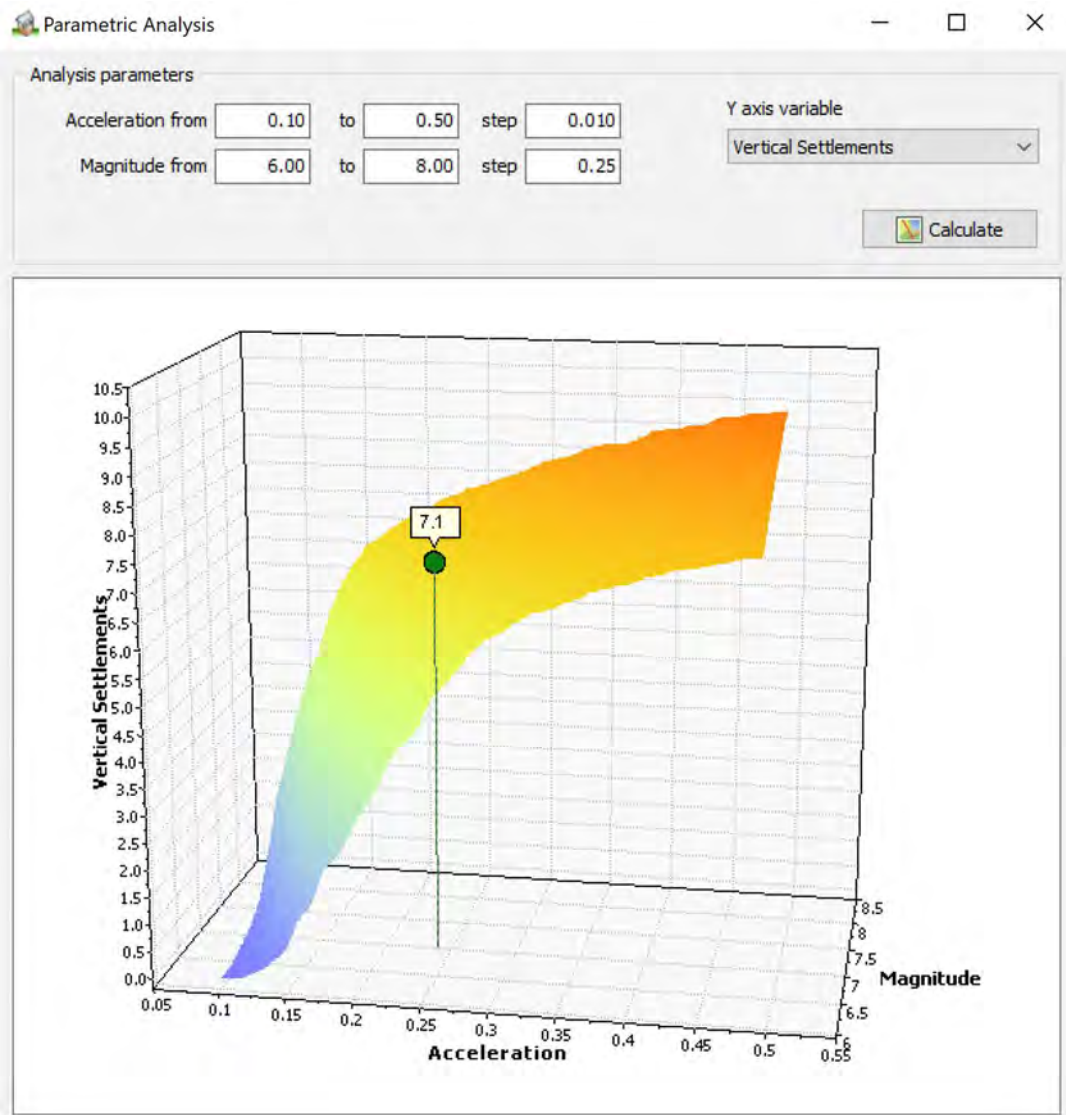


Figure 54. Example of CPT-based sensitivity to earthquake variables (M_w and a_{max})

Flow (static) Liquefaction (Steeply Sloping Sites)

Steeply sloping ground is defined as:

1. Steeply sloping ground (slope angle > 5 degrees)
2. Earth embankments (e.g., dams, tailings structures)

Flow liquefaction can occur in any saturated or near saturated loose soil, such as very loose sands and silts as well as sensitive clays and is a major design issue for large soil structures such as mine tailings impoundments and earth dams. For a slope to experience instability due to flow liquefaction the following conditions are required:

- Loose saturated or near saturated soils that are contractive at large strains and can experience significant and rapid strength loss/reduction in undrained shear
- High static shear stresses relative to the resulting large strain undrained shear strength (e.g., steeply sloping ground)
- Event(s) that can trigger strength loss
- Sufficient volume of loose saturated and near saturated soils for instability to manifest, and
- Suitable geometry to enable instability.

If a soil can strain soften in undrained shear and hence is susceptible to flow liquefaction, an estimate of the resulting large strain liquefied shear strength is required for stability analyses. Many procedures have been published for estimating the residual or liquefied shear strength of soils. Robertson (2010) outlined a method to evaluate both the susceptibility of soils to undrained strength loss that could result in flow liquefaction as well as a method to estimate the resulting liquefied undrained shear strength of predominately sand-like soils using cone penetration test (CPT) data. Robertson (2022) updated the method to extend the approach to all soils. The CPT process is essentially drained in sand-like soils and any correlation to estimate both susceptibility and undrained shear strength requires a link to an intermediate parameter, such as state parameter (ψ), which was the general approach taken by Plewes et al (1992), Jefferies and Been (2016) and Robertson (2010). In clay-like soils, the CPT process is essentially undrained, and the residual undrained shear strength can be estimated directly from the CPT sleeve resistance, f_s , since $f_s \sim s_{u(r)}$.

Sequence to evaluate flow liquefaction (i.e., strength loss/reduction)

1. Evaluate susceptibility for strength loss/reduction in undrained shear
2. Evaluate large strain (residual/liquefied) undrained shear strengths
3. Evaluate stability using the large strain undrained shear strengths
4. Evaluate if strength loss will be triggered

Case histories have shown that when significant and rapid strength loss occurs in critical sections of a soil structure, the resulting failures are often very fast, occur with little warning and the resulting deformations are often very large (e.g., Morgenstern et al, 2016, Robertson et al, 2019). Experience has also shown that the trigger events can be very small (Robertson et al, 2019). For structures where the consequences of failure are high (e.g., loss of life and/or significant environmental and reputational damage), it is prudent to assume that strength loss will be triggered since it is often impossible to design with confidence based on an assumption that strength loss will not be triggered at some time in the life of the structure. In seismic regions, even small earthquakes can trigger strength loss if the soils are susceptible and are under high static shear stresses. In general, the emphasis in design is primarily on the evaluation of susceptibility to strength loss and the resulting large strain undrained shear strength.

1. Evaluate Susceptibility for Strength Loss in undrained shear

The behavior of soils in shear prior to failure can be classified into two main groups; soils that dilate at large strains and soils that contract at large strains. Saturated (or near saturated) soils that contract at large strains have a shear strength in undrained shear that is lower than the strength in drained loading due to the resulting increase in pore pressure and decrease in effective confining stress. Saturated soils that dilate at large strains tend to have a shear strength in undrained loading that is either equal to or larger than in drained loading. However, since the benefits from dilation cannot be relied upon in the long term, it is common to apply drained shear strength parameters for dilative soil. When saturated (and near saturated) soils contract at large strains they can experience strain softening (strength loss) in undrained shearing, although not all soils that contract at large strains have a strain softening response in undrained shear (Robertson, 2017). The more contractive the soil, the larger the potential strength loss/reduction in undrained shear.

Robertson (2016) provided an updated CPT-based soil behavior type (SBT) chart that proposed a simplified boundary to identify if soils would be either contractive or dilative at large strains (Figure 52). The boundary was defined as follows, soils are contractive when $CD < 70$, where:

$$CD = (Q_{tn} - 11) (1 + 0.06 F_r)^{17}$$

The relationship applies to soils with little or no microstructure, e.g., geologically young (i.e., less than 10,000 years) and/or unbonded soils (i.e., no cementation).

The tendency for soils to change volume during shear covers a wide spectrum from highly contractive to highly dilative. Very loose soils tend to contract continuously toward critical state (CS), whereas moderately loose soils can initially contract then dilate somewhat before reaching critical state. In undrained shear, moderately loose saturated sand-like soils may experience some strain softening followed by strain hardening during strain-controlled triaxial compression testing. The strain hardening at large strains observed in moderately loose sand-like soils in strain-controlled laboratory triaxial compression tests may not be observed under load-controlled conditions in the field due to the inertia effects of the dead load (Castro, 1969). Hence, the observed strain-hardening in the laboratory on moderately loose sand-like samples under strain-controlled loading may not be experienced in the field under gravity loads. For this reason, the suggested boundary to define contractive soils based on CPT data tends to be slightly conservative, as described by Robertson (2016). Some researchers (Yoshimine et al, 1999) have suggested that the critical state line (CSL) for design should be defined using the minimum strength values, sometimes referred to as quasi-steady state, from triaxial compression tests.

If layers/zones of low permeability materials exist that could inhibit pore water redistribution after seismic loading and promote void redistribution, increase conservatism when evaluating susceptibility for strength loss.

2. Evaluate large strain (residual/liquefied) undrained shear strengths

Sand-like and transitional soils ($I_c < 3.0$)

In sand-like soils, with a soil behavior type index $I_c < 2.60$, where the CPT penetration process is predominately drained, Robertson (2010) suggested the normalized cone resistance (Q_{tn}) can be linked to state parameter (ψ) using a clean sand equivalent normalized cone resistance ($Q_{tn,cs}$) defined by:

$$Q_{tn,cs} = Q_{tn} K_c$$

Where, $Q_{tn,cs}$ is the clean sand equivalent normalized cone resistance and K_c is a correction factor to account for changing behavior with increasing fines content and compressibility.

Robertson (2010) suggested a link between $Q_{tn,cs}$ and ψ for sand-like soils, as follows:

$$\psi = 0.56 - 0.33 \log(Q_{tn,cs})$$

A similar relationship was also suggested by Been et al (2012). However, in transition soils with $2.6 < I_c < 3.0$ (e.g., silty sands and sandy silts), the CPT penetration can be partially drained where small excess pore pressures can be measured. In these soils, the correlation to state parameter becomes somewhat less reliable. To account for partial drainage, Robertson (2022) suggested that the correction factor (K_c) to obtain $Q_{tn,cs}$ be modified for $I_c < 3.0$ as follows:

$$K_c = 1.8346 I_c^5 - 23.673 I_c^4 + 124.02 I_c^3 - 320.616 I_c^2 + 405.821 I_c - 199.97$$

or the simplified version:

$$K_c \approx 15 - \frac{14}{1 + (I_c / 2.95)^{11}} \text{ for } I_c \leq 3.0$$

When $I_c < 1.7$, $K_c = 1.0$ (i.e., no correction in clean sands).

The objective of the modification was to join the relationship in sand-like soils, based on drained CPT data, to those in clay-like soils, based on undrained CPT data. The modified K_c relationship should not be extended beyond $I_c = 3.0$, where undrained penetration occurs. Robertson (2022) suggested that the modified K_c should also be used to evaluate cyclic liquefaction, since cyclic liquefaction is generally limited to sand-like soils with $I_c < 2.60$.

The correlation between $Q_{tn,cs}$ and the large strain liquefied undrained strength ratio ($s_{u(lip)} / \sigma'_{vo}$), suggested by Robertson (2010) for predominately sand-like soils, has also been updated and simplified to allow the relationship to be extended to higher values of $Q_{tn,cs}$, where the soils are dilative at large strains and where the design shear strength is controlled by the drained strength. The updated

relationship, shown in Figure 55, has been extended to include transitional soils where $I_c < 3.0$ by using the modified K_c . Included in Figure 55, for reference, are the class A and B case history data points from Robertson (2010) but updated based on modified $Q_{tn,cs}$ values and with cases removed when $I_c > 3$. Also included on Figure 55 are best estimate representative values for the coarse tailings ($I_c < 3.0$) from the Fundao and Feijao case histories (Morgenstern et al, 2016; Robertson et al, 2019). A shaded region is also added to illustrate the likely range of uncertainty for the evaluation of large strain liquefied undrained strength ratio. Figure 55 also illustrates that when sand-like soils are contractive at large strains (i.e., $Q_{tn,cs} < 70$) the undrained shear strength is less than the drained strength and when sand-like soils are strongly dilative at large strains ($Q_{tn,cs} > 80$), the drained strength is less than the undrained shear strength. Between $70 < Q_{tn,cs} < 80$ the soils can be initially contractive but become progressively more dilative with increasing strains and the undrained shear strength ratio can be high but remains slightly less than the drained strength ratio, defined by $\tan\phi'$.

The simplified and updated suggested correlation to estimate the large strain liquified undrained strength ratio, $s_{u(liq)}/\sigma'_{vo}$ for sand-like and transitional soils, when $I_c < 3.0$ is:

$$s_{u(liq)}/\sigma'_{vo} = 0.0007 \exp(0.084 Q_{tn,cs}) + 0.3/Q_{tn,cs}$$

When $Q_{tn,cs} < 20$, assume $s_{u(liq)}/\sigma'_{vo} = 0.02$ but use $s_{u(liq)} = 1\text{kPa}$, as a lower bound when $\sigma'_{vo} < 50\text{kPa}$. The minimum value of 1kPa represents the approximate undrained strength of clay-like soil when a semi-liquid (i.e., at the liquid limit) to avoid estimating lower values at low effective overburden stress. Selection of values lower than 1kPa should be supported by data from good quality samples where in-situ water contents are greater than the liquid limit.

This relationship applies when $Q_{tn,cs} < 80$, after which the drained shear strength ratio will typically control (i.e., $\tan\phi'$), as illustrated on Figure 55. The peak drained shear strength is influenced by the constant volume (critical state) friction angle (ϕ'_{cv}) and dilatancy, however, the large strain drained shear strength is controlled more by ϕ'_{cv} . Dilatancy is linked to state parameter for which $Q_{tn,cs}$ is a proxy when $I_c < 3.0$. Robertson (2012) suggested a simplified method to estimate the peak drained friction angle (ϕ') based on $Q_{tn,cs}$, as follow:

$$\phi' = \phi'_{cv} + 15.84 [\log Q_{tn,cs}] - 26.88$$

This requires an estimate of ϕ'_{cv} , that can be made using either an empirical relationship based on grain characteristic (e.g., grain roundness using Cho et al, 2006) or simple laboratory tests (e.g., measure angle of repose for very loose sand samples). The equivalent drained shear strength ratio values, shown in Figure 55, start at $Q_{tn,cs} = 50$ where $\psi = 0$. The sloping lines, shown in Figure 55 when $Q_{tn,cs} > 50$, capture the peak strength due to added dilatancy, but the values shown at $Q_{tn,cs} = 50$, for various ϕ'_{cv} , better represent the large strain shear strength ratio.

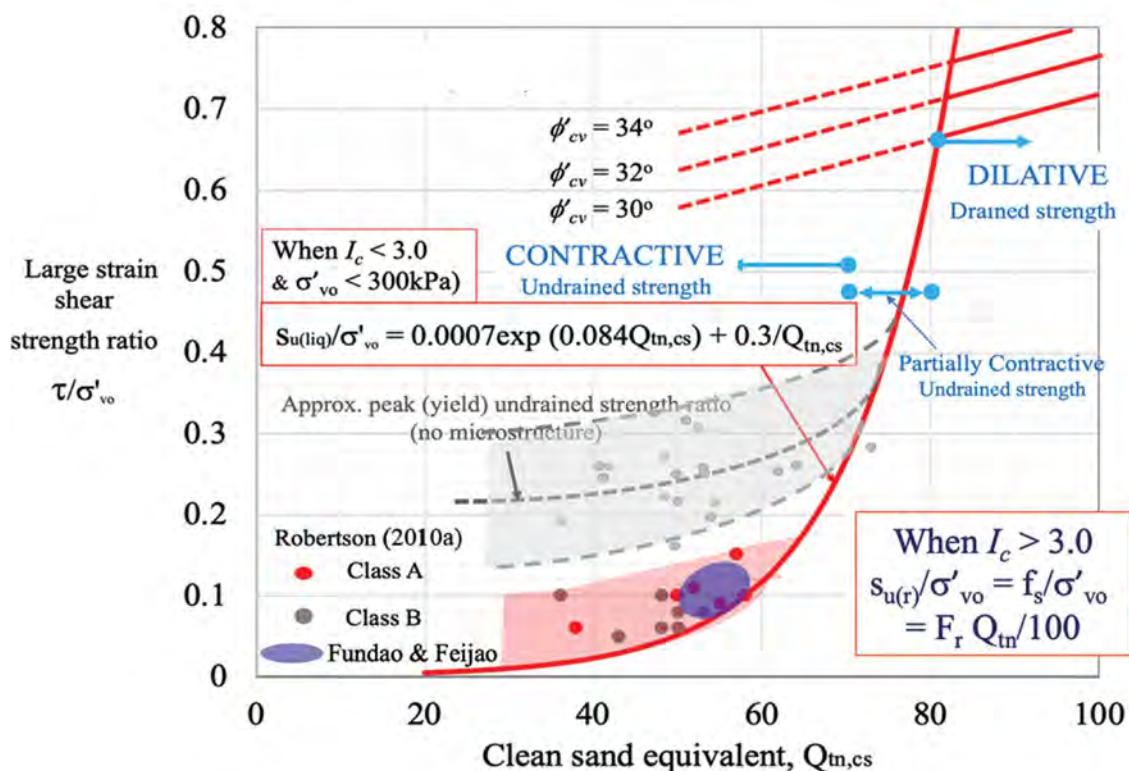


Figure 55. Relationship between large-strain shear strength ratio and $Q_{tn,cs}$ when $I_c < 3.0$ (After, Robertson, 2022)

The relationship to estimate $s_{u(liq)}/\sigma'_{vo}$ for sand-like and transitional soils and shown in Figure 55 is based primarily on case histories where the effective vertical overburden stress at failure (σ'_{vo}) was less than 3 atmospheres (i.e., $< 300\text{kPa}$) with most cases less than 2 atmospheres. Robertson (2017) showed that increasing effective overburden tends to make loose sand-like soils behave in a more ductile manner with less strength loss due to the curvature of the critical state line (CSL). The result is that $s_{u(liq)}/\sigma'_{vo}$ increases with increasing σ'_{vo} and

moves toward a value of around 0.22 to 0.25, like the peak (yield) undrained strength ratio, at high overburden stresses. The rate at which $s_{u(liq)}/\sigma'_{vo}$ increases is a function of the compressibility of the soil and the curvature of the CSL. For design purposes, the relationship shown in Figure 55 can be applied to provide a reasonable estimate of $s_{u(liq)}/\sigma'_{vo}$ up to $\sigma'_{vo} = 300\text{kPa}$. For higher stress levels the estimated values of $s_{u(liq)}/\sigma'_{vo}$ maybe conservatively low and advanced laboratory testing is required to guide any increase in $s_{u(liq)}/\sigma'_{vo}$ due to the curvature of the CSL. Robertson (2017) provided an approximate guide to estimate the effective overburden stress when the undrained behavior would become more ductile and $s_{u(liq)}/\sigma'_{vo}$ would approach a value closer to 0.25 based on the CPT friction ratio, as shown on Figure 56.

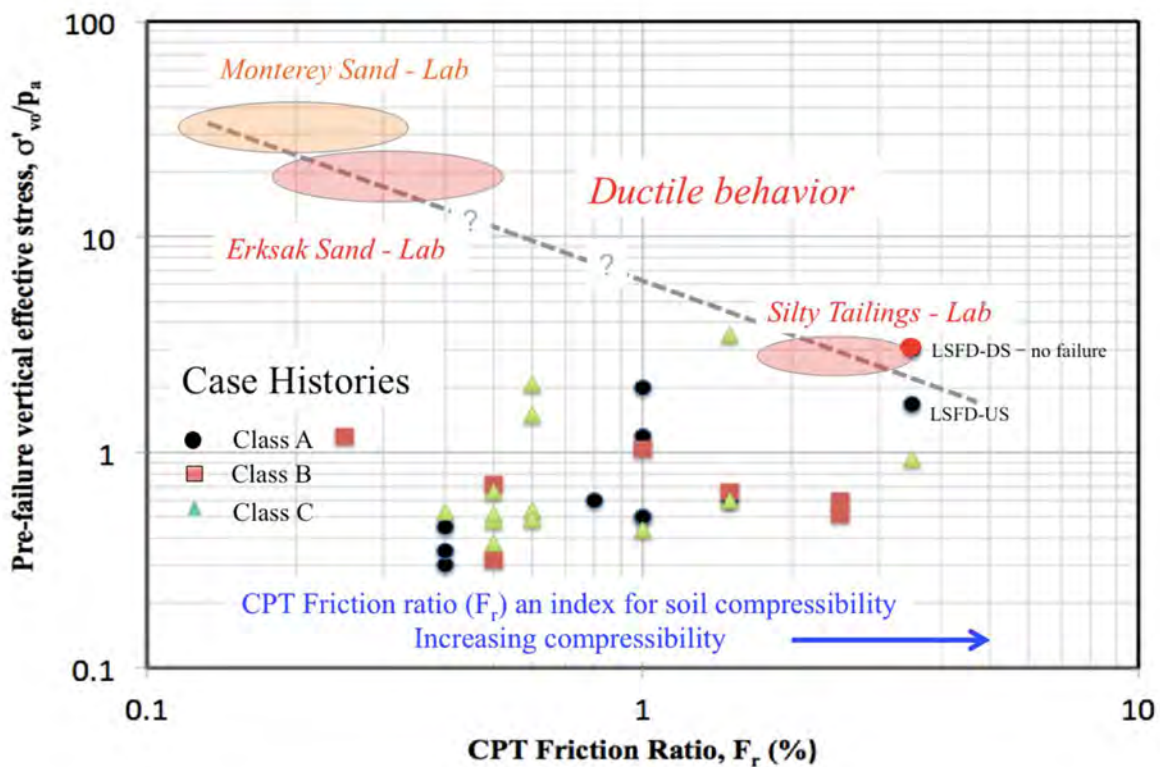


Figure 56. Relationship between pre-failure vertical effective stress and CPT normalized friction ratio for flow liquefaction case histories and selected laboratory results (After Robertson, 2017)

Olson and Stark (2003) proposed a relationship to estimate the peak (yield) undrained strength ratio for sands based on CPT data. However, estimating the peak (yield) undrained shear strength ratio in sand-like soils is very approximate due to factors such as microstructure (e.g., age and bonding), anisotropic stress

state and direction of loading. The Olson and Stark (2003) relationship used measured cone resistance, q_c , in units of MPa. Since the relationship was suggested for clean sands, it is reasonable to also represent it in terms of the clean sand equivalent ($Q_{tn,cs}$). To illustrate the difference between the peak (yield) and liquefied undrained strength ratio values as a function of $Q_{tn,cs}$ a dashed line has also been added to Figure 55 to illustrate the approximate location of the average peak (yield) undrained strength ratio for sand-like soils with little or no microstructure (i.e., little or no bonding and/or aging). Included on Figure 55 are the case history data from Olson and Stark (2003) using updated $Q_{tn,cs}$ values based on the data in Robertson (2010) to illustrate the range of uncertainty. This comparison illustrates the potentially large difference between any possible peak (yield) undrained strength and liquefied strength in loose sand-like soils. Limit equilibrium methods using peak undrained shear strengths can be misleading when applied to soils that can experience significant strength loss/reduction (Robertson et al, 2019) which introduces added uncertainty when applying peak undrained shear strength values for design. Hence, caution is needed before using peak (yield) undrained strength values to evaluate stability when there is a risk of significant and rapid strength loss/reduction. In general, the large strain liquefied/remolded undrained shear strength should be applied to evaluate the likelihood of instability when there is a risk of significant strength loss/reduction.

Clay-like soils (when $I_c > 3.0$)

In clay-like soils the liquefied undrained strength ($s_{u(liq)}$) is essentially the same as the remolded undrained shear strength ($s_{u(r)}$) since both occur at large strains. Robertson and Campanella (1983), Lunne et al (1997) and others have shown that in clay-like soils, where the CPT process is essentially undrained, the remolded undrained shear strength is approximately equal to the measured CPT sleeve friction, f_s , since both are occurring undrained and at large strains. Hence:

$$s_{u(liq)} / \sigma'_{vo} = f_s / \sigma'_{vo} = F_r Q_{tn} / 100$$

This relationship can be represented by diagonal straight lines on the Q_{tn} - F_r soil behavior type (SBT) chart, as shown on Figure 57. Figure 57 shows the resulting complete contours for $s_{u(liq)} / \sigma'_{vo}$ on the SBT chart for a wide range of soil behavior types, based on combining equations 2, 4, 5 and 7.

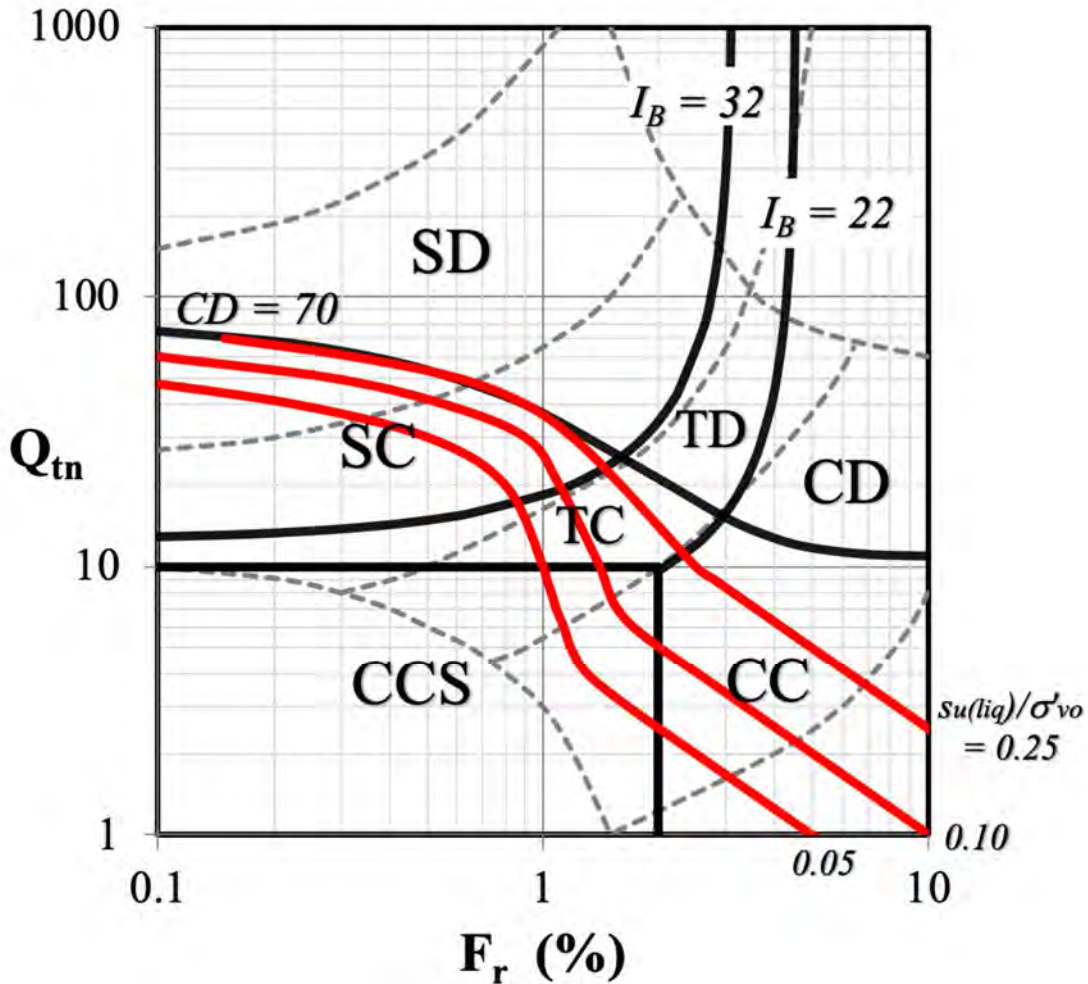


Figure 57. CPT-based SBT chart showing contours of large strain $s_{u.liq/r} = \sigma'_{vo}$

To illustrate the application in a normally consolidated clay-like soil with no strength loss (sensitivity, $S_t = 1.0$) the normalized CPT parameters are typically around $Q_{tn} = 3.5$ and $F_r = 7\%$. The contours shown on Figure 57 would correctly indicate that the estimated peak and remolded undrained shear strength ratio are the same at 0.25, where the peak undrained shear strength ratio is represented by Q_{tn}/N_{kt} (where $N_{kt} \sim 14$). If the original $Q_{tn,cs}$ (i.e., state parameter) contours are extended into the clay-like region, the estimated liquefied/remolded shear strength ratio for the same clay would have been close to 0.10, which is inconsistent with the historical CPT database for clay-like soils. For a normally consolidated clay-like soil that has a remolded undrained shear strength ratio of around 0.10 (i.e., a sensitivity of more than 2.5) the friction ratio would be expected to be less than 3% along with $Q_{tn} = 3.5$ (Lunne et al, 1997).

Jefferies and Been (2016) use a dimensionless cone resistance, Q_t that is normalized by a stress exponent of 1.0. In the clay-like region where $I_c > 3.0$, the normalization used by Robertson (2010a) is the same (i.e., $Q_{tn} = Q_t$), since both use a stress exponent of 1.0 in the clay-like region. The approach taken by Jefferies and Been (2016) attempts to capture the influence of changing drainage conditions during the CPT by incorporating the measured pore pressure behind the cone (u_2) to calculate an ‘effective’ cone resistance. However, the application of a single pore pressure measurement located behind the cone (u_2) is unlikely to fully represent the effective stresses around the cone tip and Robertson (2009) provided a more detailed discussion on the limitations of using an ‘effective’ cone resistance.

The comprehensive book by Jefferies and Been (2016) outlines a modification to their suggested correlation between state parameter and liquefied undrained strength ratio for sand-like soils based on the slope of the critical state line (CSL), λ_{10} . Essentially, for a soil with a contractive state parameter (where $\psi > -0.05$) the liquefied undrained strength ratio increases as λ_{10} increases (i.e., the steeper the CSL the smaller the strength loss for a given contractive state parameter). Previous publications (Plewes et al, 1992; Reid, 2015; Jefferies and Been, 2016) have shown that λ_{10} increases with I_c . In the clay-like region where $I_c > 3.0$, the estimated value is $\lambda_{10} > 0.15$ (Reid, 2015). Using the modified correlation suggested by Jefferies and Been (2016) for $\lambda_{10} > 0.15$ the resulting liquefied undrained strength ratio values are like those shown in Figure 57 when $I_c > 3.0$. Hence, the suggested relationship shown in Figure 57 is consistent with the updated, but more complex, relationships suggested by Jefferies and Been (2016).

Summary:

- Evaluate if soils are contractive at large strain based on the simplified CPT-based boundary suggested by Robertson (2016) using $CD < 70$. An alternate and complementary approach is to plot the CPT data directly onto the Q_{tn} - F_r SBT chart shown in Figure 57.
- If soils are contractive at large strains and predominately sand-like ($I_c < 3.0$), estimate the large strain liquefied undrained strength ratio based on $Q_{tn,cs}$. This applies to soils that have an in-situ $\sigma'_{vo} < 300\text{ kPa}$ and where $Q_{tn,cs}$ is calculated using the updated K_c correlation. When $\sigma'_{vo} > 300 \text{ kPa}$ laboratory testing is required to evaluate the curvature of the CSL that may result in modification of the suggested correlations, and Figure 56 can be used as a first estimate. Since the CSL is measured at large strains and is

controlled by grain characteristics, it is generally appropriate to determine the CSL using representative reconstituted samples. In general, increasing effective overburden stresses tend to make soil behave more clay-like and where the CPT data tend to migrate into the clay-like region on the SBT chart.

- If soils are contractive at large strain and predominately clay-like ($I_c > 3.0$), estimate the large strain liquefied/remolded undrained strength directly from f_s since the CPT penetration process is also undrained. In clay-like soils additional supporting data can be obtained from appropriate field vane testing as well as high quality sampling and laboratory testing, where possible.
- If soils are dilative at large strain and sand-like, the effective stress peak friction angle can be estimated using $Q_{tn,cs}$ and ϕ'_{cv} .

The measured penetration pore pressures (u_2) during the CPT can also be used to evaluate and/or confirm drainage conditions during the CPT as well as dilative/contractive behavior at large strains. If u_2 is small relative to the cone resistance, q_t , the penetration process is essentially drained. The rate of dissipation during CPT dissipation tests can also be used to evaluate drainage conditions in more fine-grained soils. If the time for 50% dissipation (t_{50}) is greater than about 50s the penetration process is essentially undrained (DeJong et al, 2012).

3. Evaluate stability using large strain undrained shear strengths

For soil structures where the consequences of failure are high (e.g., loss of life and/or significant environmental and reputational damage), it is prudent to assume that strength loss/reduction will be triggered, since it is often impossible to design with confidence based on an assumption that strength loss/reduction will not be triggered at some time in the life of the structure. Hence, assume that strength loss/reduction will be triggered and evaluate the resulting stability using conventional limit equilibrium methods.

If Factor of Safety (FS) > 1.1 , assume stability is acceptable. For earthquake loading evaluate seismic deformations.

For earthquake (seismic) loading, if layers/zones of low permeability exist that could inhibit pore water redistribution after seismic loading and promote void redistribution, increase conservatism when evaluating post-earthquake shear

strengths. For high-risk projects, the potential for void redistribution can be evaluated using more complex effective stress numerical models.

For high-risk projects where the consequences of instability are very high (e.g., loss of life, significant environmental damages, and loss of reputation, etc.), if $FS < 1.1$ take mitigation measures to ensure stability and reduce possible consequences. In some cases, it may be appropriate to perform advanced numerical modelling to evaluate if performance is acceptable using appropriate constitutive models and large strain shear strength values. However, overall design should be done within a risk-informed framework.

In conditions where the $FS \sim 1.0$ using best estimate residual undrained strengths, the risk of a flow failure is likely relatively low, since the inertial forces will be small, and the result from any possible instability is more likely to be a slump type failure.

4. Evaluate if strength loss will be triggered

In general, assume that if soils are susceptible to strength loss/reduction (i.e., flow liquefaction) assume that strength loss/reduction will be triggered at some time in the life of the structure.

The new Global Industry Standard for Tailings management (GISTM) and the supporting Good Practice Guide for Tailings Management, produced by International Council on Mining and Metals (ICMM), suggest a risk-informed decision-making approach in design. Risk-informed decision-making is underpinned by risk assessment, which comprises a series of steps: risk identification, risk analysis, and risk evaluation. Risk-informed decision-making improves and informs risk management (risk reduction) activities. Risk management includes the implementation of risk reduction measures, surveillance and review, risk communication, and risk recording and reporting.

For high-risk projects perform a risk assessment to aid in identifying risks and the corresponding consequences.

The simplified method to evaluate if cyclic liquefaction will be triggered during seismic loading is based on case histories with level or gently sloping ground. Application of this approach to evaluate if strength loss/reduction will be triggered (i.e., flow liquefaction) in steeply sloping ground can be misleading and unconservative. The simplified method includes a correction factor for static

shear stresses, K_α . In steeply sloping ground the static shear stresses are generally high and when soils are contractive at large strain, K_α is less than 1.0. Hence, K_α can be generally significantly less than 1.0 in steeply sloping ground with contractive soils.

Software

In recent years, commercial software has become available to aid in CPT interpretation and geotechnical design using CPT results. Robertson has been involved in the development of two programs: **CPeT-IT** (pron. *C-petit*) and **CLiq** (pron. *slick*). Both programs are inexpensive and very user friendly and can be downloaded from <http://www.geologismiki.gr/Products.html>.

CPeT-IT is an easy to use yet detailed software package for the interpretation of CPT and CPTu data. **CPeT-IT** takes CPT data and performs basic interpretation based on the methods contained in this Guide and supports output in both SI and Imperial units. Overlay plots can be generated and all results are presented in tabular and graphical format. The program also contains simple design tools for estimating bearing capacity for shallow foundations, 1-D settlement calculations and pile capacity versus depth. It also contains a tool for interpretation of dissipation tests. Example output from **CPeT-IT** is shown in Figures 58 to 60.

CLiq provides users an easy-to-use graphical environment specifically tailored for liquefaction analysis using CPT and CPTu data. The software addresses advanced issues such as cyclic softening in clay-like soils and transition zone detection. **CLiq** provides results and plots for each calculation step, starting with the basic CPT data interpretation through to final plots of factor of safety, liquefaction potential index and post-earthquake displacements, both vertical and lateral displacements. **CLiq** provides consistent output results by applying the NCEER method (Youd et al, 2001; Robertson & Wride, 1998) along with the calibrated procedures for post-earthquake displacements by Zhang et al (2002 & 2004). It also includes the latest assessment procedure developed by Robertson (2010) that is applicable to all soil type combining a check for cyclic liquefaction (sands) and cyclic softening (clays). It also includes the CPT-based liquefaction methods suggested by Moss et al (2006) and Boulanger and Idriss (2008/2014).

A unique 2D feature provides a means of creating colorful contour maps of the overall liquefaction potential index (LPI) and post-earthquake settlements in plan view thus allowing the user to visualize the spatial variation of liquefaction potential and settlements across a site. The variations of calculated post-earthquake settlements across a site allow estimates of differential settlements for a given site and design earthquake.

A parametric analysis feature allows the user to vary both the earthquake magnitude and surface acceleration to evaluate the sensitivity of both the overall

liquefaction potential index and post-earthquake settlements as a function of earthquake loading and results are presented in a 3D graphical form. Example output from *CLiq* are shown in Figures 53 and 54.

Webinars that demonstrate *CPeT-IT* and *CLiq* can be found at:
<https://www.greggdrilling.com/resources/webinars/>

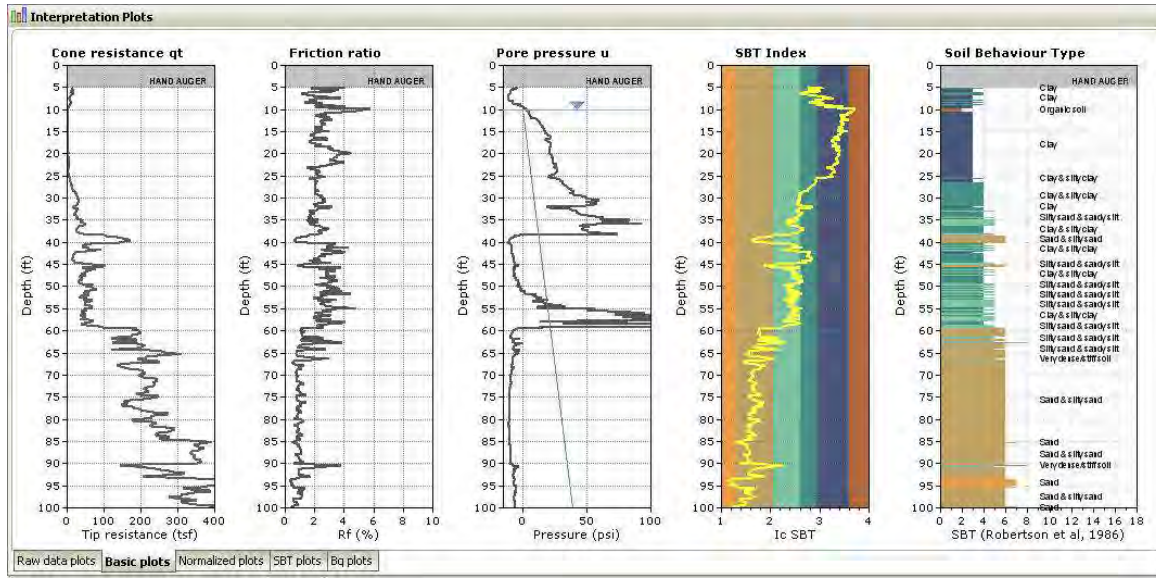


Figure 58. Example CPTu plot from *CPeT-IT*

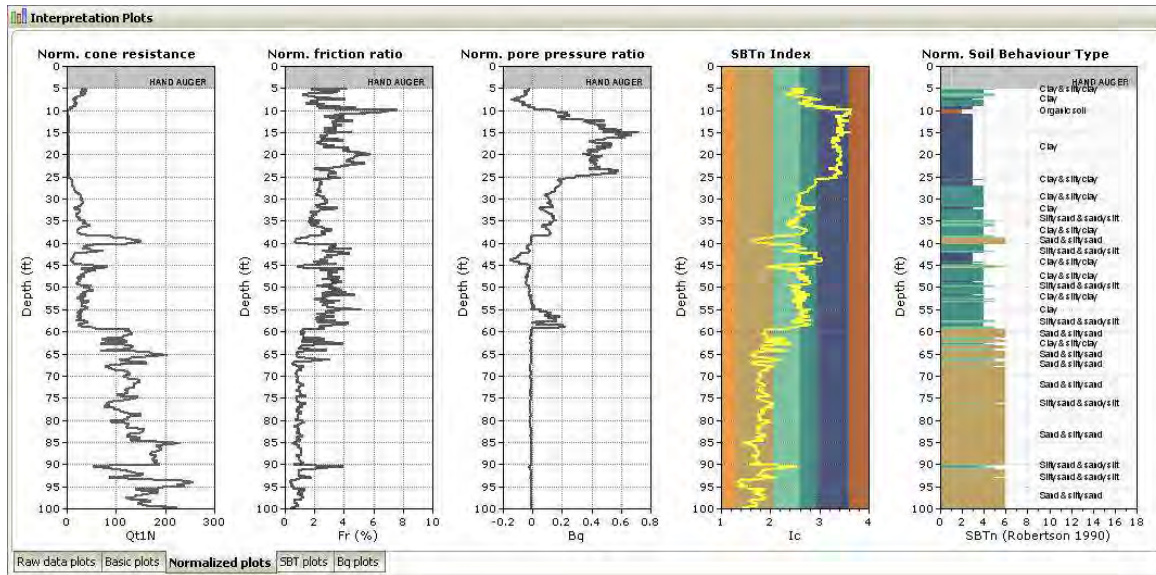


Figure 59. Example CPTu plot based on normalized parameters from *CPeT-IT*

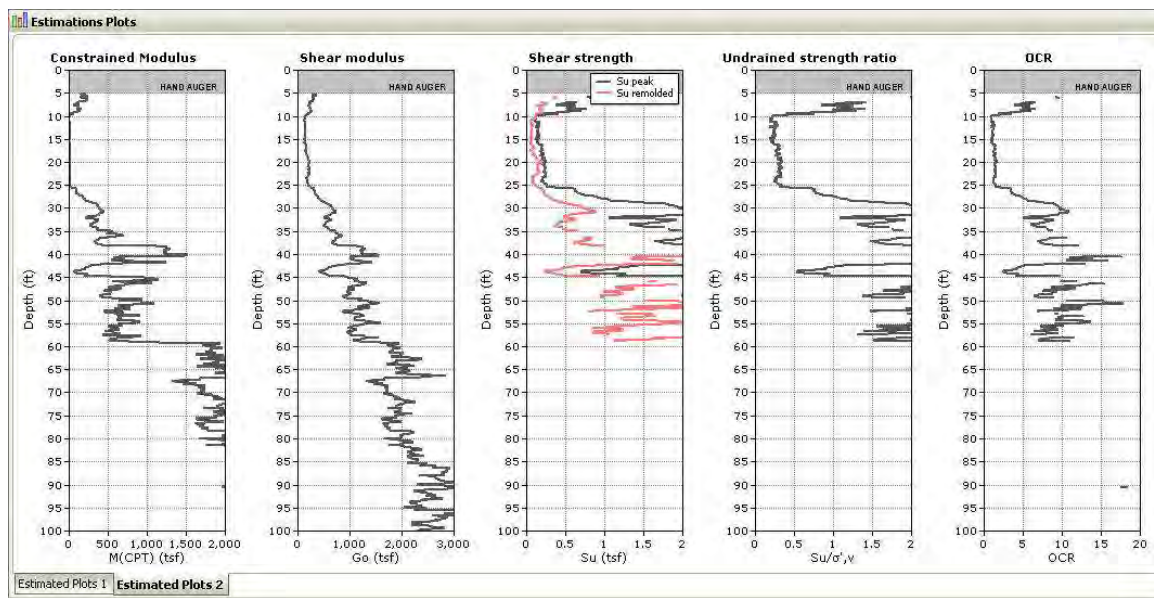


Figure 60. Example of estimated geotechnical parameters from **CPet-IT**

Main References

- ASTM-D5778-07. 2007. Standard test method for performing electronic friction cone and piezocone penetration testing of soils. ASTM International, West Conshohocken, PA, www.astm.org.
- Ahmadi, M.M., and Robertson, P.K., 2005. Thin layer effects on the CPT qc measurement. *Canadian Geotechnical Journal*, **42**(9): 1302-1317.
- ASTM D5778-12 (2012). Standard Test Method for Performing Electronic Friction Cone and Piezocone Penetration Testing of Soils, *ASTM International*. www.astm.org.
- Baldi, G., Bellotti, R., Ghionna, V.N., Jamiolkowski, M., and Lo Presti, D.F.C., 1989. Modulus of sands from CPTs and DMTs. In *Proceedings of the 12th International Conference on Soil Mechanics and Foundation Engineering*. Rio de Janeiro. Balkema Pub., Rotterdam, Vol.1, pp. 165-170.
- Bogges, R. and Robertson, P.K., 2010. CPT for soft sediments and deepwater investigations. *2nd International Symposium on Cone Penetration Testing*, CPT'10. Huntington Beach, CA, USA. www.cpt10.com
- Bolton, M.D., 1986. The strength and dilatancy of sands. *Geotechnique*, **36**(1): 65-78.
- Canadian Geotechnical Society 2006. *Canadian Foundation Engineering Manual*, 4th Edition, BiTech Publishers, Vancouver, BC.
- Campanella, R.G., and Robertson, P.K., 1982. State of the art in In-situ testing of soils: developments since 1978. In *Proceedings of Engineering Foundation Conference on Updating Subsurface Sampling of Soils and Rocks and Their In-situ Testing*. Santa Barbara, California. January 1982, pp. 245-267.
- Campanella, R.G., Gillespie, D., and Robertson, P.K., 1982. Pore pressures during cone penetration testing. In *Proceedings of the 2nd European Symposium on Penetration Testing*, ESPOT II. Amsterdam. A.A. Balkema, pp. 507-512.
- Eslaamizaad, S., and Robertson, P.K., 1996a. Seismic cone penetration test to identify cemented sands. In *Proceedings of the 49th Canadian Geotechnical Conference*. St. John's, Newfoundland. September, pp. 352 – 360.
- Eslaamizaad, S., and Robertson, P.K. 1996b. Cone penetration test to evaluate bearing capacity of foundation in sands. In *Proceedings of the*

- 49th Canadian Geotechnical Conference.* St. John's, Newfoundland. September, pp. 429-438.
- Eslaamizaad, S. and Robertson, P.K., 1997. Evaluation of settlement of footings on sand from seismic in-situ tests. In *Proceedings of the 50th Canadian Geotechnical Conference*, Ottawa, Ontario, October 1997, Vol.2, pp. 755-764.
- Fahey, M. and Carter, J.P., 1993. A finite element study of the pressuremeter in sand using a nonlinear elastic plastic model. *Canadian Geotechnical Journal*, **30**(2): 348-362.
- Hight, D., and Leroueil, S., 2003. Characterization of soils for engineering purposes. *Characterization and Engineering Properties of Natural Soils*, Vol.1, Swets and Zeitlinger, Lisse, pp. 255-360.
- Idriss, I.M. and Boulanger, R.W., 2004. Semi-empirical procedures for evaluating liquefaction potential during earthquakes. *Proceedings 11th International Conference on Soil Dynamics and Earthquake Engineering*. Berkeley, 32-56.
- IRTP, 1999. International Reference Test Procedure for Cone Penetration Test (CPT). Report of the ISSMFE Technical Committee on Penetration Testing of Soils, TC 16, Swedish Geotechnical Institute, Linkoping, Information, 7, 6-16.
- Janbu, N., 1963, Soil Compressibility as determined by oedometer and triaxial tests. *Proceedings of the European Conference on Soil Mechanicxs and Foundation Engineering*, Wiesbaden, pp 19-25.
- Jamiolkowski, M., Ladd, C.C., Germaine, J.T., and Lancellotta, R., 1985. New developments in field and laboratory testing of soils. In *Proceedings of the 11th International Conference on Soil Mechanics and Foundation Engineering*. San Francisco, California, August 1985, Vol.1 pp. 57-153.
- Jefferies, M.G., and Davies, M.O, 1991. Soil Classification by the cone penetration test: discussion. *Canadian Geotechnical Journal*, **28**(1): 173-176.
- Jefferies, M.G., and Davies, M.P., 1993. Use of CPTU to estimate equivalent SPT N₆₀. *Geotechnical Testing Journal*, ASTM, **16**(4): 458-468.
- Jefferies, M.G. and Been, K., 2006. *Soil Liquefaction – A critical state approach*. Taylor & Francis, ISBN 0-419-16170-8 478 pages.
- Kayen, R., Moss, R.E.S., Thompson, E.M., Seed, R.B., Cetin, K.O., Der Kiureghian, A., Tanaka, Y., and Tokimatsu, K., 2013. Shear-wave velocity-based probabilistic and deterministic assessment of seismic soil liquefaction potential, *J. of Geotech. and Geoenvironmental Engineering*, ASCE, 2013.139: 407-419.

- Karlsrud, K., Lunne, T., Kort, D.A. & Strandvik, S. 2005. CPTU correlations for Clays. Proc. 16th ICSMGE, Osaka, September 2005
- Kulhawy, F.H., and Mayne, P.H., 1990. *Manual on estimating soil properties for foundation design*, Report EL-6800 Electric Power Research Institute, EPRI, August 1990.
- Ladd, C.C., and Foott, R. (1974). "New design procedure for stability of soft clays." *J. of the Geotech. Eng. Div.*, 100(GT7), 763-786.
- Ladd, C.C. & DeGroot, D.J. 2003. Recommended practice for soft ground site characterization. *Soil and Rock America*, Vol. 1 (Proc. 12th PanAmerican Conf., MIT), Verlag Glückauf, Essen: 3-57.
- Lunne, T., Eidsmoen, T., Gillespie, D., and Howland, J.D., 1986. Laboratory and field evaluation on cone penetrometers. *Proceedings of ASCE Specialty Conference In Situ '86: Use of In Situ Tests in Geotechnical Engineering*. Blacksburg, ASCE, GSP 6 714-729
- Lunne, T., Robertson, P.K., and Powell, J.J.M., 1997. *Cone penetration testing in geotechnical practice*. Blackie Academic, EF Spon/Routledge Publ., New York, 1997, 312 pp.
- Lunne, T., and Andersen, K.H., 2007. Soft clay shear strength parameters for deepwater geotechnical design. *Proceedings 6th International Conference, Society for Underwater Technology*, Offshore Site Investigation and Geomechanics, London, 151-176.
- Mayne, P.W., 2000. Enhanced Geotechnical Site Characterization by Seismic Piezocone Penetration Test. Invited lecture, *Fourth International Geotechnical Conference*, Cairo University. pp 95-120.
- Mayne, P.W., 2005. Integrated Ground Behavior: In-Situ and Lab Tests, *Deformation Characteristics of Geomaterials*, Vol. 2 (Proc. Lyon), Taylor & Francis, London, pp. 155-177.
- Mayne, P.W., 2007. NCHRP Synthesis 'Cone Penetration Testing State-of-Practice'. Transportation Research Board Report Project 20-05. 118 pages. www.trb.org
- Mayne, P.W., 2008. Piezocone profiling of clays for maritime site investigations. *11th Baltic Sea Geotechnical Conference*. Gdansk, Poland., 151- 178.
- Mayne, P.W., Coop, M.R., Springman, S.M., Huang, A.B, and Zornberg, J.G., 2009. Geomaterial behaviour and testing. State of the Art (SOA) paper, 17th ICSMGE Alexandria.
- Mitchell, J.K., Guzikowski, F. and Villet, W.C.B., 1978. The Measurement of Soil Properties In-Situ, Report prepared for US Department of Energy Contract W-7405-ENG-48, Lawrence Berkeley Laboratory, University of California, Berkeley, CA, 94720.

- Molle, J., 2005. *The accuracy of the interpretation of CPT-based soil classification methods in soft soils*. MSc Thesis, Section for Engineering Geology, Department of Applied Earth Sciences, Delft University of Technology, Report No. 242, Report AES/IG/05-25, December.
- Parez, L. and Faureil, R., 1988. Le piézocône. Améliorations apportées à la reconnaissance de sols. *Revue Française de Géotech*, Vol. 44, 13-27.
- Robertson, P.K., 1990. Soil classification using the cone penetration test. *Canadian Geotechnical Journal*, **27**(1): 151-158.
- Robertson, P.K., 1998. Risk-based site investigation. *Geotechnical News*: 45-47, September 1998.
- Robertson, P.K., 2009a. Interpretation of cone penetration tests – a unified approach. *Canadian Geotechnical Journal*, **46**:1337-1355.
- Robertson, P.K., 2010a. Soil behaviour type from the CPT: an update. *2nd International Symposium on Cone Penetration Testing*, CPT'10, Huntington Beach, CA, USA. www.cpt10.com
- Robertson, P.K., 2010b. Estimating in-situ state parameter and friction angle in sandy soils from the CPT. *2nd International Symposium on Cone Penetration Testing*, CPT'10, Huntington Beach, CA, USA. www.cpt10.com
- Robertson, P.K., 2010c. Evaluation of Flow Liquefaction and Liquefied strength Using the Cone Penetration Test. *Journal of Geotechnical and Geoenvironmental Engineering*, ASCE, **136**(6): 842-853
- Robertson, P.K., 2015, “Comparing CPT and Vs Liquefaction Triggering Methods”. ASCE Journal of Geotechnical and Geoenvironmental Engineering, Vol. 141.
- Robertson, P.K., 2016. “CPT-based Soil Behaviour Type (SBT) Classification System – an update”. *Canadian Geotechnical Journal*, **53**(12); pp 1910-1927.
- Robertson, P.K., 2022. Evaluation of Flow Liquefaction and Liquefied Strength Using the Cone Penetration Test: an update. *Canadian Geotechnical Journal*.
- Robertson, P.K., Campanella, R.G., Gillespie, D., and Greig, J., 1986. Use of Piezometer Cone data. *In-Situ '86 Use of Ins-it u testing in Geotechnical Engineering*, GSP 6 , ASCE, Reston, VA, Specialty Publication, SM 92, pp 1263-1280.
- Robertson, P.K., Sully, J.P., Woeller, D.J., Lunne, T., Powell, J.J.M. and Gillespie, D., 1992. Estimating coefficient of consolidation from piezocone tests. *Canadian Geotechnical Journal*, Ottawa, **29**(4): 539-550.

- Robertson, P.K., and Campanella, R.G., 1983a. Interpretation of cone penetration tests – Part I (sand). *Canadian Geotechnical Journal*, 20(4): 718-733.
- Robertson, P.K., and Campanella, R.G. 1983b. Interpretation of cone penetration tests – Part II (clay). *Canadian Geotechnical Journal*, 20(4): 734-745.
- Robertson, P.K. and Wride, C.E., 1998. Evaluating cyclic liquefaction potential using the cone penetration test. *Canadian Geotechnical Journal*, Ottawa, 35(3): 442-459.
- Robertson, P.K., Campanella, R.G., Gillespie, D., and Rice, A., 1986. Seismic CPT to measure in-situ shear wave velocity. *Journal of Geotechnical Engineering Division*, ASCE, 112(8): 791-803.
- Sanglerat, G., 1972. *The Penetrometer and Soil Exploration*. Elsevier Pub., Amsterdam, 488pp.
- Schnaid, F., 2005. Geocharacterization and Engineering properties of natural soils by in-situ tests. In *Proceedings of the 16th International Conference on Soil Mechanics and Geotechnical Engineering*, Vol.1, Osaka, September, 2005, Millpress, Rotterdam, pp. 3-45.
- Schneider, J.A., Randolph, M.F., Mayne, P.W. & Ramsey, N.R. 2008. Analysis of factors influencing soil classification using normalized piezocone tip resistance and pore pressure parameters. *Journal Geotechnical and Geoenvironmental Engrg.* 134 (11): 1569-1586.
- Schmertmann, J.H. 1978. *Guidelines for cone penetration tests performance and design*. Federal Highways Administration, Washington, D.C., Report FHWA-TS-78-209.
- Teh, C.I., and Houlsby, G.T. 1991. An analytical study of the cone penetration test in clay. *Geotechnique*, 41 (1): 17-34.
- Wride, C.E., Robertson, P.K., Biggar, K.W., Campanella, R.G., Hofmann, B.A., Hughes, J.M.O., Küpper, A., and Woeller, D.J. In-Situ testing program at the CANLEX test sites. *Canadian Geotechnical Journal*, 2000, Vol. 37, No. 3, June, pp. 505-529
- Wroth, C.P., 1984. The interpretation of in-situ soil tests. Rankine Lecture, *Geotechnique*(4).
- Youd, T.L., Idriss, I.M., Andrus, R.D., Arango, I., Castro, G., Christian, J.T., Dobry, R., Finn, W.D.L., Harder, L.F., Hynes, M.E., Ishihara, K., Koester, J., Liao, S., Marcuson III, W.F., Martin, G.R., Mitchell, J.K., Moriwaki, Y., Power, M.S., Robertson, P.K., Seed, R., and Stokoe, K.H., Liquefaction Resistance of Soils: Summary Report from the 1996 NCEER and 1998 NCEER/NSF Workshop on Evaluation of Liquefaction Resistance of Soils,

- ASCE, Journal of Geotechnical & Geoenvironmental Engineering, Vol. 127, October, pp 817-833
- Zhang, Z., and Tumay, M.T., 1999. Statistical to fuzzy approach toward CPT soil classification. *Journal of Geotechnical and Geoenvironmental Engineering*, **125**(3): 179-186.
- Zhang, G., Robertson, P.K. and Brachman, R.W.I., 2002, Estimating Liquefaction induced Ground Settlements From CPT for Level Ground, *Canadian Geotechnical Journal*, 39(5): 1168-1180

GREGG DRILLING LLC

Southern California (Corporate Headquarters)

2726 Walnut Ave.
Signal Hill, CA 90755
Tel: 562-427-6899

Northern California

950 Howe Rd.
Martinez, CA 94553
Tel: 925-313-5800



info@greggdrilling.com
www.greggdrilling.com

Pitcher Services - Northern California

218 Demeter St,
East Palo Alto, CA 94303
Tel: (650) 328-8910
pitcherservicesllc.com



QUALITY - SAFETY - VALUE